Active Thermal Protection System for a Reusable Launch Vehicle

A Conceptual Design

Aditi Ahuja

Delft University of Technology

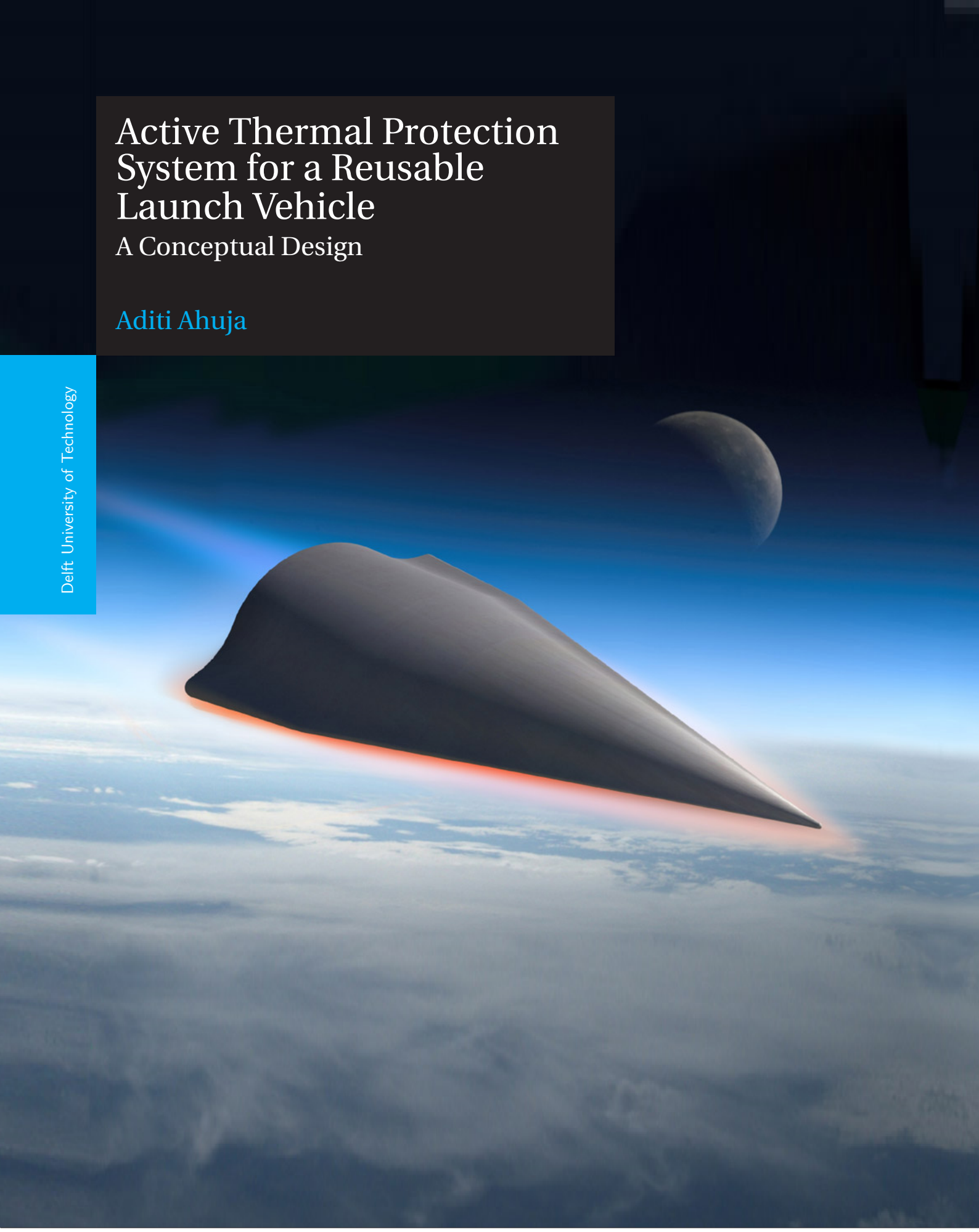

TU Delft Delft University of Technology

Challenge the future

Active Thermal Protection System for a Reusable Launch Vehicle

A Conceptual Design

by

Aditi Ahuja

in partial fulfillment of the requirements for the degree of

Master of Science
in Aerospace Engineering

at the Delft University of Technology
to be defended publicly on Monday March 30, 2020 at 10:00 AM.

Student number:	4736125	
Thesis Committee:	Dr. ir. E. Mooij,	TU Delft, supervisor
	Ir. K.J. Sudmeijer,	External, supervisor
	Dr. ir. W. van der Waal,	TU Delft
	Dr. ir. R. De Breuker,	TU Delft

TU Delft

Preface

With this report, I finally complete a two and a half year long roller coaster ride, the reward of which is a Master's degree in the field of Aerospace Engineering. I am forever grateful to my family for their unwavering support and encouragement, without which I would not have managed to succeed and make it this far.

I would like to thank both my supervisors, Erwin Mooij and Kees Sudmeijer, for their time and guidance throughout the course of this thesis. They always went beyond their basic responsibility as supervisors, and helped me grow as a person on the whole. They shared their personal experiences with me and have taught me some valuable life lessons that I will always carry with me, wherever I go. I went through some rough phases during my thesis, owing to my ill health, and without the understanding and support of my supervisors, I would not have managed to complete this thesis in time. I do not have enough words to express my gratitude.

I came to the Netherlands, a country far away from home, to pursue my dream of becoming an Aerospace Engineer and the transition was not easy. However, a crazy bunch of people who took off with me on this journey, made it so much memorable. A special thank you to each one of these people I call friends, for playing however small or big a part in this endeavour.

Aditi Ahuja
Delft, March 2020

Abstract

One of the many next steps in spaceflight is the development of reusable launch vehicles suitable for manned missions. All existing designs of re-entry vehicles are either ballistic or low L/D vehicles. In the future, the aim is to develop a high L/D vehicle, so that among others the vehicle experiences lower g-loads, making it comfortable for manned flights. Such vehicles are useful to both space (example, space tourism) and military applications (example, long-range missiles). Thermal protection system is deemed critical to the RLV development. Existing TPS solutions are not suitable for sustaining the high thermal loads for repeated flights. Therefore, arises the need to find reusable TPS solutions that can sustain the desired thermal loads. Flight testing is an crucial step for developing any hypersonic system, this applies to the TPS design as well. The aim of this study is to investigate the influence of TPS on designing the mission and vehicle for a test flight. Keeping this in mind, the research question is formulated as:

How does the thermal protection system design influence the mission and system design of an experimental winged RLV?

For proposing a TPS solution, it is important to understand the requirements that are imposed by the mission and system. A study of past and present space vehicles provided insight for future reusable launch vehicle missions and designs, i.e., vertical take-off and horizontal landing configurations, long range gliding entries (small entry flight-path angles) with global crass-range and ability to land on multiple sites across the globe (controllability), high thermal loads, low g-loads, is obtained. Based on these expectations, mission and system requirements that influence the TPS design are identified, such as the stagnation point heat flux lies within 1-2 MW/m^2. A litrature survey conducted prior to this thesis lead to identifying cooled metallic TPS as a suitable solution for future space vehicles.

Enhanced radiation cooling is one such cooled metallic TPS solution proposed by Buursink (2005). It consists of a coolant filled porous layer covered with a metallic outer skin with a small gap in between the two layers. The outer skin, which is heated up by mainly due to convection by the aerodynamic heat flux, radiates heat in both directions, inwards and outwards. The incoming heat flux is taken away by the evaporating coolant such that the underlying structure does not heat up. The preliminary investigation of the TPS concept lead to identifying suitable materials for the TPS along with the thickness of the layers.

To investigate the performance of the ERC design, a one-dimensional transient thermal analysis tool is developed. This thesis provides the mathematical formulation of the cooling phenomena and a description of the tool development. The performance of the design did not meet the thermal requirements imposed on the design. Therefore, modifications are

proposed to the design, including a change in material of the outer skin and introduction of holes in the stagnation region of the outer skin for venting the evaporated coolant. Carbon/ Carbon - Silicon Carbide (C/C-SiC) material is proposed in place of the metallic skin and the venting of evaporated coolant in the stagnation regions provides a thermal barrier for the TPS from the hot air. Both these modifications are accompanied with consequences that must be addressed, the most crucial ones are discussed and possible solutions are proposed. The poor oxidation resistance of C/C-SiC at high temperatures is one such problem and application of oxidation resistant coatings is proposed to address it. The performance of this new modified ERC design is found to satisfy the thermal load requirements.

The modified ERC has a relatively complex system, as compared to the original ERC design and a gap pressurisation system is a crucial element of this design, because it is an open system. Nitrogen gas is proposed for pressurising the gap, to ensure the gap pressure is above the coolant's triple point pressure as well as the stagnation region pressure. A sensitivity analysis of the modified ERC with respect to uncertainties in physical properties of the TPS material, and the blocking effect is conducted. The design is found to have negligible sensitivity to the material property uncertainties, unlike the blocking effect that has a significant influence. Also, a robustness investigation of the design helped understand the influence of mission and system parameters, namely nose radius, entry velocity and maximum heat load constraint, on the performance. For each parameter combination, the performance in terms of maximum temperature and total coolant mass is obtained, which is found useful in answering the research question. The entry velocity does not affect the temperature performance, however when combined with a change in heat load constraint or nose radius, a significant variation is observed. As for coolant mass, it is seen to increase in entry velocity because of longer flight time. Similarly, trends for other parameters are observed and provide a good first estimate for designing a test mission and vehicle. Intuitively, one would choose a parameter combination that requires least amount of coolant and operates within the working temperature of the material. However, this might not be the most optimal design from the overall mission and system aspect. To find an optimal solution, an integrated trajectory- vehicle shape-TPS design is recommended, as three are interrelated.

The overall outcome of the thesis is a TPS solution that is found to have the potential to be implemented in future reusable launch vehicles. However, a detailed design and experimentations, both ground-based and in-flight, are required to increase the technology readiness level of the concept. This thesis provides a conceptual design of a TPS, along with a first estimate of its thermal performance.

Table of Contents

Acronyms

AKTiV	Aktive Kühlung durch Transpiration im Versuch
ANOVA	Analysis of variance
C/C	Carbon fibre reinforced carbon
C/C-SiC	Carbon/Carbon Silicon Carbide composites
CCC	Circumscribed Central Composite Design
CCD	Central composite design
CCF	Face Centred Central Composite Design
CCI	Inscribed Central Composite Design
CMC	Ceramic Matrix Composites
DLR	Deutsches Zentrum für Luft- und Raumfahrt e.V.
ESA	European Space Agency
FESTIP	Future European Space Transportation Investigations Program
ISRO	Indian Space Research Organisation
IXV	Intermediate eXperimental Vehicle
MR	Mission requirement
NASA	National Aeronautics and Space Administration
NASP	National Aero-Space Plane
OAE	Once-Around Earth
ODS	Oxide dispersion strengthened
RLV	Reusable launch vehicle
SHEFEX	SHarp Edge Flight EXperiment
SiC	Silicon carbide
SOH	Sub-Orbital Hopper
SR	System requirement
SSTO	Single-stage to orbit
STS	Space Transportation System
TPS	Thermal protection system
TSTO	Two-stage to orbit
USAF	United States Air Force

List of symbols

Roman

$\dot{M}$	Mass flow rate	[kg/s]
$\dot{m}$	Mass flow rate per unit area	[kg/s/m^2]
A	Area	[m^2]
c_1	Heat flux constant	[−−]
c_2	Heat flux exponent	[−−]
C_D	Drag coefficient	[−−]
C_d	Discharge coefficient	[−−]
C_L	Drag	[N]
c_p	Specific heat capacity	[J/kg · K]
D	Drag	[N]
d	Diameter	[m]
g_0	Standard gravitational acceleration at Earth's surface	[m/s^2]
h	Altitude	[m]
H_{lv}	Latent heat of evaporation	[J]
k	Specific heat ratio	[−−]
L	Lift	[N]
L/D	Lift to drag ratio	[−−]
M	Mach number	[−−]
m	Mass	[kg]
n_g	g-load	[−−]
P	Pressure	[Pa]
Q	Volume flow rate	[m^3/s]
q	Heat flux	[W/m^2]
R	Specific gas constant	[J/kg/K]
r	Radius	[m]
r_p	Pressure ratio	[−−]
R_N	Nose radius of vehicle	[m]
Re	Reynold's number	[−−]
S_{ref}	Aerodynamic reference area of vehicle	[m^2]
T	Temperature	[K]
t	Time	[s]
V	Velocity	[m/s]
v	Volume	[m^3]

V_c	Local circular velocity	[m/s]
x	Thickness	[m]
Y	Expansion factor	[−−]

Greek

γ	Flight-path angle	[rad]
λ	Thermal conductivity	[W/m · K]
ϕ	Porosity	[−−]
ρ	Density	[kg/m^3]
ρ_0	Atmospheric density at sea level	[kg/m^3]
σ	Stefan-Boltzmann's constant	[W/m^2 · K^4]
θ	Surface inclination with respect to stagnation point	[rad]
ε	Emissivity	[−−]

Subscripts

blck	Blocking
c	Coolant
E	Entry condition
F	Final condition
i	Node in space
in	Inward
j	Node in time
max	Maximum
out	Outward
p	Porous layer
s	Skin
stag	Stagnation point

Chapter 1

Introduction

The aim of this chapter is to provide a comprehensive overview of the present-day engineering challenge that motivates this research project, including the objective and scope of this work. In addition to this, the basic structure of this report is described. A brief background is provided in Section 1-1, the purpose of this section is to address the problem and provide the necessary context. Additionally, the current knowledge gap that must be filled by means of this research is discussed. Based on this discussion, purpose of the research is stated and an overall methodology is described. In Section 1-2, the research question for this work is formulated. The aim of this question and its sub-questions is to unpack the problem such that answers to these questions will provide a complete solution to the problem. In Section 1-3, an outline of this report is provided, which is useful for the reader to understand, not only the structure of this report, but also to get an idea about the flow of work carried out for this research.

1-1 Background

Over the past few decades, increased demand for commercial global transportation and economical access to space have renewed interest of the space industry in reusable hypervelocity aerospace vehicles. Reusable launch vehicles (RLVs) have a high potential to be used in low-cost space and time-critical military missions (Mahulikar et al., 2008). The past few years have seen an increased interest in RLVs, which will have more airplane-like features, such as horizontal takeoff and landing capabilities, wings, air-breathing (jet) propulsion and landing gear. The National Aerospace Plane (NASP), a concept proposed by NASA, is an example of such a vehicle. Spaceplanes are expected to be more versatile, have short turn-around time between flights, increased reliability due to improved abort and return capabilities at any time during the mission, as well as have a reduction of the loads during launch. Two of the many applications envisioned for these vehicles are, delivery of crew/ cargo to the low-Earth orbit (LEO) and passenger/ cargo transportation to any location on Earth in a much shorter time compared to current air transport.

RLVs with an airbreathing propulsion system requires extended periods of acceleration in the denser part of the Earth's atmosphere to reach cruise and orbital velocities, as

Table 1-1: Space Shuttle and NASP Wing Maximum Surface Heating Comparison (Modlin, 1991)

Case	Maximum heat flux [kW/m^2]	Radiation equilibrium skin temperature [K]
Space Shuttle descent	400	1697
NASP descent	2000	2538
NASP ascent	10,000	3795

compared to existing rocket powered launch vehicles. The need for configurations with low aerodynamic drag combined with longer flight durations will lead to severe aerodynamic heating of the vehicle's surface. Air has a large amount of kinetic energy at hypersonic velocities (M>5), a significant part of which is converted to internal energy due to the decrease in air velocity caused by the viscous boundary layer at the surface of the vehicle, that in turn, leads to a substantial increase in the air temperature of the boundary layer. This change in air velocity becomes an important design consideration as its magnitude increases, because severity of the heating problem increases and the vehicle's design must be capable of managing the increased heating rates. Researchers have identified the nose and leading edges of the vehicle as critical regions in this aspect.

For flights at hypersonic speeds, the nose and leading edges must be blunt to some extent, to ensure the heat transfer rates remain manageable. However, for spaceplanes to achieve desired propulsion system performance and aerodynamic control, smaller nose radius and sharper leading edges are ideally required (Reed and Lister, 2015). This design will lead to an increase in the heating rates as compared to the surface heating experienced by existing hypersonic vehicle configurations (Anderson Jr, 2006). Examples of the maximum heat flux data for the wing section of the Space Shuttle and National Aero-Space Plane (NASP) are listed in Table 1.1. From these data, it can be observed that the maximum heat flux for the NASP vehicle is an order or two higher in magnitude than for the Space Shuttle. In case of the descent phase, the difference in order of magnitude is due to the spaceplane's low drag configuration (sharper nose and leading edges). In case of the ascent phase, the longer flight duration through the Earth's dense atmosphere, in combination with the vehicle's configuration, causes the maximum heat flux to be much higher, becoming one of the most critical factors for the vehicle's thermo-structural design.

The radiation equilibrium skin temperatures, seen in Table 1.1, are higher than the maximum temperature limits of the commonly used materials. Thus, a solution must be found to protect the vehicle surface from intense heat. Several methods have been developed in the past for surface cooling. For example, thermal barrier coatings could be attached to outer skins, internal convective cooling could be used as a structural heat sink by circulating the vehicle's cryogenic fuel through the hot structures, surface mass transfer cooling techniques (transpiration, film, or ablation) could be considered, or liquid metal heat pipes could be placed in critical regions.

The thermal protection system (TPS) occupies a huge acreage on the vehicle exteriors and forms a major part of the launch weight. Therefore, it is imperative that apart from making the TPS suitable for thermal protection purposes, it should be made lightweight, to keep the launch costs down. Also, it is required to present a robust external surface for the vehicle. Development of subsystems for hypersonic vehicles requires high confidence design data, which unfortunately, cannot be fully validated in ground test facilities. The acquisition of high resolution, high precision, coherent data is possible by means of flight

tests. For conducting these tests, a test vehicle and a trajectory must be designed such that the design requirements of the TPS are fulfilled. The trajectory flown by the test vehicle, should be optimised for aero-thermodynamic performance. To design such a trajectory, TPS design requirements have to be taken into consideration. Therefore, identifying the TPS requirements is a first step towards acquiring coherent and useful data from flight tests that can be used and extrapolated for detail design of the TPS.

The purpose of this study is to propose a suitable TPS concept, deemed critical to the realization of next generation hypersonic aerospace systems, and to identify its requirements for conducting flight tests. The research generates basic design data and performance analysis of a TPS design for a test vehicle, flying a nominal trajectory. The successful completion of this effort hopefully advances the design database for aerospace vehicles and accelerate the maturation of TPS technologies that have been deemed critical to development of emerging RLVs. Before proceeding, however, it must be noted that the underlying theme throughout the study is to conduct a thermal analysis of the proposed TPS design, by means of a thermal analysis tool developed during the course of this work. In this thesis, emphasis is placed on studying the TPS response to severe aerodynamic surface heating effects and the limitations of the proposed cooling method. No attempt is made to analyse, in great detail, the complicated hypersonic and surface boundary layer flow-field. Rather, empirically verified results reported in literature and simplifying assumptions, considered applicable to the problem of interest, are used. Additionally, the structural requirements of the TPS design is not considered. It is assumed that the mechanical and thermal stresses can be sustained by the design, and the TPS structure can be integrated with the vehicle. However, this must be verified and is proposed for study in the future.

1-2 Research goal

The goal of this thesis is to identify a reusable TPS design that can handle the high heat flux and total heat load experienced by a winged RLV, and to identify the influence of the TPS on designing a flight test. Therefore, the research question for the thesis is,

How does the thermal protection system design influence the mission and system design of an experimental winged RLV?

This question has further been broken down into sub-questions as given below:

1. What are the mission and system requirements that must be fulfilled by a TPS for an experimental winged re-entry vehicle?

2. Which TPS design is expected to satisfy the desired mission and system requirements?

3. How can the performance of the TPS design be analysed?

4. Is the TPS design suitable for multiple flights?

5. How do the limitations of the TPS design influence the flight test mission and the vehicle design?

1-3 Outline of report

This report documents all the work carried out during the course of this thesis. This report consists of seven chapters, including this chapter. In Chapter 2, mission and system requirements have been identified, after a detailed study of past, present and future missions. These requirements help guide the work carried out in this thesis. Based on these requirements a nominal trajectory is defined at the end of the chapter, and is used for analysing performance of the proposed TPS design. In Chapter 3, the preliminary design investigation carried out during the course of this work is discussed. This includes a description of the TPS concept that is selected for study. Additionally, to assess performance of the concept, some preliminary design is required which consists of identifying suitable materials and sizes for the TPS layers. Existing literature is used to make these choices and develop an initial system. Next, in Chapter 4, a description of the mathematical model used to simulate the physical phenomena of cooling in the TPS is described, including the assumptions made in the model. Followed by, a description of the thermal analysis tool developed, based on the mathematical formulation of the problem, to asses the TPS concepts performance. In Chapter 5, the results obtained by simulating the initial concept design using the tool developed is discussed. In addition, design modifications have been identified and implemented. This includes a discussion about the limitations of these modifications. Additionally, the design sizing is analysed, to identify the impact of sizing on the performance. Lastly, a conceptual design is proposed based on the findings and analysis carried out. A discussion about the operation of the system is included, along with schematic and CAD drawings. In Chapter 6, the results from the sensitivity and robustness analysis of the design are discussed. This helps to understand how the design would be influenced by different known and unknown changes in the design. Lastly, in Chapter 7, conclusions are drawn from the work and recommendations for the future are discussed.

Chapter 2

Mission Heritage

A reusable launch vehicle is a space launch system, which can be recovered after a flight for future reuse with minimum maintenance. RLVs can be both sub-orbital and orbital vehicles with single or multiple stages. Two-stage to orbit (TSTO) vehicles using a reusable hypersonic aircraft as the booster and a smaller vehicle to attain orbit, are amongst the most common RLV concepts. Single-stage to orbit (SSTO) vehicles have also been proposed in the past however, they can be more challenging to design in terms of weight, material and propulsion system requirements. These two concepts differ in terms of the thermal loads, which lead to a difference in the TPS design. Vertical launch from launch pads, horizontal launch from airports or air-dropped configurations and many more such ideas have been proposed for launching RLVs. Multiple landing scenarios, vertically or horizontally, using parachutes, parafoils, rotors or water landings have also been considered by designers over the years. These take-off and landing considerations are critical to the design characteristics and payload carrying capability of a vehicle.

Unfortunately, there are some challenging issues with designing such a system because of which a fully reusable launch system has not been successful till date. Typical design problems include the design of guidance and control systems capable of guiding the vehicle along an optimum trajectory and controlling it over the full flight range, structures and materials offering an improvement in structural efficiency as compared to existing airplane structures and thermal protection systems capable of withstanding high heat loads in the range of 1-5 MW/m^2. One of the main reasons for prominence of expendable launch vehicles over RLVs has been the higher up-front development costs of RLVs. Nonetheless, over the years many system concepts have been proposed as well as various experiments have been conducted and the development continues.

Reviewing past and present work is important, because it gives an overview of the technology evolution. Additionally, it helps us better define the requirements for designing efficient systems. The main aspect (out of many) that needs focus while designing a RLV, identified in this work, is a reusable (with a relatively low maintenance cost) TPS, that can sustain high in-flight thermal loads/ gradients. Various missions and vehicles were reviewed, and the most relevant ones are discussed in this chapter. Most of the missions and vehicles discussed in this chapter are high L/D vehicles or missions and many of them have proposed metallic TPS as a solution to the heating problem. This is the reason why it is important

to have a look at them before proposing a conceptual design. Based on these past, present and future missions/ vehicles, a reference mission is selected, for which a preliminary set of mission requirements are identified. The reference mission and the relevant requirements are discussed in Section 2-4. Before the proposed TPS design can be implemented for this mission, it must reach a desired technology readiness level (TRL). This requires the design to undergo various ground and in-flight tests. As discussed in the previous chapter, for a hypersonic vehicle, wind tunnel tests are insufficient and in-flight data is required. Therefore, to test the TPS concept in-flight, a test vehicle must be chosen that is capable of flying a nominal trajectory, which meets the mission requirements. This test vehicle will impose additional system requirements that must be considered while designing a suitable TPS, and is discussed in more detail in Section 2-5. Also, a nominal trajectory is needed, which can be obtained using the identified requirements. The nominal trajectory used for this thesis is described in Section 2-6.

2-1 Past

Over the years, many spaceplane concepts have been proposed, most of which were cancelled before they could be fully developed. Till date, only three orbital spaceplanes have been successfully flown, and include the United States Space Shuttle, the Soviet Buran and the Boeing X-37. All three were launched vertically using rocket propulsion and landed horizontally like an aircraft by using atmospheric lift. Although, vehicle designs such as the X-30 were proposed to take-off like a conventional aircraft, using aerodynamic lift in the ascent phase, no such flight has been successfully demonstrated. Suborbital vehicles such as the X-15, performed a successful horizontal launch, but did so after being taken to a higher altitude by a carrier aircraft. X-30 and X-33 were technology demonstrators for the National AeroSpace Plane (NASP) and VentureStar missions, respectively. Both were SSTO designs, the difference being that X-30 was a waverider configuration capable of carrying two crew members to orbit whereas the X-33 was to be an unmanned, lifting body configuration designed for a sub-orbital flight. The above discussed vehicles and other past RLV programs such as the Future European Space Transportation Investigations Program (FESTIP) are discussed in this section.

2-1-1 Boeing X-20 Dyna-Soar

The Boeing X-20 Dyna-Soar was a manned re-entry vehicle developed by USAF, designed to be launched vertically by means of an expendable rocket. Unfortunately, the development was stopped before a prototype was built. Nonetheless, a lot of research was conducted and wind tunnel tests were performed that lead to the design being ahead of its time, especially in terms of the materials and their manufacturing techniques. The concept of this vehicle was based on Eugen Sänger's Silbervogel, a rocket-powered sub-orbital bomber.

A rocket booster would launch the vehicle to an altitude in the range of 50-150 km with a speed greater than 5.5 km/s. The winged vehicle would then perform a boost-glide (skipping) entry back into the Earth's atmosphere using aerodynamic lift along with a Transtage rocket engine and cover a cross-range of roughly 2800 km (Buursink, 2005). This vehicle had a high L/D ratio of approximately 2 and was planned to be recovered by making it a manned bomber, to make it reusable. The high speed sub-orbital flight with a glide-skip entry into the Earth's atmosphere imposed thermal requirements on the structure and materials of the vehicle, other than them having to be reusable.

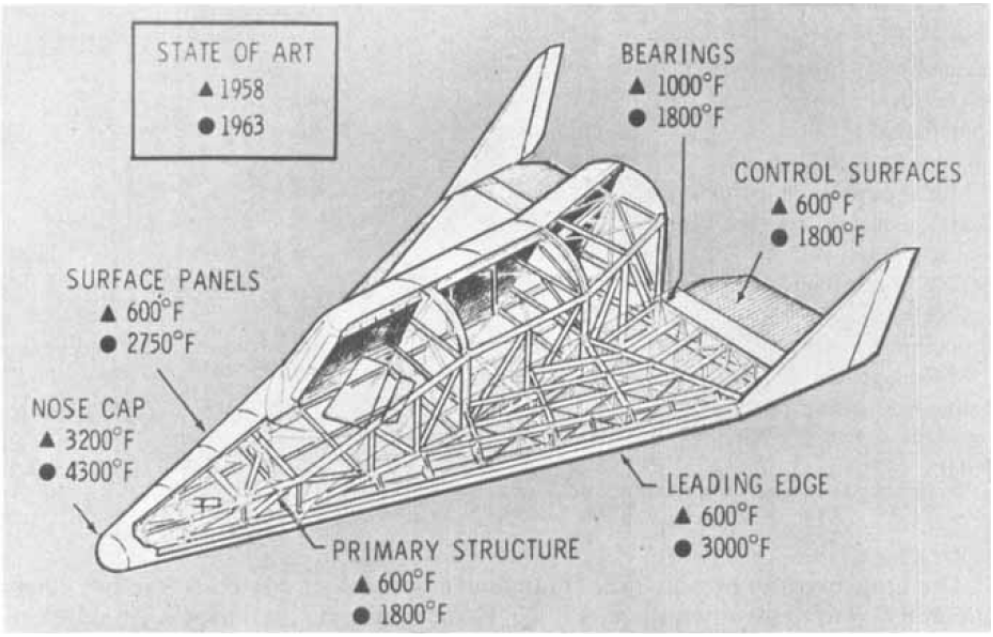

Figure 2-1: X-20 material temperatures (Rotelli, 1965).

In Figure 2-1, the temperatures that could be sustained by the materials on different parts of the vehicle can be seen. From this figure, the material development, over the four year period, is distinctly visible. For example, the preliminary design of the primary structure and leading edge could sustain temperatures up to 588 K ($\approx$ 600°F), but the new materials and designs developed during the research were a major improvement and could sustain temperatures up to 1255 K ($\approx$ 1800°F) and 1922 K ($\approx$ 3000°F), respectively. The X-15 had introduced heat sink fabricated from Inconel X, a nickel steel. Dyna-Soar went considerably further, developing radiation-cooled insulated structures fabricated from René-41 superalloy and refractory materials. The X-20 Dyna-Soar was the first re-entry vehicle designed to have a fully metallic TPS. Corrugated René-41 panels were used after reinforcement with a thin-gauge made from René-41 on the outer side and with insulation or refractory alloys on the inner side of the panel. Also, the nose cap of this vehicle was made of Carbon and Zirconia (2644 K) (Rotelli, 1965). Active cooling was also proposed for reducing temperatures within the crew compartment and two equipment bays. An absorbent material between sheet metal panels filled with water and gel would be used. Purpose of the gel was to retard the fluid flow, while the absorbent wicking kept it distributed uniformly to prevent hot spots (Heppenheimer, 2007). The windward side was covered with a TPS made from Molybdenum (1755 K) and the leading edges were coated with TZM Molybdenum (1920 K) (Rotelli, 1965). This TPS configuration for the X-20 vehicle was expected to be reused for a minimum of four re-entry flights (Heppenheimer, 2007).

The advance materials and active cooling concepts developed during this program set a precedent for the designs that followed and were found to be very relevant to the proposed work. The mission profile is interesting, because a sub-orbital flight at hypersonic speeds was planned, followed by a gliding-skipping entry into Earth's atmosphere.

2-1-2 Lockheed SR-71 (Blackbird)

SR-71, also known as Blackbird, is developed by Lockheed and was in service from 1964 to 1999. It is known for being the fastest and highest flying manned aircraft. It had a

Figure 2-2: The SR-71 fleet (Lockheed Martin).

horizontal launch from an airfield and achieved a maximum altitude of 25.9 km, which is record breaking, because other vehicles that achieved this altitude were all launched vertically. SR-71 is claimed to achieve Mach 3.2 (894 m/s) and it could cruise for almost an hour at Mach 3. Also, it could fly over a range of almost 3200 km, without having to be re-fuelled. At such high speeds, the heat produced due to friction with the atmosphere was very high and could melt conventional airframes. Even though this vehicle cannot be officially classified as a spaceplane, it is of much interest to this study because of the hypersonic long range flight performed and technologies developed to meet the thermal requirements.

At full speed, the front edge of the windscreen and front wing edge reached a temperature of 340°C and 427°C, respectively. Normal airframe materials could not withstand such high temperatures and therefore, SR-71 is built with a Titanium alloy frame. Advantage of such an airframe is its strength, which is comparable to that of stainless steel, but at the same time, it is light weight and durable at high temperatures. The disadvantage was its sensitive and brittle nature. To further enable the vehicle to withstand the excessive heat, it is coated with a special paint, consisting of billions of microscopic iron balls. Also, the SR-71 has a corrugated skin, which expands at higher altitudes due to heating. This helped the vehicle to handle the high thermal stresses that are developed. The tyres are impregnated with aluminum powder to withstand heat damage. Yet after landing, the vehicle had to be left to cool for over half an hour, before the ground crew could handle it.

2-1-3 Space Shuttle

The Space Shuttle, officially known as the Space Transportation System (STS), was a human spaceflight program carried out by NASA, which successfully transported Earth-to-orbit crew and cargo from 1981-2011, after which it was decommissioned. Also, it was the only winged, manned semi-reusable spacecraft to have achieved orbit and landing multiple times. The Russian Buran was very similar in design to the Space Shuttle, but it managed to make only one unmanned flight, before the program was cancelled. The Space Shuttle system consisted of an orbiter, two semi-reusable solid rocket boosters and a disposable external fuel tank. After completing its mission, the orbiter would re-enter the Earth's atmosphere

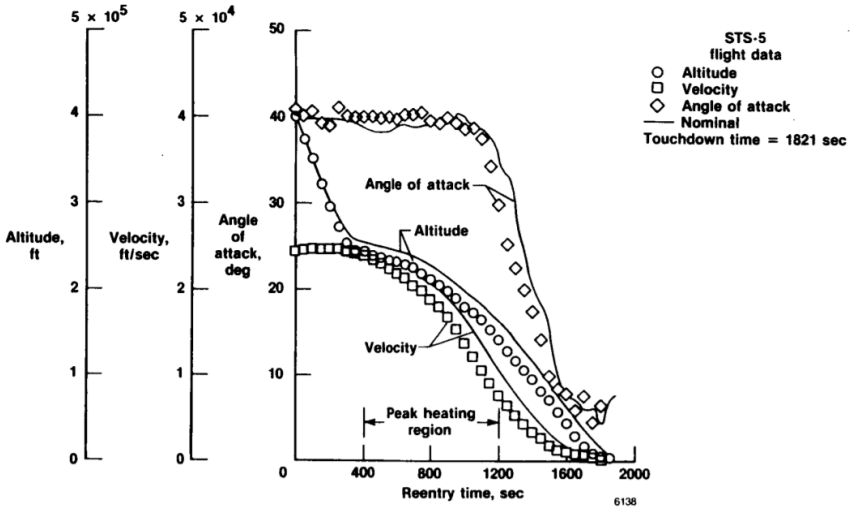

Figure 2-3: STS re-entry flight parameters (Gong et al., 1987).

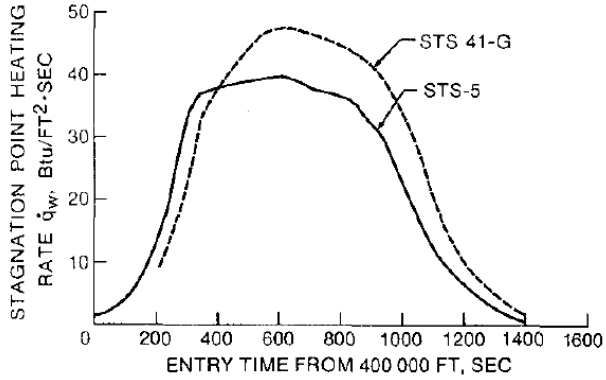

Figure 2-4: STS Stagnation-point heat flux during re-entry (Curry et al., 1986).

and glide back. The Space Shuttle TPS was composed of silica tiles.

The re-entry profile of a typical Space Shuttle can be seen in Figure 2-3. The re-entry begins at an altitude of 120 km, with a 40° angle of attack and entry velocity of 7.5 km/s. The peak heating region starts at an altitude of 75 km, lasts for roughly 800 secs, till the vehicle reaches an altitude of 45 km. During this period, the angle of attack remains roughly constant and reduces once the vehicle achieves an altitude of 45 km. In Figure 2-4, the stagnation point heat flux for the Space Shuttle trajectory can be seen. The heat flux shows little variation in the peak heating region and remains approximately constant at 432 kW/m^2, after which it gradually decreases till the vehicle lands. The Space Shuttle, being one of the few partial reusable vehicles, to have been flown, provides vital input to this study, in form of requirements and TPS technologies.

Passive TPS systems were used for the Space Shuttle. In Figure 2-5, the various materials used as TPS on different parts of the Space Shuttle, which experience varying heating, can be seen. The nose cap and wing leading edge of the Space Shuttle, experience the highest heat flux and dynamic pressure, are covered with Reinforced carbon-carbon (RCC) shell. The lower surface is made of high- temperature, reusable surface insulation (HRSI) tiles, whereas the control surfaces and part of the upper surface is covered with

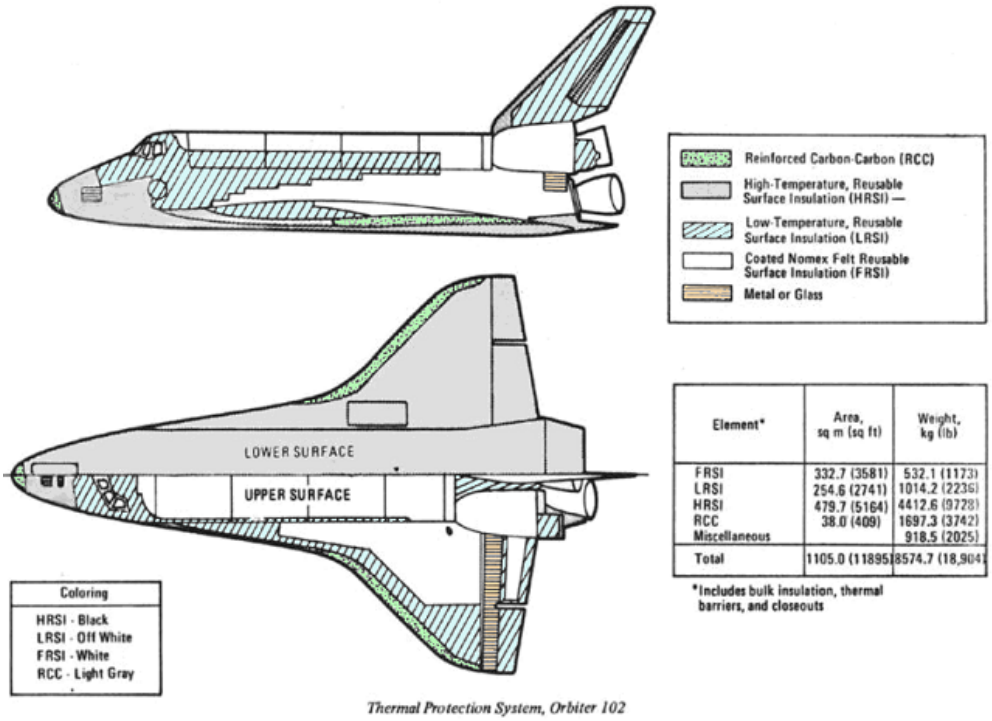

Figure 2-5: STS thermal protection systems (NASA).

low-temperature, reusable surface insulation (LRSI). Rest of the upper surface is coated with Nomex felt reusable surface insulation (FRSI). Most of the vehicle's outer surface area is covered by HRSI and FRSI.

2-1-4 X-33

The X-33 was designed as a prototype (approximately half scale) for a potential future RLV proposed by Lockheed Martin, called the Venture Star. NASA's wedge-shaped, sub-orbital X-33 vehicle was supposed to be a technology demonstrator providing useful information for development of the full-scale model, however, due to budget issues, it was cancelled before it could be built. The X-33 was designed to test unique aerospike engines, composite liquid hydrogen tanks and a metallic thermal protection system. (Jenkins et al., 2003). The vehicle was a lifting body design and was expected to have a seven day turnaround period between flights.

Test flight would involve launching the X-33 from a vertical position like a conventional space launch vehicle, to reduce weight of the landing gear and wheels such that it is only required to support empty mass of the vehicle (baseline dry mass 29,500 kg, compared to total mass 123,800 kg). The vehicle would be accelerated to a maximum speed of 4,500 m/s and reach altitudes up to 75-80 km, after which the engines would be shut down and the vehicle would glide over long distances up to 1,530 km, downrange of the launch site. Following this, terminal area energy maneuvers would be conducted to reduce speed and altitude; and finally the vehicle would land like a conventional airplane.

Stagnation heat load was about 193 kW/m2 (giving a temperature of 1165°C); windward it was just 35-45 kW/m^2 (650-700°C). There is no radius of curvature on the X-33 smaller than 12 inches (305 mm) because of thermal reasons. Figure 2-6 shows the expected heating (h is heat transfer coefficient and h_{FR} is the Fay-Riddell heating coefficient) along

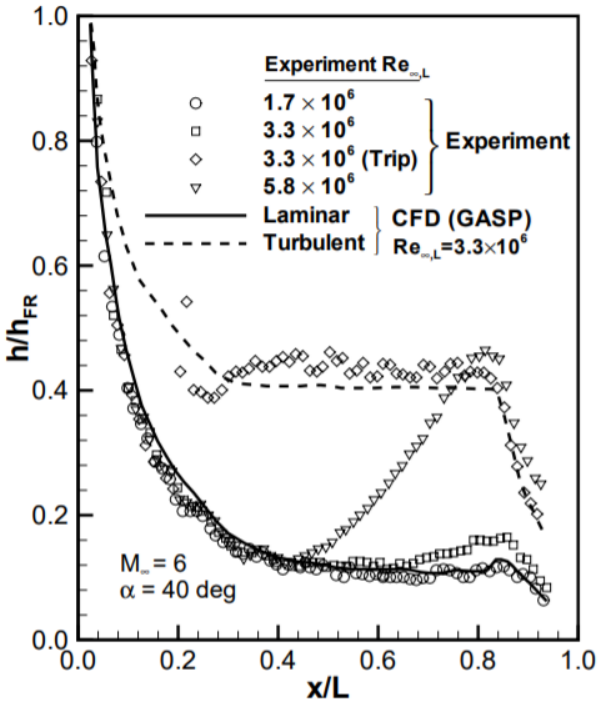

Figure 2-6: Predicted and measured heating for the X-33 vehicle along the windward centreline (Hollis et al., 2001).

the windward centreline of the vehicle, measured in wind tunnel tests and predicted through engineering models. To combat this heating, the TPS design proposed for X-33 can be seen in Figure 2-7. The metallic TPS panels proposed for the windward surface of the vehicle was a unique feature. These panels had varying sizes as per their location on the vehicle and to reduce the gaps and fillers between the panels, a herringbone pattern with overlapping edges was proposed (Hollis et al., 2001). The planned mission and proposed X-33 vehicle provided valuable insight for identifying the requirements of a flight test mission for testing hypersonic subsystems. Additionally, the use of metallic panels as TPS, proposed for this mission, provided a direction for designing future reusable TPS.

2-1-5 European eXPErimental Re-entry Test-bed (EXPERT)

Aim of the EXPERT vehicle was to acquire aerothermodynamic flight data which could be used to validate various tools and test facilities. One of its main goals was to test materials for ESA's Intermediate eXperimental Vehicle (IXV), an unmanned, delta-winged plane. Unfortunately, the EXPERT vehicle was not flown due to problems with the launcher availability. The vehicle's design is different as compared to other capsules, it is shaped like an elongated cone and is meant to be flown with the nose in front. The mission is to fly a sub-orbital trajectory and perform a ballistic entry into the Earth's atmosphere. As per the trajectory design, the vehicle is predicted to have an initial re-entry velocity and flight-path angle of 5 km/s and -5.5°, respectively at an altitude of 100 km. The expected maximum heat flux was 1.7 MW/m^2. The maximum temperature at stagnation point was expected to reach 2000°C. In Figure 2-8, the variation of heat flux and dynamic pressure over time in the stagnation region can be seen. The different TPS types are used for different regions on the vehicle, C/SiC for the nose, an metallic shell (PM1000) for the conical and flat surfaces,

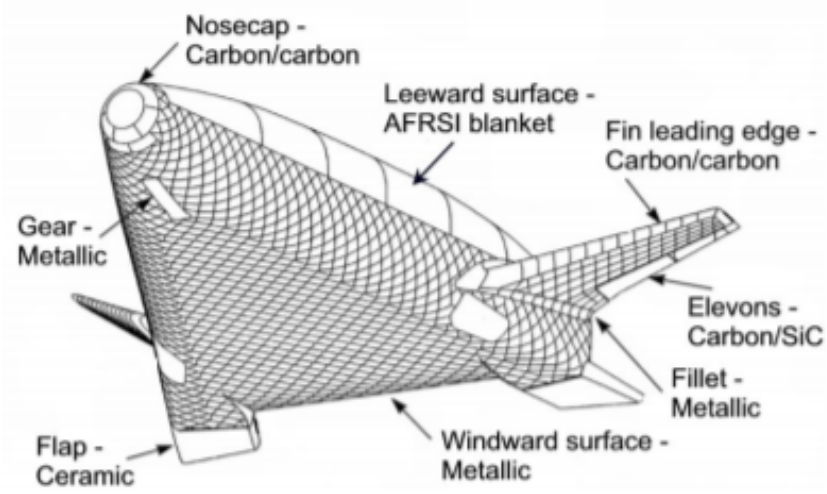

Figure 2-7: TPS material design for the X-33 (Hollis et al., 2001).

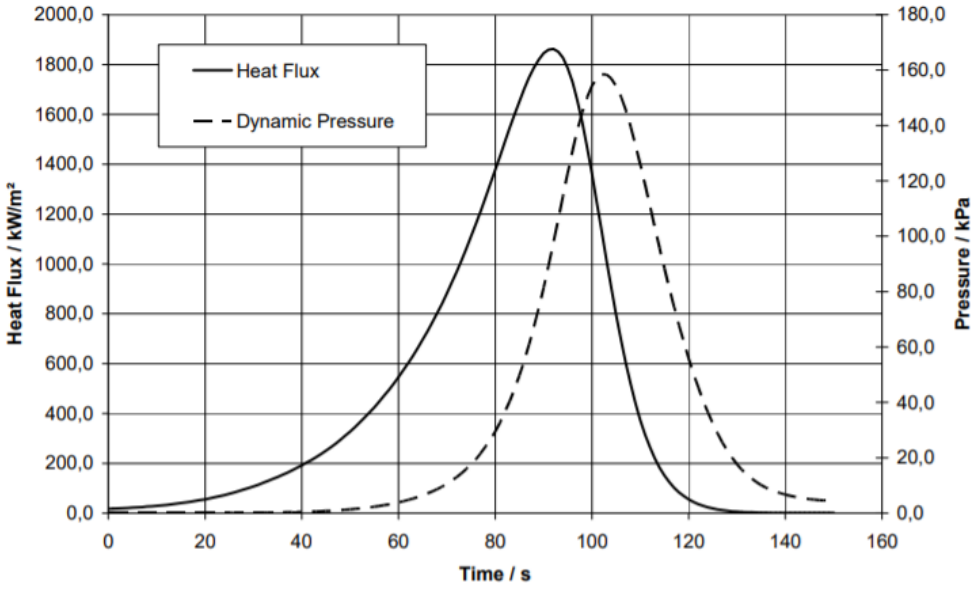

Figure 2-8: Heat flux and dynamic pressure variation for the EXPERT vehicle nose over time (Reimer et al., 2009).

and ceramic for the flaps (Ratti et al., 2009).

This vehicle and mission are interesting to this work, for many reasons, of which the main one is that an active cooling system is to be carried as payload for flight testing its performance. A small enhanced radiation cooling experiment is installed in the forward part of one of the flat panels and has an circular exposed diameter of 100 mm, as can be seen in Figure 2-9 (Sudmeijer, 2005). The experiment consists of an integrally machined container made of PM1000, with the porous water absorbed material inside, as is seen in Figure 2-10. The evaporated water vapour leaves the container in the centre and is exhausted through pipes to the vehicle's base in order to avoid contamination of the boundary layer. Thermocouples are used to measure the temperature of the outer skin of the experiment, the surface of the porous material and the exhaust vapour (Sudmeijer, 2005).

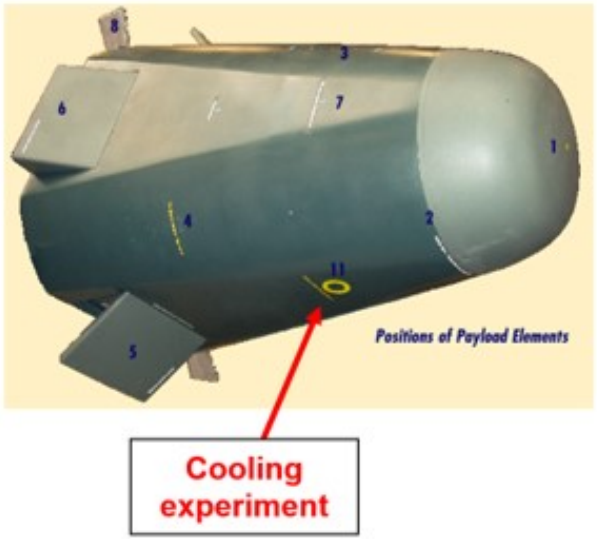

Figure 2-9: Location of the active cooling experiment on the vehicle (Sudmeijer, 2005).

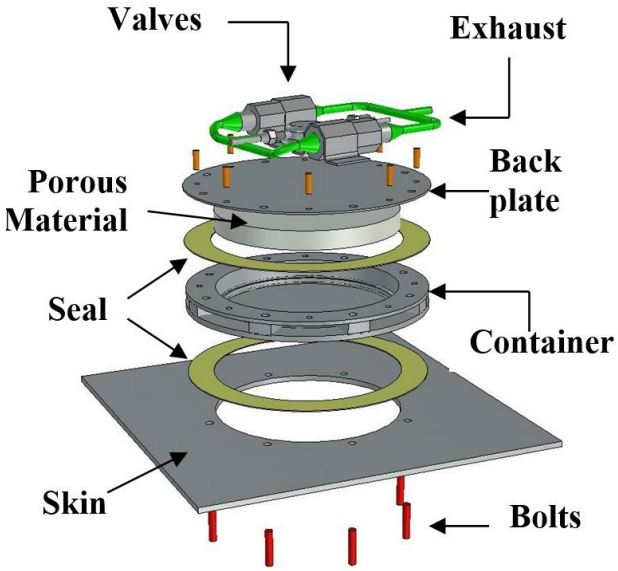

Figure 2-10: Enhanced radiation cooling experiment fitted on-board the EXPERT vehicle (Sudmeijer, 2005).

2-1-6 FESTIP

From 1994 to 1998, European Space Agency (ESA) conducted the Future European Space Transportation Investigations Program (FESTIP), with the objective to identify promising concepts and technologies that are needed to reduce the cost of going to space. A variety of system concepts were investigated, 8 of which, were finally chosen for a detailed design study. These included various SSTO/ TSTO vehicle configurations, with horizontal/ vertical launch capabilities, reusable and semi-reusable systems, winged and lifting bodies. Among many, some of the main selection criteria were technical feasibility and commercial applicability (considering various factors such as mass efficiency and cost savings) of a concept (Dujarric, 1999). The sub-orbital hopper (concept 15) and the semi-reusable TSTO (concept 16) seemed within Europe's technical reach and were further analysed during the Future Launchers Technologies Programme (FLTP) (Dujarric, 1999). This program provided de-

tailed insight for designing a hypersonic mission. The methodology used for identifying different design concepts along with the analysis and shortlisting of these designs, is very useful for developing future technologies.

2-2 Present

Some of the latest RLV projects will be discussed in this section. Studying the latest RLV missions, vehicles and technologies is important, because it helps identify the current and future technology development trend. Most of the projects today are aimed at reusability and improving the system technologies for a hypersonic flight. Sub-orbital experimental vehicles are being developed to perform in-flight tests of various sub-systems such as the guidance, navigation and control system and thermal protection system. Many current projects were reviewed, three of which - namely, the German SHarp Edge Flight EXperiment (SHEFEX), SpaceLiner and India's Reusable Launch Vehicle-Technology Demonstrator (RLV-TD)- were found relevant to this research and will be discussed in this section.

2-2-1 SHarp Edge Flight EXperiment (SHEFEX)

German Aerospace Center's (DLR) program, known as SHEFEX, is a platform for testing various re-entry experiments. Till date, the program has successfully performed two sub-orbital re-entry flight experiments, the SHEFEX I, launched in 2005, and SHEFEX II, launched in 2012. Both vehicles were launched vertically with the use of a rocket.

One important and interesting SHEFEX II experiment was the AKTiV (Aktive Kühlung durch Transpiration im Versuch) transpiration-cooled experiment. For this experiment, a tile of the TPS system was replaced by a porous tile made of permeable C/C-SiC, which was cooled down by nitrogen passing through the porous sample. In-flight measurement showed a significant cooling effect where the C/C-SiC tile was used in comparison to a similar surface without the permeable tile (Böhrk, 2015).

To further advance the technological evolution, SHEFEX III (a high-lift vehicle) is planned to perform a suborbital re-entry with an entry velocity of 4800 m/s at Mach 17 at 100 km altitude (Dittert et al., 2015). As a result of the much higher re-entry velocity, the expected heat load will be much higher compared to SHEFEX II. The stagnation point heat flux and heat flux on the windward side of the vehicle at three different points behind the nose, is seen in Figure 2-12 (a). Also, the pressure variation on the SHEFEX III vehicle along the trajectory, is seen in Figure 2-12 (b). The maximum pressure of 60 kPa and a corresponding maximum heat flux of 10 MW/m^2 is experienced at the stagnation point during re-entry. The peak heat flux at the stagnation point is very high, however, the thermal gradient is relatively gradual during descent.

2-2-2 SpaceLiner

Since 2005, the Space Launcher System Analysis (SART) department at the German Aerospace Center (DLR) has been working on a hypersonic spaceplane concept, known as SpaceLiner. The aim of this concept is passenger transportation over ultra-long distance, i.e., to fly from Australia to Europe in 1.5 hours (Foreest et al., 2009). It is designed for a vertical launch by means of two rocket powered stages. After engine burnout, the remaining part of the flight is a powerless skip trajectory. Such a skip trajectory introduces extremely high heat loads on the vehicle. To illustrate this, Foreest et al. (2009) compares the trajectory flown

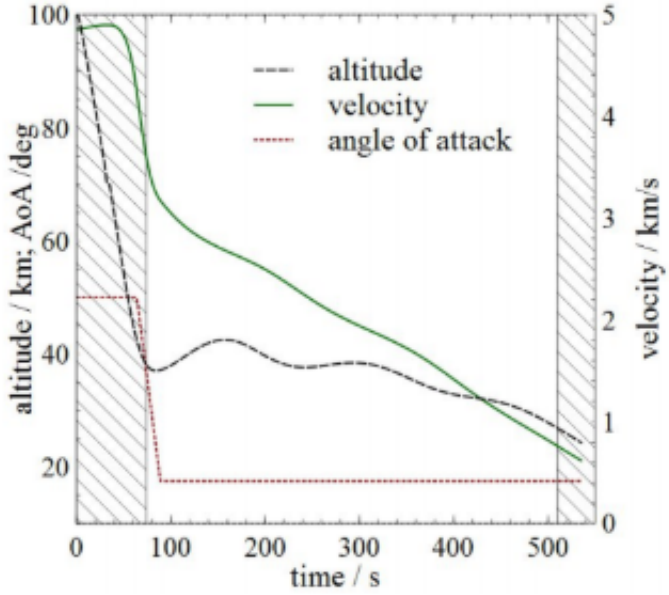

Figure 2-11: SHEFEX III trajectory design (Dittert et al., 2015).

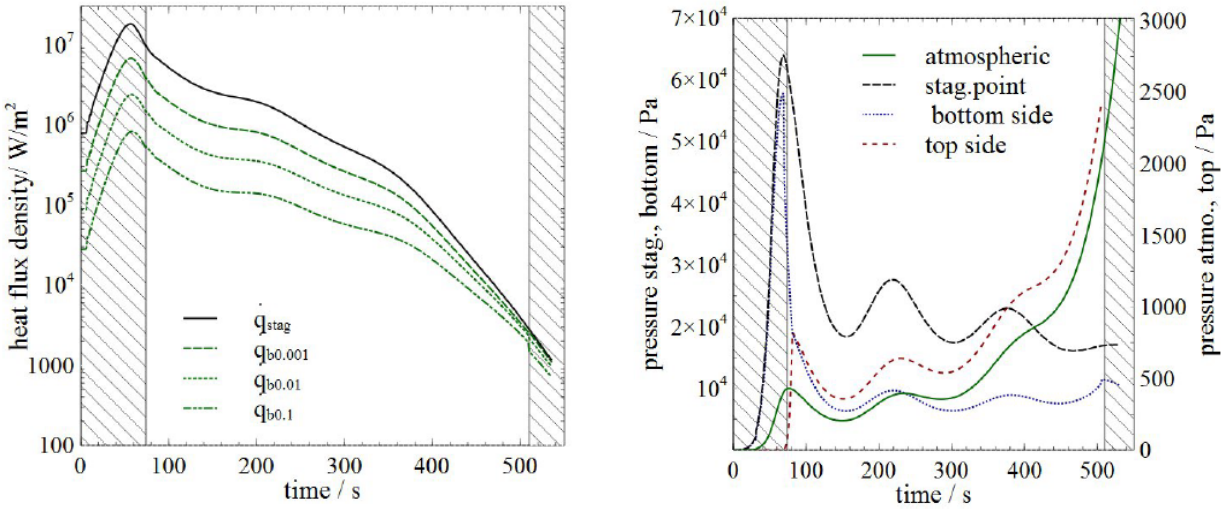

(a) (b)

Figure 2-12: (a)Heat flux predicted for stagnation point and bottom side and (b)Pressure distribution and atmospheric pressure variation for SHEFEX III (Dittert et al., 2015).

by the SpaceLiner to the re-entry trajectory of the Space Shuttle (as seen in Figure 2-13). From this comparison, it is clear that the SpaceLiner flies in approximately the same speed regime, but at lower altitudes. This means that heat loads on the SpaceLiner will be more severe as compared to the Shuttle.

Analysis has showed that temperatures at leading edge and nose will be approximately 1000K higher (Foreest et al., 2009). As can be seen in Figure 2-14, the nose and leading edges have the highest maximum surface temperature. The dynamic pressure is around 2,500 N/m^2 and the heat rate for a leading edge with a radius of 0.1 m would be 2,200 kW/m^2

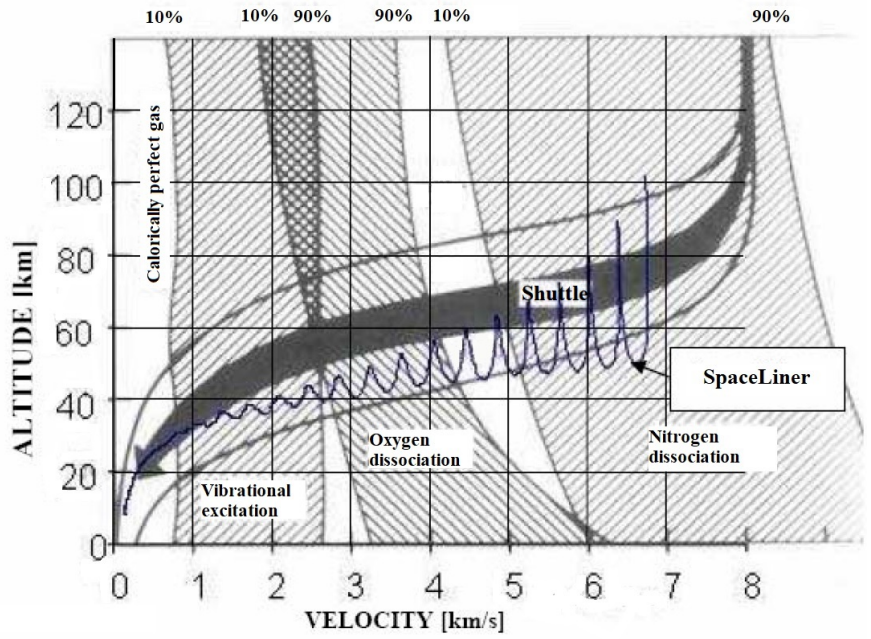

Figure 2-13: SpaceLiner skip trajectory vs. Shuttle re-entry (van Foreest et al., 2007).

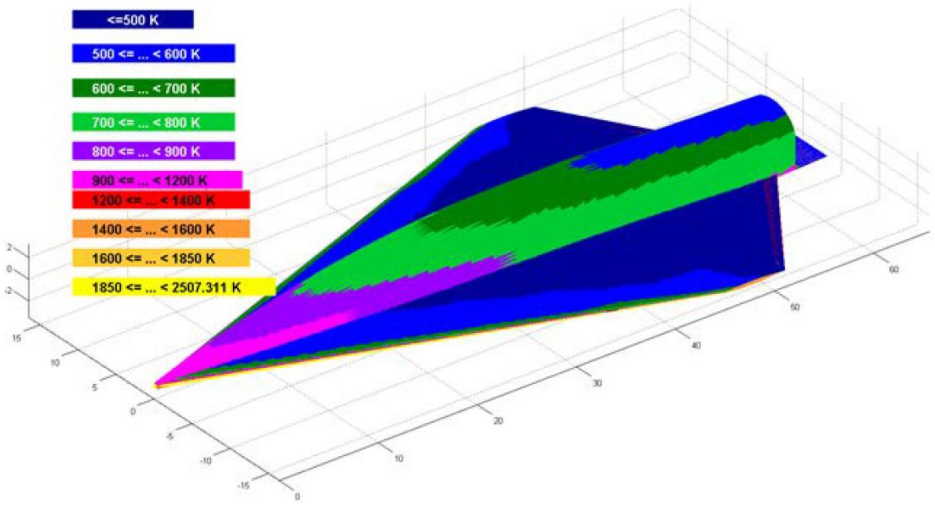

Figure 2-14: Overall maximum surface temperature areas reached on the upper side of SpaceLiner (Sippel, 2015).

(Sippel, 2015). Aerodynamic performance has been given higher importance and therefore, methods have been developed to tackle the high thermal loads. Foreest et al. (2009) proposed an active cooling system, known as transpiration cooling. Various wind tunnel experiments were performed using different coolants and water was found to be the most suitable coolant. This vehicle concept is still undergoing development and in-flight experiments are yet required to test the proposed TPS system.

Besides the overall promising results, some technical challenges of the active transpiration cooling system have been detected in the FAST20XX-investigations (Sippel et al., 2011). Precise controllability of the water flow through the porous ceramic media has been found difficult (Schwanekamp et al., 2015). The vehicle would require a more sophisticated coolant supply system when in flight and real flight conditions are usually more complex

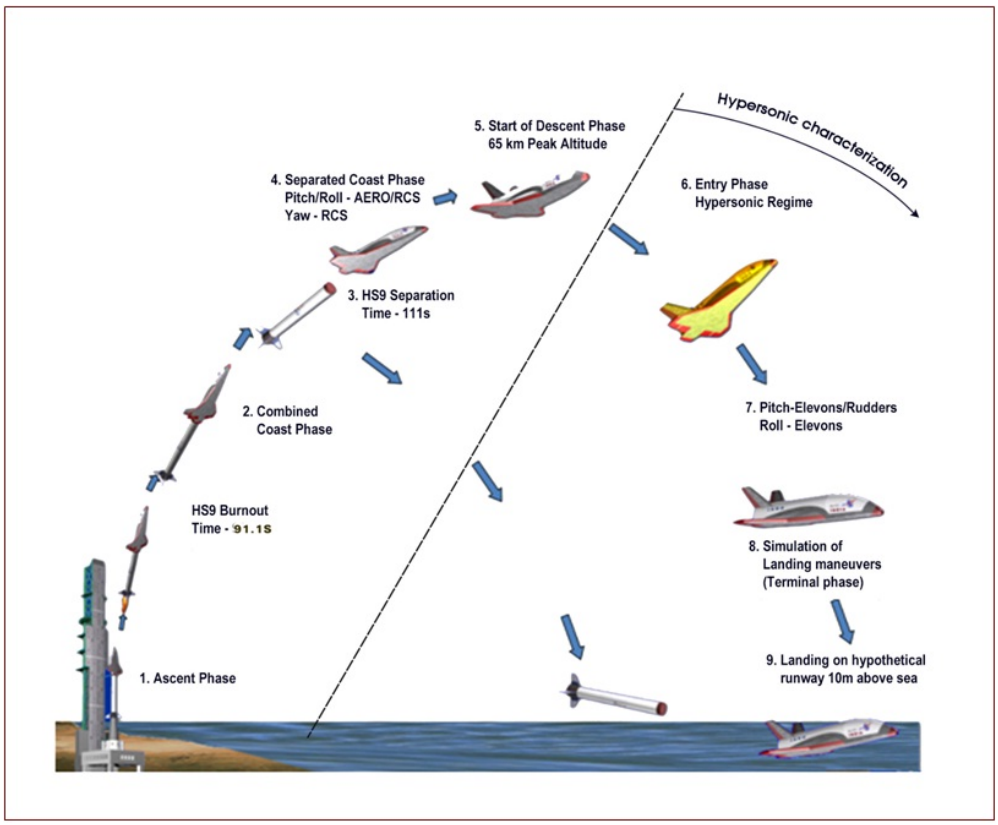

Figure 2-15: Mission profile of RLV-TD (ISRO).

and demanding, as compared to those in a laboratory. Early boundary layer transition due to injection of coolant into the boundary layer is predicted, which will require additional reinforcement for certain areas on the vehicle. Therefore, transpiration cooling is a reference design at this point, and better active cooling concepts are being researched (Schwanekamp, 2014). In the coming years, a more detailed system assessment of the different design choices will be performed (Sippel, 2015). The application of this vehicle concept is similar to the current work and the cooling system proposed for this vehicle, was a starting point for the conceptual TPS design in this work.

2-2-3 Reusable Launch Vehicle-Technology Demonstrator (RLV-TD)

Indian Space Research Organisation (ISRO) took its first step towards developing a fully reusable launch vehicle to enable low cost access to space. The RLV-TD is a winged vehicle developed to act as a flying test bed for conducting the hypersonic aerothermodynamic characterisation of wing body, evaluating the autonomous navigation, guidance and control (NGC) schemes and the TPS. A first prototype of the RLV-TD performed a successful sub-orbital flight in May, 2016. The vehicle was launched vertically to Mach 5 by a conventional solid booster (HS9) designed for low burn rate. As can be seen in Figure 2-15, the vehicle reached an altitude of 65 km, after which it performed a gliding entry using aerodynamic lift and landed 450 km away from the launch site. In the future, this vehicle will be scaled up to become the first stage of India's reusable two stage orbital launch vehicle

In Figure 2-16, the various materials used for the vehicle's TPS and the cold wall heat flux at different parts of the vehicle can be seen. As per this figure, the nose cap, wing leading

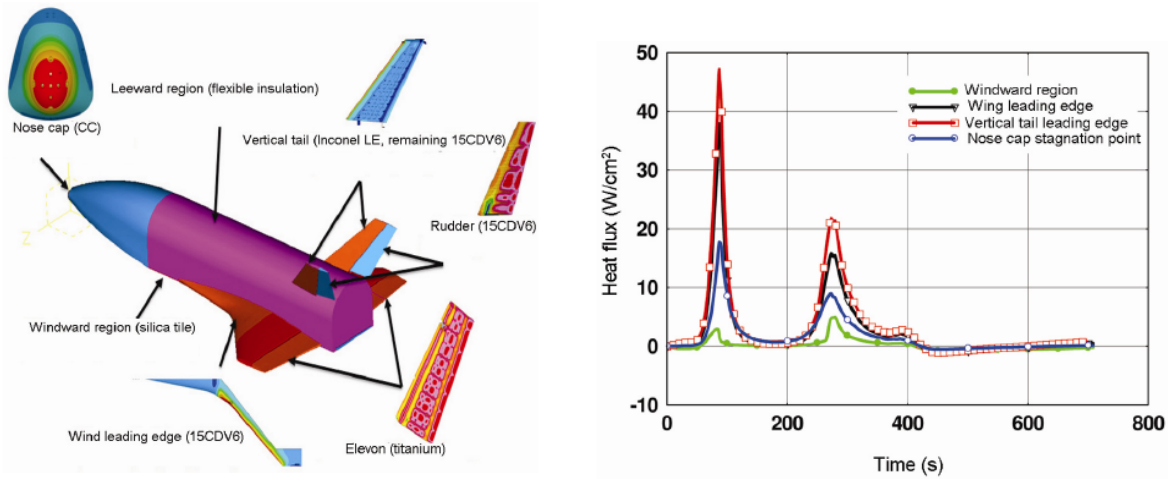

(a) (b)

Figure 2-16: (a) Various structures and (b) Cold wall heat flux estimated at various locations of RLV-TD (Sivamurugan et al., 2018).

Table 2-1: Past and present RLV mission/ vehicles.

Vehicle	**Sub-orbital/ Orbital**	**Take-off/ Landing**	**Stages**	**Propulsion system**
X-20	Sub-orbital/ Orbital	VTHL	Two stage	Rocket engine
SR-71	Sub-orbital	HTHL	Single stage	Air-breathing engine
Space Shuttle	Orbital	VTHL	Two stage	Rocket engine
X-33	Sub-orbital	VTHL	Single stage	Rocket engine
EXPERT	Sub-orbital	VTHL	Two stage	–
FESTIP	Sub-orbital	HTHL	Single/ two stage	Rocket engine
SHEFEX	Sub-orbital	VTHL	Two stage	–
Spaceliner	Sub-orbtital	VTHL	Two stage	Rocket engine
RLV-TD	Sub-orbital	VTHL	Two stage	Rocket engine

edge, elevon, vertical tail and rudder is designed as a hot structure, i.e. these structures can withstand structural load at higher temperatures as well. For windward and leeward regions, TPS like silica tiles and flexible insulation is used. The Carbon–carbon nose cap is attached with an aluminium alloy ring through molybdenum bracket, molybdenum bolt and molybdenum nut. This dissimilar metal joint was tested in a 9MW plasma wind tunnel, total heat load was simulated and it was found that the joints withstood the load. The specimen qualified for 900 kW/m^2 heat flux for 30 s duration (Sivamurugan et al., 2018).

2-3 Future

Based on the past and present RLV missions and vehicles, the future of RLVs can be predicted. As is seen in Table 2-1, the vehicles can be classified into various categories, based on the type of propulsion, the number of stages, the launch and landing orientation and the flight regime. A choice made in each of these categories has a significant impact on the design of a vehicle, as is already seen in the previous sections.

Having only one stage means no assembly of stages is required, saving time, crew and

facilities on the ground. Furthermore, only one vehicle needs to be developed, parked and flown. Although this single-stage airplane-like vehicle seems ideal, experience has shown that developing such a vehicle is extremely difficult. The lack of technology readiness is also why the FESTIP study did not include air-breathing SSTO concepts (Dujarric, 1999). Furthermore, with TSTO configurations, the vehicle that finally goes into orbit is smaller. This helps in reduction of fuel consumption and can result in a larger payload capacity. TSTO concepts like SpaceCab and SpaceLiner could thus be interesting configurations for the near future. Meanwhile, experience with these concepts could pave the way towards SSTO concepts in the future.

Rocket engines have been the major propulsion method for spacecraft up to now. With the prospect of SSTO concepts in mind, air-breathing engines will become more important. Air-breathing engines have the advantage of using oxygen from the air, thereby reducing the required fuel mass on board. In addition, they have a higher specific impulse in the lower Mach number range than rocket engines (Kors, 1990). The need for rocket engines will still exist, for final insertion and manoeuvrability in space, since air-breathing engines do not work outside the atmosphere. It is not always recommended to use both engines, because it could have a negative impact on the weight and size of the vehicle, nullifying the positive impact of reduced fuel mass. Nonetheless, such an engine combination was proposed for NASP.

Air-breathing SSTO concepts were eliminated during FESTIP on the grounds of technological difficulty. The X-30 was an example of such a challenge. Concepts using existing/ planned commercial aircraft to carry an upper stage, as seen in the X-15 vehicle, are not tolerant to performance requirement changes, because the carrier aircraft introduces a limitation and constrains launcher performance growth potential. Also, the thermal loads on a vehicle powered by an air-breathing engine, during the ascent phase is very high.

The hope is that HTHL vehicles can be operated similar to an aircraft, resulting in a number of advantages like: no extra costs for launch facilities, faster turn-around time and lower launch costs. However, HTHL launch vehicles weigh approximately 4 times more during take-off than landing due to the large propulsion mass fraction (Dissel et al., 2006). Nonetheless, the final goal for manned RLVs in the future would be to take-off horizontally. Also, horizontal landing requires less or no thrust while vertical landing comes with considerable safety issues including possible engine failure on landing (Ashford, 2002). A combination of horizontal take-off and horizontal landing, thus seems to be a most promising configuration.

2-4 Reference mission

The previous sections have explained the evolution of space-plane missions throughout the last decades. This resulted in the definition of the most promising configuration for the future. Based on these observations a reference mission is selected in this section. Plus, a set of mission requirements are defined in Section 2-4-1.

The most promising RLV design is found to have the following configuration:

- The vehicle shall perform a sub-orbital flight, this will help gather sufficient in-flight data, before an orbital flight can be attempted.

- A vertical take-off and horizontal landing vehicle design has been successful in the past, however, a HTHL will be the final goal for a future RLV.

Table 2-2: Major activities carried out in OAE and SOH mission (Vollmer, 1992).

Mission Type	OAE	SOH
Inject into	sub-orbital	sub-orbital
Drift to/ Culminate to	$\approx$ 150 km	$\approx$ 150 km
Circularise in LEO	No	No
Wait & phase in LEO	No	No
Deploy cargo at	130 km	130 km
Orient for de-boost	No	No
De-boost	No	No
Re-orient for re-entry	No	No
Re-enter	Yes	Yes
Glide to/ Land at	Launch site	Downrange landing site
OMS/ RCS required	No/yes	No/yes
MECO velocity deficit	$\approx$ 87 m/s	$\approx$ 2300 m/s
Exospheric time slot	$\approx$ 25 minutes	$\approx$ 3 minutes
Duration of flight mission nominal	$\approx$ 2hours	$\approx$ 25 minutes
Duration of contingency mission	$>$2.5 hours	$\approx$ 30 minutes
Downrange	1 x around Earth	Transatlantic ($\approx$ 4500 km)
Cross-range	$\approx$ 3000 km	$\approx$ 700 km

- A SSTO RLV is desired in the future, but will require technology development.
- Air-breathing SSTO vehicle is a desired configuration, however, it is not feasible with the current engine technology. So in the meantime, focus is still on rocket powered SSTO vehicles.

Keeping these objectives in mind, the various missions/ vehicles, as seen in Table 2-1 were compared. The FESTIP concept 15 was found to be a suitable reference mission for this study, as it meets most of the objectives discussed above.

There were two main missions proposed under this concept namely, Once-Around Earth (OAE) and Sub-Orbital Hopper (SOH). Both were a rocket engine powered, winged SSTO vehicle, with a horizontal take-off and landing mission, launched by a rail guide, to follow a sub-orbital elliptical trajectory and deliver the cargo to a specified altitude, followed by an unpowered gliding entry into the Earth's atmosphere. Main difference between the two missions was that the OAE mission, as the name suggests, had to glide around the Earth to land on the launch site itself, whereas the SOH mission would glide partly around Earth and land on a downrange landing site. Due to the difference in flight range, the total integral heat load acting on the vehicle flying the OAE mission is much higher. The once-around or half-around variants are nearly the same size and involve the same technological challenge as the fully orbital SSTO. Consequently, they can be considered as particular operating modes of a full SSTO concept, offering increased performance capabilities.

For this study, the OAE mission is selected as the reference mission. The nominal trajectory of this mission is compared with that of Space Shuttle and Buran in Figure 2-17 by Marini (2001). The FSSC-15-OAE follows, for most of its ascent, the theoretical high lift path, while the winged re-entry is similar to that of Space Shuttle and Buran. At higher altitudes the vehicle experiences low Reynolds number conditions at large Mach numbers, thus enhancing viscous effects, while transition occurs at lower altitudes and Mach numbers (transition Reynolds number is conventionally assumed to be $\mathrm{Re}_t \approx 10^6$). Such a flight path

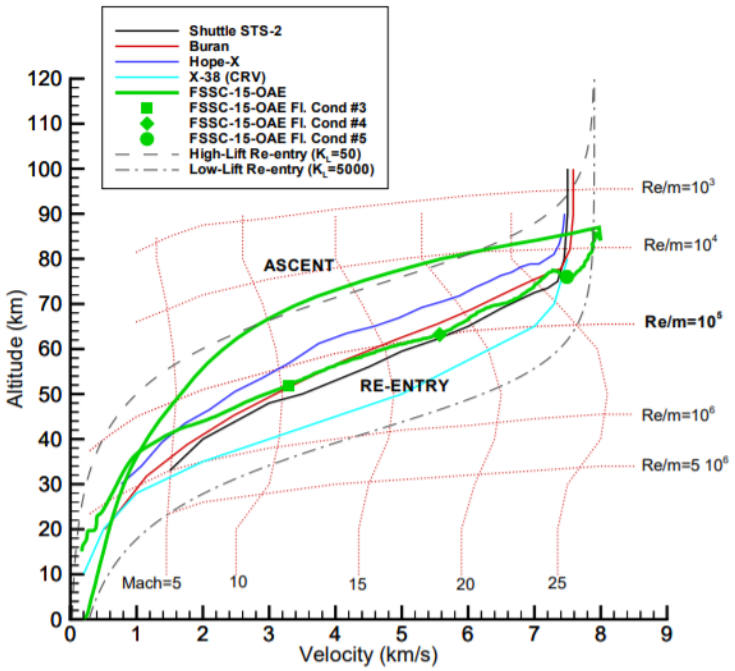

Figure 2-17: Comparison of the FSS-15 (OAE) trajectory with other missions (Marini, 2001).

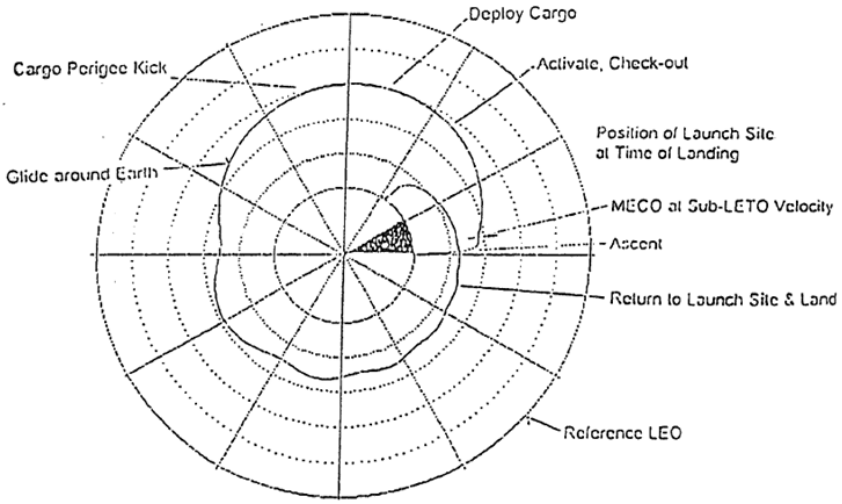

Figure 2-18: Mission profile for FSS-15 (OAE) (Vollmer, 1992).

is an interesting thermal challenge to study and is in line with the goal of this work. The mission profile for the OAE can be seen in Figure 2-18 and nominal trajectory parameters are given in Figure 2-19. The engine was to cut-off at an altitude of 100 km, after which the trajectory would culminate at 150 km. The cargo would be ejected at 130 km. The temperature profile along the windward centreline of FSSC-15 OAE is as seen in Figure 2-20 and is estimated assuming a fully catalytic wall. The maximum heat flux and integrated heat load are 500 kW/m^2 and 850 MJ/m^2.

It must be noted that air-breathing SSTO vehicles have the most demanding thermal design during ascent phase. The selected mission, even though it is a SSTO mission, is a

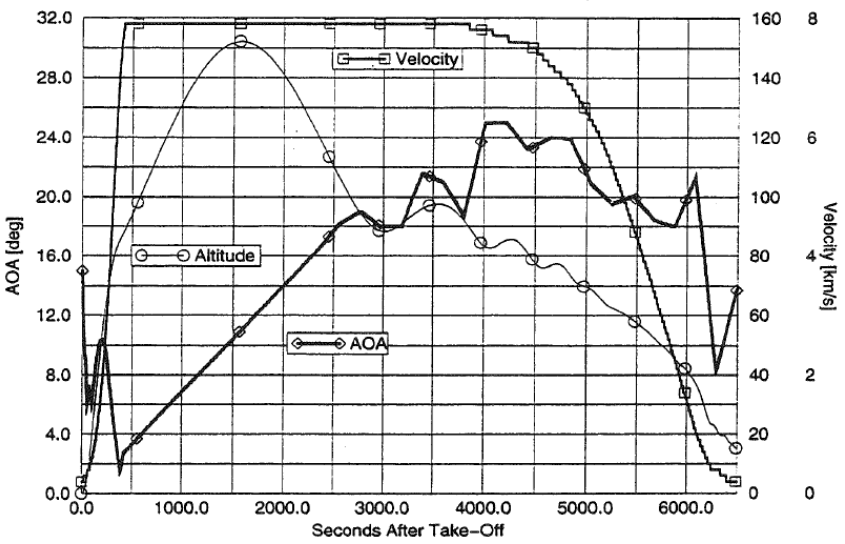

Figure 2-19: Nominal trajectory for FSS-15 (OAE) (Vollmer, 1992).

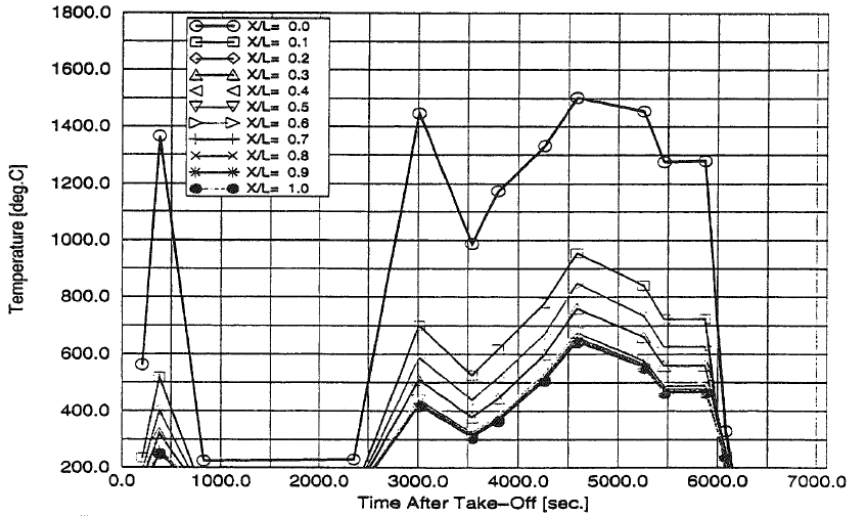

Figure 2-20: Temperature profile on windward centreline of FSS-15 (OAE) (Vollmer, 1992).

rocket powered launch and the thermal design during the long range glide entry is more demanding. Therefore, in this study, the focus of the TPS design will be on the stagnation point and total heat load (per unit area) experienced during the re-entry phase into the Earth's atmosphere. In addition, the reference mission is a sub-orbital flight, the entry velocity lies between 7-8 km/s and the flight-path angle is small (given a gliding entry).

2-4-1 Mission Requirements

For raising the TRL of any promising technology, in this case the TPS to be designed, in-flight experiments must be performed. Based on the mission concepts discussed and for the chosen reference mission i.e., FSSC-15-OAE, certain mission requirements can be identified, that form an important consideration for selection of a suitable test vehicle and the TPS design. These requirements define the expected mission profile and are as seen in Table 2-3. MR01 and MR02 suggest the design of a long range mission, like the selected reference mission, extending experimental time as far as possible. MR04 is identified to closer define

the experimental vehicle. MR01, MR02, MR04 and MR05 were defined because they point the vehicle design in a specific direction, based on the survey of past and present RLVs. MR06 is a direct requirement derived from the reference mission.

Table 2-3: Mission requirements.

MR01	The trajectory shall ensure a sub-orbital flight with a gliding entry.
MR02	The landing site shall be within 100 km from the launch site.
MR03	The descent shall begin at 120 km with an entry velocity in the range of 2500 m/s $<V<$4500 m/s and flight-path angle of -10°.
MR04	A constant Mach number ($\geq$ 10) shall be maintained for at the least a time period of 30 s, along with a variable Re (5e5 $<Re<$2e6).
MR05	The heat flux during the constant Mach flight period shall lie in the range of 1 MW/m^2 $< \dot{q} <$2 MW/m^2 and not exceed 2 MW/m^2 during the entire flight.
MR06	The integrated heat load shall not exceed a maximum value of 850 MJ/m^2.

2-5 Test vehicle

To successfully design and implement the reference mission selected in the previous section, every system must be tested and the engineering tools must be validated. This requires experimental data which can be obtained by performing test flights. As is seen in most past and present missions, scaled down experimental vehicles are built first, to perform in-flight experiments and gather sufficient data. Wind tunnel testing is not enough in case of hypersonic flights. Therefore, to test the TPS that is designed in this research, a vehicle must be selected for experimentation. This vehicle must satisfy the mission requirements identified in the previous section. In addition, sufficient data with respect to the vehicle and its design must be available.

The Hyperion is a small low-cost re-entry vehicle that is being used at Delft University of Technology (TU Delft) in the Netherlands, for conducting various studies. Hyperion-I and II have been officially designed over the years for varying performance and characteristics. A total of 27 sub-class designs of the same shape (small nose radius) as the Hyperion-II, with some different geometrical parameters that lead to a variation in aerodynamic characteristics, having a nominal mass of 250 kg were analysed by Mooij et al. (1999). Out of these, design 5 was found to have a maximum aerodynamic performance $L/D_{max} = 2.21$. A visualisation of the geometry of Hyperion-II vehicle (design 5) is shown in Figure 2-21.

For this vehicle, Dijkstra (2012) proposed an optimal re-entry trajectory to obtain aerothermodynamic data in hypersonic flight regime. Two flight missions were studied, a constant Mach number flight and a levelled flight. Each mission had its own advantages and disadvantages as discussed by Dijkstra (2012). Various constraints were applied, one of them being that the maximum heat flux should be limited to 5 MW/m^2. Although, the levelled flight mission is safer in terms of heat load (seen in Figure 2-22), the constant Mach number flight with a large Reynolds sweep is very attractive for obtaining aerothermodynamic data in the boundary layer transition flow region (Dijkstra, 2012). Therefore, it is a preferred mission profile. The same Hyperion – II design has been selected as the test vehicle for this study, because it satisfies the mission requirements identified in the previous section. Also, since it is an in-house project, all relevant data for the vehicle is readily available.

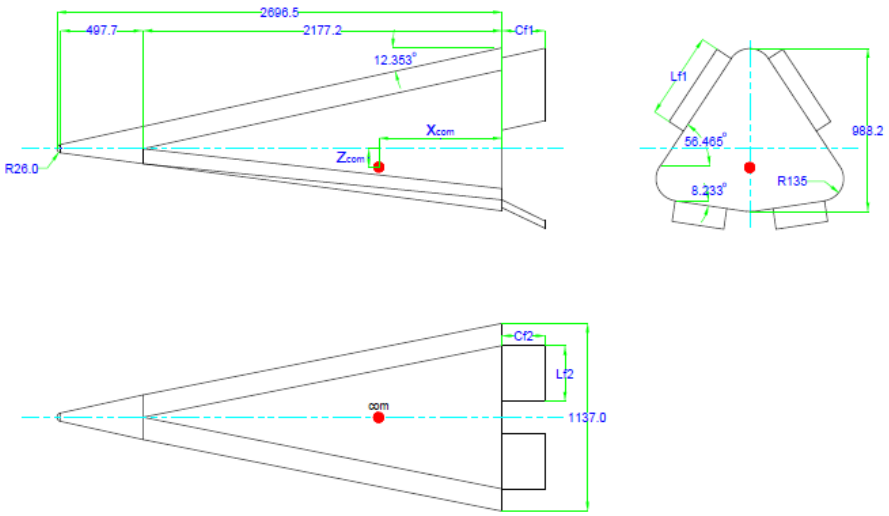

Figure 2-21: Hyperion-II design 5 geometry, as drawn by Dijkstra (2012).

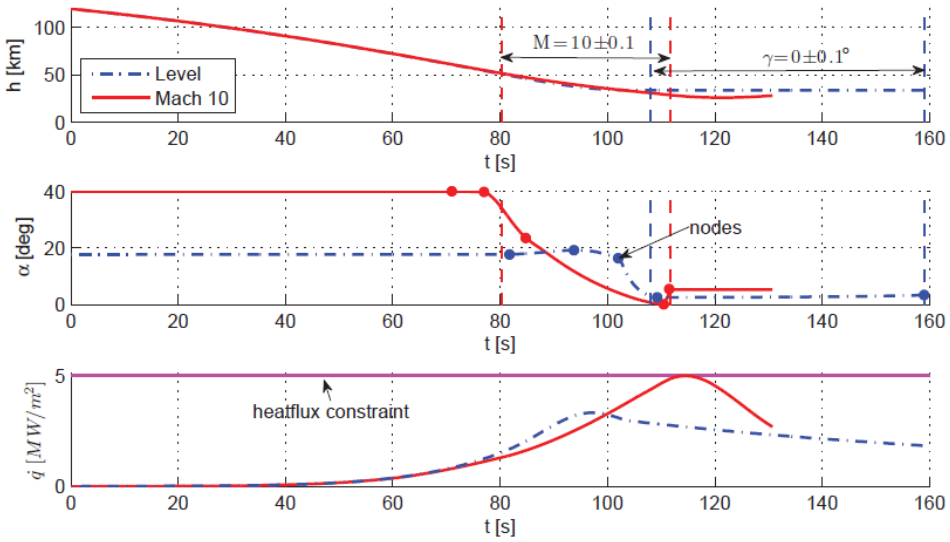

Figure 2-22: Hyperion-II optimal trajectory parameters Dijkstra et al. (2013).

2-5-1 System Requirements

The system requirements that shall be met are specified below. These are not the complete set of requirements for such a vehicle, but are the most relevant requirements chosen for this thesis. These requirements have been set to ensure that the vehicle experiences a range of high heat flux for a substantial time period, as the reference mission is a long range flight. These requirements define the expected capabilities and performance of the vehicle, based on the reference mission. They are given in Table 2-4. SR01 is derived directly from the mission requirement. SR02 has been set to ensure that the vehicle meets the future goal of a manned mission. SR04 is a necessary requirement to ensure MR04 is satisfied. SR06, SR07 and SR08 have been identified from past RLV missions.

Table 2-4: System requirements.

SR01	The vehicle shall perform an unpowered, gliding entry into the Earth's atmosphere.
SR02	The vehicle shall not exceed a maximum acceleration of 2g.
SR03	The vehicle shall be designed to ensure reliability and reusability. It shall have the ability to perform 10 flights at least, with minimum maintenance.
SR04	The vehicle shall have suitable guidance and control to ensure a constant Mach number flight for at the least a time period of 30 s. (If needed, it shall perform a pull up manoeuvre.)
SR05	The vehicle shall have a high L/D ratio (>2).
SR06	The maximum temperature of the nose and leading edges shall not exceed 2000 K.
SR07	The maximum temperature of the internal structure shall not exceed 300 K.
SR08	The maximum pressure at the stagnation point on the vehicle shall not exceed 60 kPa.

2-6 Nominal trajectory

A nominal trajectory is required in this study, to analyse the performance of the proposed TPS design. It is important to note the trajectory used in this work is not obtained by conventional methods. Only the vehicle's mass, nose radius and L/D ratio is considered, and it is assumed that the vehicle has the required guidance and control capabilities, to fly along this path. This is an acceptable assumption for this study, as trajectory design is out of the scope of work. Also, to analyse the thermal performance of a TPS system at such a preliminary level, an approximate estimation of the stagnation heat flux is sufficient.

A very simple analytical approach is used to obtain a nominal trajectory. The objective of the nominal trajectory is to include both aspects, minimum heat load (to ensure minimum TPS mass) and maximum range (to allow maximum manouverability). However, both these objectives cannot be fully satisfied because they are counterproductive. Optimal solution is not the aim for a nominal mission, therefore, an approximate solution is applied to obtain an acceptable compromise between the two objectives. The nominal trajectory is designed such that the vehicle flies along the maximum heat flux constraint for the maximum possible time period, to reduce the total heat load as flight time is the shortest. To enable this flight, the vehicle is expected to sufficient bank angle control. The vehicle begins its re-entry with a maximum angle of attack, to reduce the peak heat load in the initial phase and then gradually reduces the angle. To avoid very large mechanical loads, after a certain point the vehicle is made to fly along the g-load constraint.

The constraints for heat load and g-load, along with entry conditions are obtained from the requirements. Other data such as vehicle mass, nose radius and L/D ratio is known for the chosen test vehicle. Using these values, the Chapman's (cold wall) equation for heat load constraint (Equation (2-1)) and the equation for g-load constraint (Equation (2-2)) are solved simultaneously. The values for C_L and C_D are assumed to be independent of Mach number. These equations are solved using the values given in Table 2-5 and as plotted in Figure 2-23.

$$q = \frac{c_1}{\sqrt{R_N}} \sqrt{\frac{\rho}{\rho_0}} \left(\frac{V}{V_c} \right)^{c_2} \tag{2-1}$$

Table 2-5: Parameter setting for nominal trajectory

Parameter	Value
R_N (mm)	26
L/D	2.21
ρ_0 (kg/m^3)	1.225
V_c (m/s)	7905
c_1 (W/m$^{3/2}$)	1.06584*10^8
c_2	3
n_g	2
q_{max} (kW/m^2)	1500
m (kg)	250
g_0 (m/s^2)	9.81
S_{ref} (m^2)	0.7

$$n_g = \frac{\sqrt{C_L^2 + C_D^2}}{mg_0}\rho V^2 S_{ref} \tag{2-2}$$

Next, the vehicle is assumed to have a free fall flight before it reaches the maximum heat load constraint, which means a simple free fall equation can be solved to obtain the first leg of the flight. The vehicle accelerates as it undergoes a free fall flight for the first leg of the flight, once it approaches the maximum heat load constraint, it requires a pull up manoeuvre, whic enables it to fly along the maximum heat load constraint line. As soon as the g-load constraint line is met, the vehicle is reoriented using controls such that it can fly along the g-load constraint line.

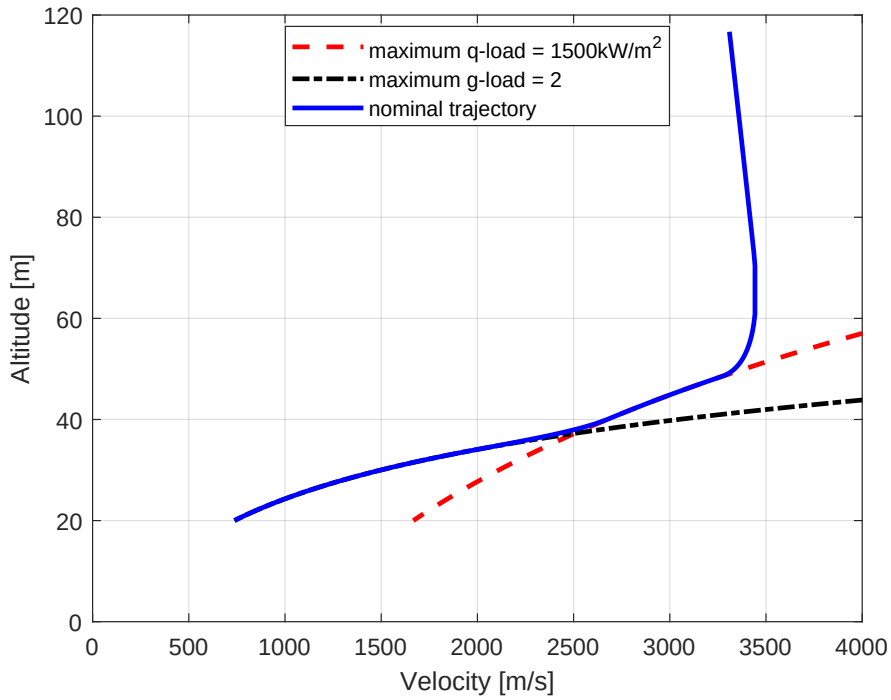

Figure 2-23: Altitude-velocity profile for nominal trajectory.

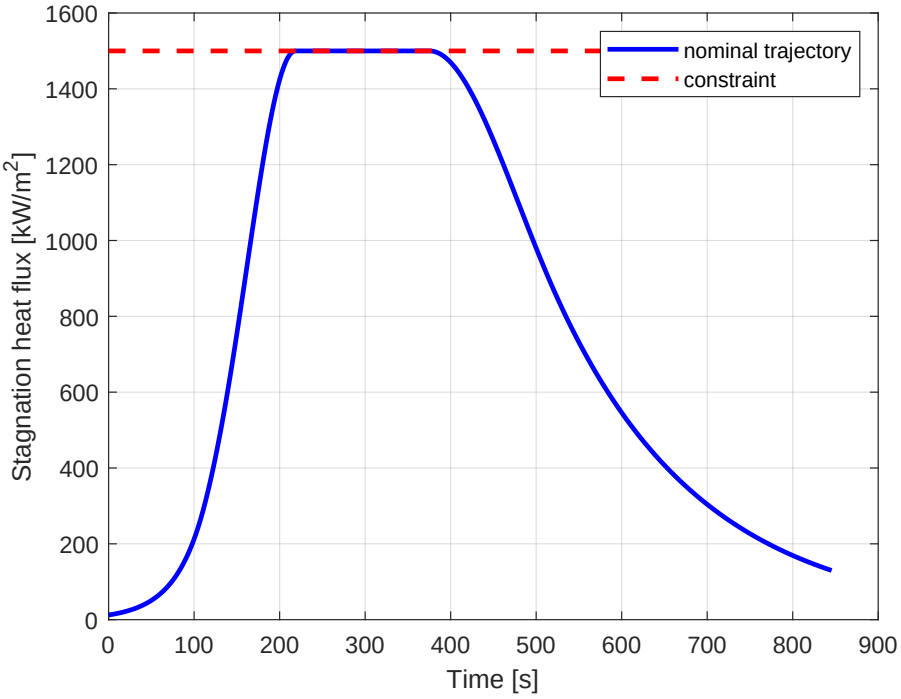

Figure 2-24: Stagnation heat flux profile for nominal trajectory (Nose radius (R_N) = 26 mm).

Chapter 3

Preliminary Design Investigation

In this chapter, a preliminary TPS design investigation for nose of the Hyperion II test vehicle is proposed. It must be noted that a conceptual design based on thermal analysis is the expected final outcome of this work, and in this chapter the initial design, which will be analysed later in Chapter 6, is described. After analysis of this design, improvements and changes will be implemented/suggested, which will result in the final proposal of the conceptual design. The focus in this chapter is only on a preliminary choice of material and size, which in the end can be looked at as variable factors/ parameters that influence the performance of the design.

To begin with, in this chapter, the selected design concept is discussed in Section 3-1, which includes an explanation of the design and a brief description of the basic operating principle. In Section 3-2, the coolant requirements along with the choice of the coolant is discussed. The coolant's physical properties will have a considerable influence on the heat transfer and performance of the design. The limitations of the selected coolant and consequences of selecting another coolant are also briefly discussed. In the following section, Section 3-3, the material choice for outer skin and porous layer is discussed. Material selection is an important step in any design process and careful consideration of the TPS requirements is necessary, in combination with experimental data. The possible material options, along with their advantages and limitations are described, and based on material requirements identified at the start of the section, a suitable choice is made. Lastly, in Section 3-4, thickness of the TPS layer is determined based on literature.

3-1 Design concept

Based on an intensive literature survey carried out prior to this thesis, various TPS concepts were studied. TPS can be classified based on type of material used, into three categories, namely ablative TPS, ceramic TPS and metallic TPS. Out of these three, metallic TPS (uncooled) is found to be an attractive solution, because of its improvements over ceramic TPS in terms of robustness and maintainability, while being mass-competitive. Additionally, based on the type of cooling, TPS can be classified as an active and passive system. Most of the existing TPS deigns are passive systems, they either absorb the incident heat flux and

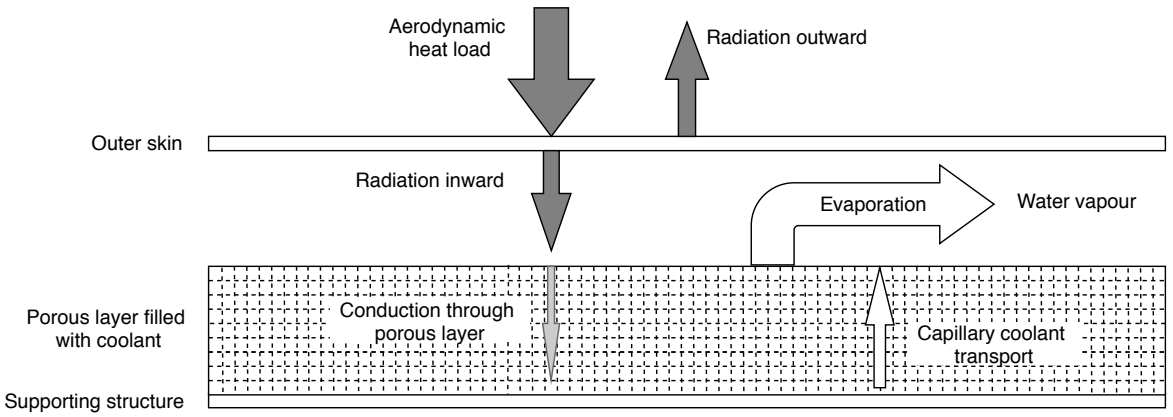

Figure 3-1: Schematic representation of energy flow in Enhanced radiation cooled TPS.

distribute it uniformly over the vehicle or radiate it outwards. This includes, heat sinks, hot structures and insulated structures. Alternately, some materials burn away, consuming a large portion of the heat energy in the process, however, these are not suitable for reusable systems. Existing passive TPS technologies are operating at almost their maximum capacity and little improvement in performance is expected from these designs. Active cooling, on the other hand, has been investigated for many years, however, has never been implemented for an actual mission. Active cooling consists of a coolant that is actively supplied to the system and is used for heat dissipation in different forms. The different types of active cooling include, transpiration cooling, convective cooling, heat pipes, etc. Past studies have shown that active cooling TPS has great potential to be used for reusable launch vehicles, however the lack of flight test data and the costs involved has deprived its development.

The cooled metallic TPS, one such active cooling system, is found suitable for the current application. Ideally, the advantages of a metallic TPS (uncooled) should also apply to a cooled metallic TPS. The mass competitiveness is likely to be less for cooled TPS, because the coolant mass has to be added. This can be offset to some extent by the removal of internal insulation. Moreover, cooled metallic TPS can sustain higher heat loads as compared to a metallic TPS. Reducing the nose radius of a vehicle, improves the aerodynamic performance by reducing the drag on the vehicle, however leads to a higher stagnation point heat flux. To solve this problem, cooled metallic TPS is proposed, because from past studies it has been proven to perform better than a metallic TPS.

Enhanced radiation cooling is a relatively new concept in the category of cooled metallic TPS, patented in 2001(Van Baten and Buursink, 2002). Unlike classic thermal protection systems, that provide insulation to the inner layers only by radiating heat outwards, enhanced radiation cooling allows the heat to be radiated inwards as well. A coolant is allowed to evaporate by using the heat that is radiated inwards, thereby cooling the TPS. Since, an additional means of losing the heat is used in this concept, the allowable heat load for a particular temperature of the TPS is increased or for a given heat load, a lower temperature is reached. The evaporated coolant is removed from the system, which basically means that the heat energy radiated inwards is expended. The coolant may or may not be actively supplied to the system, depending on the cooling requirements.

During operation, the aerodynamic heat load will cause the outer wall to heat up mainly by means of convection. It will radiate the thermal energy outwards as well as inwards. The porous layer underneath, which is filled with a coolant, will experience a temperature rise due to the heat load from the outer wall. When the outer surface of the porous layer

reaches the boiling temperature of the coolant, evaporation starts. Simultaneously, heat is conducted through the porous layer until the entire layer, along with the coolant, achieves the boiling temperature of the coolant. The evaporated coolant is vented from the vehicle and capillary action pushes more coolant to the outer surface of the porous layer. If the coolant is not actively supplied to the porous layer, the capillary action will continue only till the critical saturation level of the porous layer is reached. After this, the cohesive forces of the water in the capillaries is stronger than the capillary force, inhibiting transport. As the evaporation plane descends into the porous layer, it causes the temperature of the porous layer to rise above the boiling point, drying it out completely and eventually achieving a temperature equivalent to the outer wall. At this point, the heat radiated inwards is negligible. This means that temperature of the outer wall will also start to increase. In this scenario, there is a serious risk of damage to the outer skin, the material could melt due to the excessive heating. If that happens, the porous layer will come directly in contact with the environment and will be used for its insulating properties. Therefore, once the critical saturation level of the porous layer is reached, the useful operation of the cooling system ends. This simply means that sufficient coolant should be available for the entire re-entry flight. Either, the porous layer is thick enough to carry the required coolant mass, or a tank filled with coolant is connected by means of a pipe to replenish the porous layer. The amount of water required depends on the evaporation rate, which is directly related to the temperature difference between the outer wall and porous layer. So a higher outer wall temperature means that the evaporation rate will be higher, correspondingly the rate of capillary transport will be higher.

3-2 Coolant selection

Just like for selecting a material, there are requirements that must be fulfilled by the selected coolant. Some of these requirements include high heat of evaporation, non-toxic, high conductivity, low freezing point, low triple point pressure and relatively low evaporation temperature.

Although there are many requirements, a low boiling temperature and a high heat of evaporation, are the most important criteria. A boiling temperature in the range of 0°C and 150°C is preferred, because a lower temperature could be difficult to handle and higher temperatures would reduce the heat radiated inwards, between the outer wall and porous layer. Heat of evaporation is the energy required by the coolant to change its phase from liquid to vapour. If the heat of evaporation is higher, lesser coolant mass is required to take away heat load radiated from the outer wall. For this reason, water is selected as a coolant for this system. It has the highest heat of evaporation i.e., 2256 kJ/kg at 100°C, as compared to other liquids, due to substantial hydrogen bonding in the liquid phase which must be broken. At lower temperatures, the bonding is higher and so is the heat of evaporation (2500 kJ/kg at 0°C). It is very difficult to find a coolant having a similar evaporation temperature and heat of evaporation combination, or just have a higher heat of evaporation. Additionally, water is non-toxic, has less safety hazards and handling requirements as compared to other coolants like liquid nitrogen or hydrogen and is not costly. One of the reasons for using a different coolant would be, if the materials used for the TPS layers have poor resistance to water vapour. However, this change in choice would probably mean an increase in coolant mass, because of lower heat of evaporation.

As for the triple point pressure, for water the value is 6 mbar (0.006 atm, see Figure 3-2). Below this pressure, water does not exist in liquid form. Even in frozen state, cooling

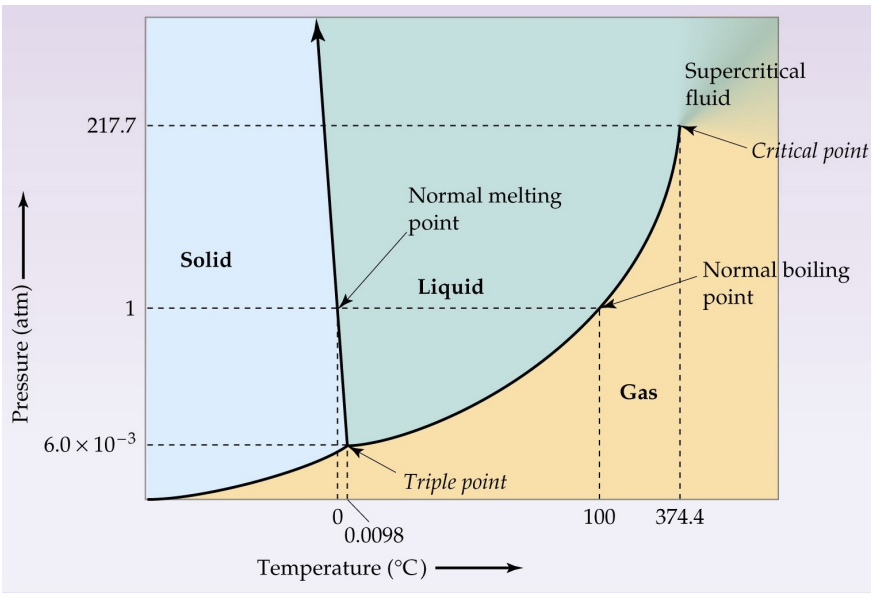

Figure 3-2: A phase diagram of water (McMurry and Fay, 2004).

will happen due to sublimation. However, due to lack of capillary transport, the evaporation plane will shift inside the porous layer, instead of on the surface, and eventually could lead to the system not being actively cooled. Therefore, it is important to ensure that the system should always be operated at a pressure higher than the triple point pressure.

There is a possibility of using hydrocarbon fuels, which as per literature take up larger amount of heat while cracking, in the range of 8-10 MJ/kg (Korabelnikov and Kuranov, 2005). However, residue of carbon in the system is expected, if such a coolant were used, which is a major drawback. This option has not been considered in this study. It can be studied in the future, but would require additional testing.

3-3 Material selection

Material selection is a systematic procedure that aims at finding materials which meet the functional/ performance requirements of the design along with minimising cost. Based on the design concept and TPS general requirements, some material requirements have been identified and discussed in Section 3-3-1. Followed by a discussion on the material selected for the outer skin and porous layer in Sections 3-3-2 and 3-3-3, respectively.

3-3-1 Material requirements

1. High maximum operating temperature.
   The outer skin and porous layer should have a high operating temperature. A higher maximum operating temperature of the outer skin, will increase the maximum allowable heat flux of the design (considering everything else remains constant). And as for the porous layer, the temperature under nominal operation is not expected to be very high, however, in case of failure, its insulating properties are relied upon to safeguard the underneath structure, because of which a higher maximum operating temperature is preferred.

2. High emissivity.

The emissivity of both layers, outer skin and porous layer, is an important parameter, because radiation cooling is one of the physical phenomena implemented in the selected design concept.

3. High specific heat.
   Specific heat capacity is the amount of heat energy required per unit mass of the material, to increase its temperature by 1 K. This means that a material with higher specific heat capacity, will require more energy to be added for the temperature to rise, which in simple words means a higher allowable heat flux (considering everything else remains constant).

4. High thermal conductivity.
   Thermal conductivity is a measure of the material's ability to conduct heat. A higher value simply means better heat distribution in the material. Also, the outer and inner surface temperature of a TPS layer achieves equilibrium more rapidly, which helps in reducing the thermal stresses developed if the temperature gradient were steep.

5. Oxidation resistance. This is an important requirement, because abundant nascent oxygen is present in the surrounding environment, produced due to the high temperatures, which can react with the material and lead to degradation.

6. Low coefficient of thermal expansion.
   Coefficient of thermal expansion expresses the change in the dimensions of the material due to change in temperature. A lower value is required to reduce thermal stresses and avoid cracks/ ruptures due to expansion and contraction of the material.

7. Manufacturability and machinability.
   The materials selected should be relatively easy to manufacture, such that costs of manufacturing are not too high. This value cannot be quantified at this point. Materials requiring complex and costly processes for manufacturing are avoided, unless some of the above mentioned properties lead to a significant improvement in performance. Plus, it is preferred if the material can be easily machined, to take the necessary shapes and forms.

8. Reusability and maintainability. This requirement cannot be quantified at this point. However, in general, if the material is resistant to impacts and oxidation, and does not ablate, it can be considered reusable. However, with reusability comes inspection and maintenance requirements. So a material that can be reused, with minimal inspection and maintenance is always preferred.

Other than the requirements listed above, the material properties such as density, ductility, Young's modulus, yield strength, ultimate strength, flexural strength, impact resistance, etc. are also important parameters, that must be taken into account. However, for the purpose of this work, these factors are given lesser importance. This does not mean that while making a material choice, these parameters are neglected. These requirements are considered as secondary and are not used while making a trade-off or during analysis. It is assumed that the structural integrity is maintained, using any additional supports if needed.

At this point, it is important to note that since no form of experimentation was involved during this study, the choice of material has been solely made using existing literature and logical reasoning, both of which are discussed below. Moreover, it is also vital to state

that a preliminary material selection has been carried out in this section and the choice can be further optimised by means of a study solely focused on material selection. An optimal choice of material is not essential to this research, because the aim is to propose a conceptual design for which choosing the most suitable material would be ideal, but is not always necessary. Selecting an optimal combination of materials happens through various stages of design development. Therefore, optimised material selection has been considered out of scope for this study.

3-3-2 Outer skin

As per the design concept, the outermost layer of the TPS is a thin metallic skin. Most metallic materials have been developed for applications like (aircraft) gas turbines, waste incinerators, chemical processing and the glass industry, other than for TPS application. All these other applications also pose a range of requirements with regard to operating temperature, (specific) strength and resistance to different types of corrosive and chemically active environments. Therefore, these materials can be applied for TPS as well, provided the requirements are met. The different metallic material types are briefly discussed below. An extensive study of materials was not conducted, as this would be a complete study in itself. Nonetheless, a broad overview was obtained as seen below. It should be noted that all material properties have been obtained from the respective material datasheets, available on the manufacturer's website, unless stated otherwise.

1. Superalloys – These are alloys of Nickle, Chromium, Iron and Cobalt; and have high heat resistant properties even at higher temperatures, in the range of 800°C to 1250°C. Recognised manufacturing brands such as, Hastelloy and Inconel, are developing a range of these alloys for the past few decades. Superalloys exhibit a range of yield strength at temperatures below 600 °C, 200 to 1000 MPa, however, at temperatures above 700 °C, a drastic drop in the strength is observed, 30 to 150 MPa. Another drawback of these alloys, especially Nickel-Chromium, Iron-Chromium and Cobalt based alloys, is that they are heavy, having a density in the range of 8000 to over 9000 kg/m3.

2. Oxide Dispersion Strengthened (ODS) alloys – These alloys are very similar to most superalloys, except for the addition of oxide having high melting temperature, in the form of small particles, for example Yttrium oxide particles. A very small percentage by mass of oxide is added, in the range of 0.5-0.6%. To make a homogenous structure, mechanical alloying, more commonly known as powder metallurgy, is used. This involves mixing the powdered form of the alloy with the oxide particles, followed by mechanical alloying in a ball mill and hot pressing. The oxide particles added to the alloy help increase the creep strength at high temperatures by blocking the movement of dislocations. Therefore, compared to normal superalloys, these ODS alloys have a higher creep strength even at temperatures above 1000 °C. Metallwerk Plansee manufactures two such ODS alloys, namely PM1000 (Nickle-Chromium alloy) and PM2000 (Iron alloy), that have been extensively used in the past by the Dutch space industry, namely DutchSpace, NLR etc., for research based on TPS applications. Buursink (2005) has also used PM1000 for performing experiments on the enhanced radiation cooling concept. Moreover, the manufacturer's datasheet does not provide all the required material properties, especially the thermal emissivity. Therefore, researchers in the Netherlands, such as Buursink (2005), conducted various experiments

on these materials to obtain this data. The main difference between PM1000 and PM2000 is the higher percentage of aluminium in PM2000, that leads to deposition of a layer of stable aluminium oxide during operation. In case of PM1000 a chromium oxide layer is formed, which is unstable at higher temperatures, leading it to vaporise. The drawback of ODS alloys is that it is more costly as compared to normal alloys, plus there are problems with machinability. This is because while machining if the material melts, the improvement in properties due to dispersion strengthening is lost. Alternate methods for machining are being developed in the Netherlands for the past few years. For example, welding can be replaced by high temperature brazing, to join ODS alloys.

3. Intermetallics - Gamma Titanium Aluminide (γ-TiAl) is a relatively new material, for which a lot of research was carried out during the NASP program (for X-30). After a lot of research, it has been proven to be a competitive material for use at temperatures between 250 °C and 850-900°C, with a higher yield strength as compared to Nickel alloys. Plasma wind tunnel tests were conducted on this material by Fischer et al. (2003), for the FESTIP program, to be used as TPS on the Hopper mission. These experiments indicated a very low catalicity and erosion rates, and an emissivity of about 0.8. However, these results were found for moderate enthalpies, and further tests are required to study the materials performance at higher enthalpies with full oxidation. Nonetheless, overall good characteristics and low density / high specific strength, make γ-TiAl the most attractive material for the above mentioned temperature range.

4. Silicides and Nitrides – Silicate materials exhibit usefulness at temperatures above 1000 °C, where superalloys cannot be used. Plus, these have high melting points, low density and good oxidation resistance, such as $MoSi_2$ melts at 2030 °C and has a density of 6.24 g/cm^3. However, at temperatures below 1000 °C, issues arise with low fracture toughness and low ductility. Many composites such as, MoSi2-Si3N, MoSi2-SiC and MoSi2-Al2O3, are currently under study for application in turbine engines and their performance, at temperatures above 1200°C, is found to be comparable to PM1000, and in some cases even better. Therefore, making them interesting for detailed study and application in the future. However, development will take a lot of time and the potential is very uncertain today.

5. Refractory alloys and metals - Molybdenum, Tungsten, Niobium and Tantalum, are some of the main refractory metals. These materials are said to have extraordinary heat and wear resistance, manufactured using powder metallurgy because of their high melting point, in the range of 2000°C. These materials are chemically inert. However, the main drawbacks are high density, poor oxidation resistance and difficulty in processing to required forms (due to hardness). Table 3-1 shows the melting temperature and density of the refractory metals. Additional coatings need to be applied, to make the material resistant to oxidation, however this limits the use of the material to the maximum operating temperature of the coating, around 1650°C. Due to this, the use of these materials is not justified, given their high density. Other alloys are available, that have much lower density and can be used for this temperature range. The high densities make these materials not suitable for TPS that covers a large portion of the vehicle.

Of the available alloys, the ODS alloys have high strength even at extreme temperatures

Table 3-1: Melting point and density of refractory metals.

Material	Melting temperature [°C]	Density [kg/m^3]
Niobium	2477	8570
Molybdenum	2623	10200
Tantalum	3017	16400
Tungsten	3422	19300

(over 1100°C) (see Figure 3-3), however lower than ceramics and refractory metals. As discussed earlier, refractory metals have a very high density, which makes it not suitable for this application. The problem of oxidation in both ceramics and refractory metals, are severe and till date no self-healing coatings have been developed, although plenty of research on oxidation resistant coatings is being carried out, which if successful, would make ceramics the best choice. At temperatures up to 700°C, a number of alloys have much higher strength. γ-TiAl is very interesting, because of its low density giving high specific strength. However, it is a complex material where the strength and ductility are dependent very much on the grain structure and different atomic lattices, and the angles under which they are loaded (Yamaguchi et al., 2000). Nevertheless, for the current generation of materials, PM1000 and PM2000 (and their US counterparts) give highest strength at high temperatures. γ-TiAl can be very interesting for low-intermediate temperatures. However, experience in working with this material will have to be gained. Also, Molybdenum-silicides appear to be a very good candidate. Some of the materials characteristics are not good, but a lot of effort is ongoing to improve these by adding alloying elements and making composites with e.g. SiC.

Therefore, based on the above discussion, the most suitable metallic material for this study is found to be ODS alloys. Extensive material data is available for PM1000 and PM2000, other than the material properties data sheet from the manufacturer (Metallwerk Plansee), due to the research of these materials for TPS applications in the Netherlands. For the purpose of this study PM2000 has been selected as the outer skin material. As discussed earlier, at high temperatures an unstable layer of chromium oxide is formed, in case of PM1000, because of which it is not suitable. There are many other companies that make ODS alloys, that have similar compositions as PM2000, such as Inconel MA754. However, most of them have a lower percentage of aluminium, except for HAYNES 214. It is important to note here, that although PM2000 is chosen for this research, Metalwerk Plansee has discontinued bulk manufacturing if this material and manufactures it only for special orders, which makes it more costly. HAYNES 214 on the other hand is bulk manufactured and therefore, might be more cost effective. Here, PM2000 is being used because abundant material data is available.

3-3-3 Inner porous layer

Other than the material requirements listed above, the porous layer should be able to hold a large amount of water and retain it even under high g-loads. Moreover, it should be chemically inert, have low density and coolant supply to the surface by means of capillary transport should be possible. ZIRCAR Ceramics' Alumina Type ZAL-15 was chosen as the porous material for this design, the reason for this choice will be clear by the end of this section. ZAL-15 is a low density, refractory structure composed of alumina fibres and

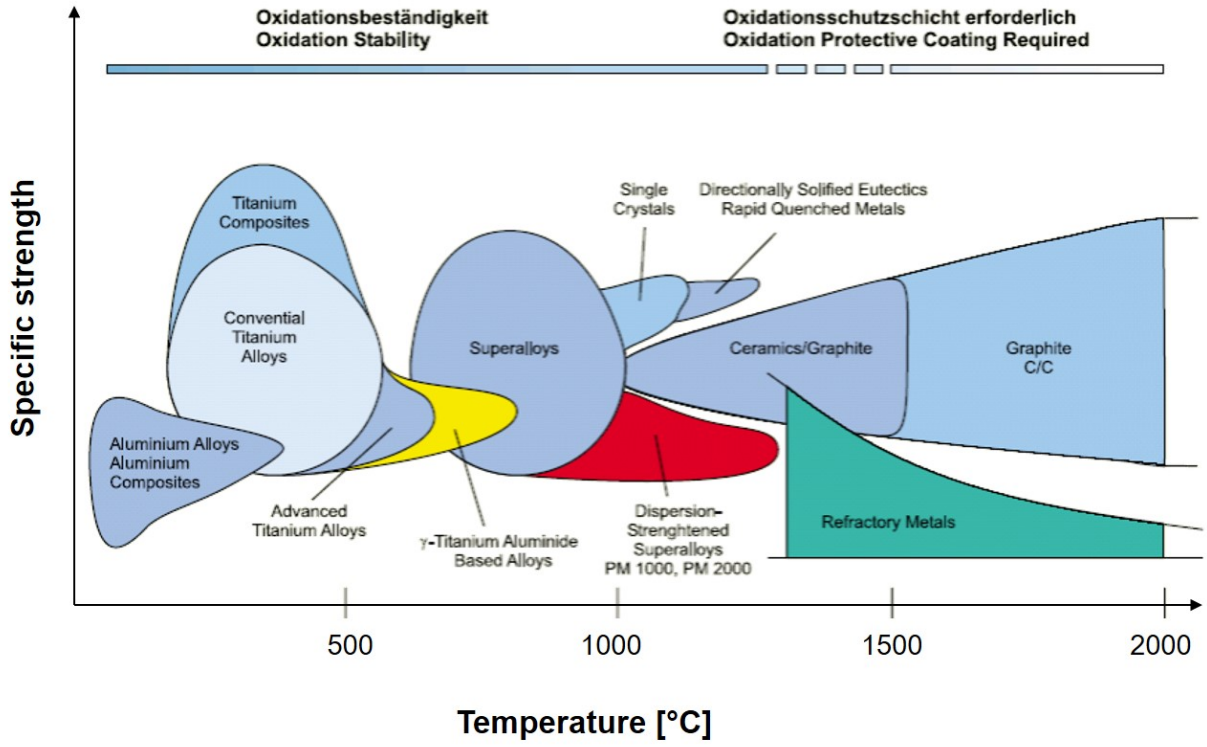

Figure 3-3: Comparison of different types of materials based on their operating temperature and strength (Buursink, 2005).

Table 3-2: Properties of ZAL-15 from ZIRCAR Ceramics' data sheet (Zir, 2019).

Density (kg/m^3)	240
Maximum use temperature (°C)	
Continuous	1550
Intermittent	1650
Thermal expansion coefficient from room temperature to 1000°C (/°C)	5.0 * 10^{-6}
Melting point (°C)	1870
Specific heat (J/kgK)	1047
Thermal conductivity (W/mK)	
250°C	0.06
525°C	0.08
800°C	0.12
1075°C	0.16
1250°C	0.22
1350°C	0.25
Flexural strength (MPa) at 25% strain	1.6

silica binders (85% Al_2O_3 and 15% SiO_2) (Zir, 2019). As per the company's data sheet, the porosity is 93% i.e., the theoretical amount of water by volume that can be held by the material. However, in actual practice, this value could be lower due to presence of air bubbles. All the other relevant material properties can be seen in Table 3-2.

Buursink's (2005) research involved experiments on ZAL-15, which showed the ability

to hold 75% water by volume. The capillary transport could fill up a 35-40 cm thick layer of the porous material under 1-g load conditions. Detailed analysis was not conducted, these were simple experiments, nonetheless a first assumption was made such that the thickness of porous layer that can be filled up is a ratio of the g-load and will be smaller in the direction in which g-load is more. Therefore, there is a limitation on thickness of the porous layer, if the filling up relies only on capillary action, and the g-load is the limiting factor. For this study, a maximum g-load of 2g has been considered, which means that the porous layer should not be thicker than approximately 20 cm. If a thicker layer is required, then a possible solution to the problem would be to make compartments and have multiple filling points. Many other tests were performed by Buursink (2005), including a vacuum test, which showed that if water was filled into the porous material at pressures lower than the triple point, ice would freeze and capillary transport would be restricted, however no significant damage was observed to the material's microstructure. Emissivity of the material was measured at room temperature, for both wet (0.91) and dry (0.81) conditions, and it was assumed that it remains constant even at relatively higher temperatures, therefore it can be assumed constant for the expected operational temperature range i.e., between 0°C and 150°C, at the least.

The experiments performed by Buursink (2005) showed that the ZAL-15 (as porous layer) and water (as coolant) combination was very effective, in terms of emissivity, water retention, water transport and overall cooling performance. Therefore, ZAL-15 was an obvious choice for this study. Though there is one known drawback, the material's response to vibration is not known. This is necessary to be tested in future.

3-4 Preliminary sizing

The preliminary design is incomplete without having an initial dimension of the TPS layers, in this case the outer skin, porous layer and the gap in between these two layers. Ideally, a structural analysis would be required to determine the size, however this was defined out of scope for this work. Therefore, to start with, an initial size is proposed based on literature. The nose radius of the Hyperion-II vehicle is known i.e., 2.6 cm. Buursink (2005) carried out experiments on enhanced radiation cooling panels using a PM 1000 skin of 1 mm thickness, ZAL-15 with a thickness of 12.7 mm, 19 mm and 26 mm, with a gap of 1 mm, 3 mm and 5 mm in between the two layers. For this design, outer skin thickness is set at 1 mm and gap is sized at 5 mm, this leaves a porous layer thickness of 20 mm, for a 26 mm nose. As was discussed in Section 4.3, the porous layer thickness is limited by the g-load and for a 2-g load case, maximum recommended thickness was 20 cm. Therefore, it can safely be assumed that for a 20 mm porous layer, water transport to surface of the porous layer by capillary action, would be sufficient, provided enough water i.e., for the entire re–entry trajectory, is supplied to the porous layer. In detailed design phase, discussed in Chapter 6, these sizes will be varied to study the influence of sizing on thermal performance of the design, and based on the results the sizing will be revised. Once again, it is important to note that ideally structural integrity would also be considered in the detailed design step. However, it has been neglected and it is assumed that the proposed sizing can handle the structural/ mechanical loads.

Chapter 4

Software

Based on the cooling concept discussed in the previous chapter, in this chapter, mathematical models are proposed, that describe the physical phenomena of cooling, to perform a thermal analysis of the concept and in turn acquire information about the system's performance. A steady and a transient thermal analysis is carried out, therefore both mathematical models must be formulated. This is seen in Section 4-1, including the assumptions made in the model and the corresponding consequences or outcomes of these assumptions. Mathematical models generally comprise of complex equations, depicting the interdependence of parameters, sometimes these relations can be solved by hand. However, in many cases, the system's complexity requires the use of computers. So the next step is to convert the model from mathematical form to a logic that can be easily understood by the computer. Before making a computer software, it is important to prepare a software architecture, such that the software logic is streamlined. This has been described in Section 4-2, including a brief discussion about the software philosophy. Lastly, in Section 4-3, the software model developed is verified using simple hand calculations or data from existing literature. This is a mandatory step in the process of developing any software, as the quality of the results is not justified if the model is not verified.

4-1 Mathematical model

A mathematical model can be described as, a general description of a process or concept, in a mathematical language, allowing a relatively straightforward means of handling the variables, to determine how the process or concept would behave under different conditions. To gain understanding of the physical phenomena and to obtain a prediction tool for design of the cooling system, a mathematical model is needed. Heat transfer can occur under steady or unsteady (transient) conditions. Steady conditions mean that the temperature of the system does not vary with time, whereas for an unsteady state temperature is time dependent. For this study, an unsteady state heat transfer model is developed, because the vehicle experiences variable heat flux along the trajectory, correspondingly the temperature of the TPS layers is time dependent. Obviously, the system does reach steady state at some point, when the vehicle is flying along the maximum heat load constraint, however prior and

after this segment of the re-entry flight, the temperature is not steady. Also, the heat flux gradient is pretty steep, and is expected to be similar for the temperature profile. Therefore, a transient state model is developed for use in this study. Mathematical formulation of a transient state model for the ERC concept is described in this section (in Section 4-1-2), including assumptions made and their expected consequences (inSection 4-1-1).

4-1-1 Assumptions and consequences

The transient model is developed using certain simplifying assumptions, as discussed below, including the consequence of each assumption.

1. *Only 1D heat flow is taken into account, in the direction opposite to the coolant flow.* This is an acceptable assumption, so as to simplify the thermal model, and to obtain a first estimate of the concept's performance. For better accuracy of the results, a full 3D heat flow analysis is recommended, however this will be computationally expensive, so improvement in accuracy and its impact on the results will have to be analysed, against the increase in computation costs.

2. *It is assumed that sideways heat conduction in both, outer skin and porous layer is negligible.*
   This is because heat incident on the complete surface of the nose is of a similar magnitude, such that the entire surface is heating up simultaneously. If taken into account, this is not expected to have a significant impact on the results.

3. *Physical properties of a material at any node are assumed to be constant and depend on the temperature at that node.* This is seen from the material datasheets, the material temperature has an influence on the physical properties. However, the data provided in these datasheets is limited and is obtained from ground testing at normal pressures. In flight, the property variation might be different, and might have an impact on the results. To check for this, a sensitivity analysis, with respect to uncertainty in physical properties is conducted and discussed in Chapter 6.

4. Fluid properties at a node are assumed to be dependent on the system pressure. As system pressure increases, the saturation properties for water, such as evaporation temperature and heat of evaporation are seen to vary from the NIST Chemistry WebBook, SRD 69. Since a significant variation in properties is observed, it must be taken into account. Therefore, this is a justified assumption.

5. *Emissivity of porous media (ZAL-15) is assumed to be constant at all temperatures.* This assumption is made because, there is little to no variation in the emissivity of this material within the temperature range of this analysis, according to the findings of Buursink (2005).

6. *No heat is generated in the TPS.*
   There could be some heat generating elements in the system, such as a pump, however, the heat generated by these elements are neglected in this preliminary estimation. This can be included only after a detailed design has been developed and more information about all elements is known.

7. *Chemical reactions, such as oxidation, on the surface of the nose, are neglected i.e., surface is considered to be noncatalytic.*

This is a simplifying assumption, to make a first estimate. For future development, this should be taken into account. The heating incident on the surface of an entry vehicle is primarily convective heat transfer from the hot boundary layer next to the vehicle surface. In the presence of dissociated air (nascent oxygen), convective heating may be enhanced significantly by a phenomenon known as surface catalysis. The material of the vehicle surface may act as a catalyst to the recombination of dissociated air, thereby releasing the associated chemical energy in the form of increased surface heating. Surface catalysis tends to be more significant near the nose or wing leading edges, where shocks are generating dissociated air. It is seen that the stagnation point heat flux increases as the surface catalysis increases (Anderson Jr, 2006). Aluminium content present in PM2000, reacts with nascent oxygen to form a stable layer of aluminium oxide, which is an exothermic reaction. This additional heating must be taken into for more accurate results.

8. *Coolant mass flow is assumed to be mono-dimensional.*
This assumption is made for simplifying the model, and is in line with the first assumption. In reality, this is not true, but considering coolant flow in the other dimensions, is recommended to better understand the system. Although, impact on the results is not expected to be significant.

9. *The pressure in the system is higher than the triple point of water.*
More than an assumption, this is a necessity, to avoid freezing the water present in the porous layer. Freezing of water hinders the transport of coolant to the porous layer surface, causing the sublimation plane to descend into the porous layer and a rise in the temperature of both, skin and porous layer. This means the system is not performing as expected and is not recommended.

10. *Cold wall heat transfer between the surrounding and outer skin layer is assumed.*
This assumption is a conservative approach. In reality, this is not true and the heat flux is expected to be lower. Nonetheless, it is an acceptable assumption for a first estimate.

11. *Heat transfer due to convection in the air gap is neglected.*
This is assumed because the gap thickness is very small (5 mm) and the convection current/ density gradient is not significant, as compared to the radiative heat transfer at high temperatures. If included, this expected to improve the accuracy of the results, but not have a significant influence on the performance.

12. *Heat transfer due to conduction in the air gap is neglected.*
This is an acceptable simplifying assumption, because the gap thickness is too small and the radiation heat transfer at high temperatures is such a large value, such that the contribution of conduction heat transfer seems less significant. If included, this expected to improve the accuracy of the results, but not have a significant influence on the performance.

13. *Radiation in the air gap is the dominant mode of heat transfer.*
This assumption is in line with the previous two assumptions and holds true for high temperatures, which is expected for most of the re-entry flight. In the beginning, when temperatures are lower, this may not hold true. However, the influence of that is not significant when the overall performance is being studied.

14. *The outer skin is assumed to be a lumped system and conduction through it is neglected.* This is an acceptable first assumption because, the skin is very thin (1 mm) and is expected to have uniform temperature across its thickness (Biot number < 0.1).

15. *The porous medium is neglected in the heat balance relations, instead only coolant layer is considered and its physical properties are modified to take into account the physical properties of porous layer. For example, effective density is $\rho = \phi * \rho_c + (1 - \phi) * \rho_p$, where ϕ is the porosity. This can be termed as effective physical properties.*
The porous medium is completely filled with coolant from the onset of heating. Considering the porous medium, which in this case is ZAL-15, has a porosity of 91%, the ratio of coolant to porous medium is very high. Plus, effective physical properties are taken into account, which makes this an acceptable assumption for first estimate. Considering the porous layer as a separate element will make the system more complicated and not have a significant effect on the results.

4-1-2 Mathematical formulation

The outer skin is directly in contact with the surrounding environment. At the stagnation point, heat flux q_{stag} is incident on the skin. Temperature of the skin rises due to convective heating and considering it is a metallic skin, it radiates some portion of this heat outward as well as inward. Therefore, the change in enthalpy of the skin is estimated by taking a summation of the incoming aerodynamic heat flux and outgoing radiation in both directions. The thermal analysis for the skin is done using lumped system analysis. The 1-dimensional transient heat transfer equation for the skin is given as seen in Equation (4-3),

$$q_{out} = \sigma \epsilon_s T_s^4 \tag{4-1}$$

$$q_{in} = \frac{\sigma \left(T_s^4 - T_p^4\right)}{\left(\frac{1}{\epsilon_p}\left(\frac{R_N}{R_i}\right)^2\right) + \left(\frac{1-\epsilon_s}{\epsilon_s}\right)} \tag{4-2}$$

$$\rho_s c_{p,s} x_s \frac{dT_s}{dt} = q_{stag} - q_{in} - q_{out} \tag{4-3}$$

$$T_{s,new} = T_{s,old} + \frac{dt * (q_{stag} - q_{in} - q_{out})}{\rho_s c_{p,s} x_s} \tag{4-4}$$

where the subscript s stands for skin and p stands for porous medium. Equation (4-2) is the part of heat being radiated inwards and is incident on the porous layer, which heats the coolant as well. Now, the heat incident on the porous medium will be transferred to both, the solid material and coolant. However, based on the assumptions made earlier, heat transfer to the porous layer is neglected. The heat radiated inwards, heats up the coolant mainly through conduction. The 1-dimensional transient conduction heat equation for the coolant is given as seen in Equation (4-5). It must be noted that the physical properties considered in these equations are effective properties, as described in the last assumption. Also, the temperature obtained is same for both coolant and porous layer i.e., $T_c = T_p$, where subscript c stands for coolant and p stands for porous layer.

$$\rho c_p \frac{\partial T_c}{\partial t} = -\lambda \frac{\partial^2 T_c}{\partial x^2} \tag{4-5}$$

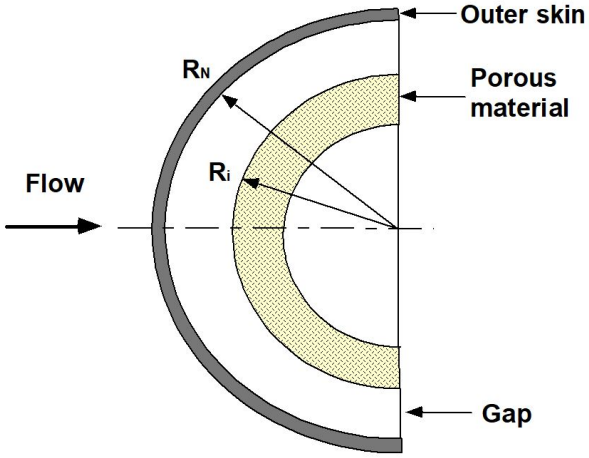

Figure 4-1: Configuration of Enhanced radiation cooling.

To solve Equations (5-1) to (5-5), an initial condition must be defined, in this case, for the skin and coolant temperature, an initial guess of 298K will be used. The boundary conditions required to solve the second order differential equation seen in Equation (4-5) are as follows,

1. The lower surface of the porous layer, where the thickness of the porous medium is $x_p = L$ and is in contact with the supporting back plate (Figure 3-1), an adiabatic wall is considered.

2. On the air gap side, where x_p=0, a constant heat flux per time instant is considered i.e., $q\left(t\right) = -\lambda \frac{dT_c}{dt}$.

Here, $\dot{q}\left(t\right)$ is the heat radiated inwards from skin to porous layer per time instant. Equation (4-5) is a second order differential equation and will be solved using the Binder-Schmidt method (see schematic in Figure 4-2), as per which

$$u_i^j = \frac{1}{2}\left(u_{i-1}^{j-1} + u_{i+1}^{j-1}\right) \tag{4-6}$$

where i stands for the space step and j stands for a step in time. To ensure stability, the condition, $\frac{a\Delta t}{\Delta x^2} = \frac{1}{2}$ must be fulfilled at all times.

The coolant, in this case water, will start heating and once the temperature crosses its boiling point, evaporation of the coolant will start. This means that a constraint must be applied on the air gap side i.e., x_p=0, to take into account evaporation of coolant. Therefore, the coolant temperature at the first node is calculated using Equation (4-7),

$$T_c\left(i,j\right) = T_c(i,j-1) \; + \; \frac{q_{in}dt}{\lambda} \tag{4-7}$$

However, if the coolant temperature is found to be greater than the boiling point of water, the value is considered incorrect. This is because beyond the boiling point, incoming heat is utilised in change of phase of coolant, and the coolant evaporation rate is estimated as is seen in Equation (4-8).

$$\dot{m} = \frac{q_{in}}{H_{lv}} \tag{4-8}$$

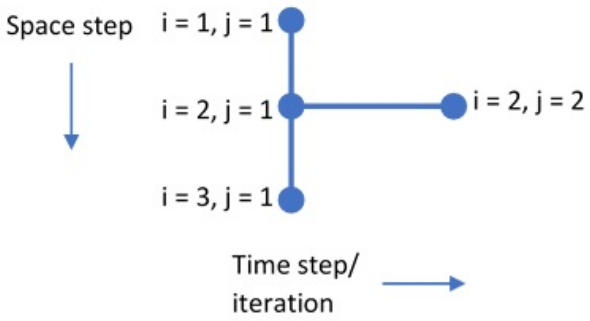

Figure 4-2: Schematic for Binder-Schmidt approach.

The term $\dot{m}$ stands for the coolant mass flow rate. This will give the rate at which the coolant will evaporate so as to absorb the incident heat flux. Therefore, the coolant mass flow rate must always be equal to or slightly more than the rate at which the coolant evaporates, to make sure that the porous medium is always filled with coolant. As for the coolant temperature, it will be equal to the boiling point of the coolant.

One additional step must be considered here, if the temperature at the previous step was less than the boiling point and the temperature estimated for the current step is more than the boiling point. This means that part of the incoming heat was utilised in raising the temperature, as is seen in Equation (4-9) and the remaining was used in evaporation.

$$\Delta T = T_c\,(boil) - T_c\,(i, j-1) \tag{4-9}$$

We use the ΔT found in Equation (4-9), to calculate the amount of heat flux that was used in heating up the coolant by using Equation (4-10),

$$q = -k\frac{\Delta T_c}{dt} \tag{4-10}$$

Now, this heat is subtracted from the incoming heat flux, before estimating the rate of evaporation.

$$\dot{m} = \frac{q_{in} \;-\; q}{H_{lv}} \tag{4-11}$$

Note, this additional step is required if and only if the temperature in the previous iteration is less than boiling point of the coolant and the temperature estimated for the current step is more than the boiling point. In this manner, the coolant temperature at the first node is estimated. For the consecutive nodes, the temperature is estimated using Equation (4-6). An example can be seen in Equation (4-12), where the temperature of the 2^{nd} node for the 2^{nd} time step is estimated.

$$T_c\,(2,2) = \frac{T_c\,(1,1) - T_c\,(3,1)}{2} \tag{4-12}$$

This way, temperature for all the following nodes are estimated. Based on the estimated coolant temperatures, the skin temperature is re-calculated. The difference between the previously calculated skin temperature and the re-calculated value is negligible, less than 10^{-4}, because of which re-calculation is not always necessary, but is a good check.

To compare the improved performance of a cooled metallic TPS, to an uncooled system, the uncooled system must also be modelled. This is much easier now, since the cooled model

has already been developed. In case of the uncooled model, the heat radiated inwards will lead to a rise in temperature of the porous layer. Since the coolant is absent, the physical properties of only the porous layer are considered. In this model, Equations (5.1) to (5.7) remain the same, except for the physical properties in Equation (5.5) are no longer effective values. Also, in all equations, the temperature obtained is only for the porous layer, as coolant is absent, so T_c is replaced by T_p. Equations (5.8) to (5.11) are not applicable to this model.

4-2 Code architecture

A software tool is developed using MATLAB, based on the mathematical model described in Section 4-1, for analysing the thermal performance of the proposed TPS concept. The software architecture for this tool has been discussed in this section. This is useful in understanding how the tool is modelled. Also, a code architecture is an important step in translating the mathematical formulation of a physical phenomenon, into a logic that can be understood and simulated by a computer system.

4-2-1 Transient model (Main)

A flow chart of the transient model is as seen in Figure 4-3. The flow chart depicts flow of information through the software. There are two models, namely cooled and uncooled, which when simulated with the required inputs, provide the output to the transient model. Flow chart for the cooled and uncooled model is seen in Figure 4-4 and Figure 4-5, respectively. The main transient model starts with an input from the user, depending on if the user selects a cooled or uncooled system, the respective model is initiated. Now if a cooled model is selected, the user must also indicate if, the blocking effect should be considered. Based on the user input, the appropriate information is passed on to the cooled model. The system provides the cooled or uncooled model with the other required inputs such as, the trajectory data (including pressure and stagnation heat flux profile), physical properties of the materials and coolant and size of the TPS layers. The output from the cooled or uncooled model is sent back to the main transient model, this includes the temperature and mass flow rate profile. A warning is issued if any material's maximum operating temperature is exceeded. Here, manual intervention is necessary, to update one of the input files i.e., the trajectory, TPS size or TPS materials. If the material maximum operating temperature is not exceeded, the total coolant mass per unit area is estimated as and published as the output of the transient model, along with the data obtained from the cooled or uncooled model.

4-2-2 Cooled model (Sub-routine 1)

Cooled model receives input from the transient model as described earlier. First the problem is initialised, next using the inputs, heat radiated outwards and inwards from the skin is estimated and using this the heat stored in the skin material is obtained, which in turn is used to determine the skin temperature. An iterative process is involved, where outer surface temperature of the porous layer is assumed from the previous time step and the skin temperature is estimated. Using the new skin temperature, the temperature profile for the porous layer is calculated. Also, once the coolant evaporation temperature is reached, evaporated coolant mass flow rate is estimated. This continues for each time step and the

data is stored, till the final time step is reached. After that the stored data is passed on as output to the transient model.

4-2-3 Uncooled model (Sub-routine 2)

Difference between the cooled and uncooled model, as the name suggests, is active cooling using a coolant. Therefore, in case of the uncooled model, all input from the transient model remains the same except for, physical properties of coolant are not provided. Also, output from the model is only the skin and porous layer temperature profile. In most cases, the maximum operating temperature of the materials is exceeded, for the uncooled model. Similar to the cooled model, the skin and porous layer temperature are iteratively estimated for each time step, and the output is stored for all time steps, after which it is sent back to the transient model.

4-3 Verification

Verification can be defined as the process of inspecting a tool or software, to check if it is correctly representing the proposed mathematical model. The thermal analysis software developed in this work was verified in multiple stages during its development. As is discussed in this section, first unit/ function wise verification was carried out. This means that each function in the software was checked to see if it is producing the expected output, more about this is discussed below. Next, a complete system verification was carried out, using the experiment results from Buursink's (2005) research.

Unit/ function verification includes verification of every sub-routine as well as verification of the information flow between sub-routines. As is seen in Section 4-2, the main transient model has two in-built models and multiple input files. The first step is to make sure that the input data is supplied in the correct units. To check this, other than visual checks, error messages were programmed in the software, that checked for the order of magnitude of a parameter value. In case an erroneous input was provided, the software immediately flags an error message and exits the simulation. Next step was to ensure that the correct information was being passed on between sub-routines, which was carried out by simple visual checks using garbage data. The cooled and uncooled models were programmed in Excel, to compare the output results. For this, simple numbers were used, only to check if the output from both programs is the same. It must be noted that this step was performed only to ensure that correct information is being passed between functions and the mathematical formulas are correctly programmed.

To verify the complete system, final output of the cooled and uncooled model was compared to existing data from literature. Buursink (2005) performed ground based experiments on the ERC system, consisting of a 1 mm thick PM1000 outer skin and a 12.7 mm thick ZAL15 porous layer, with a 5 mm gap in between the two layers and water as the coolant. The sample is fitted in a ZAL45 frame and heated using 10 quartz heater lamps of 1000W each, giving a thermal radiation of approximately 400 kW/m^2 (Buursink, 2005). Also, the test setup consists of thermocouples installed at various locations on the skin and porous layer (as seen in Figure 4-6), to measure the temperature during the experiment. The temperature profile obtained from one of the many experiments, was used for verification of the tool.

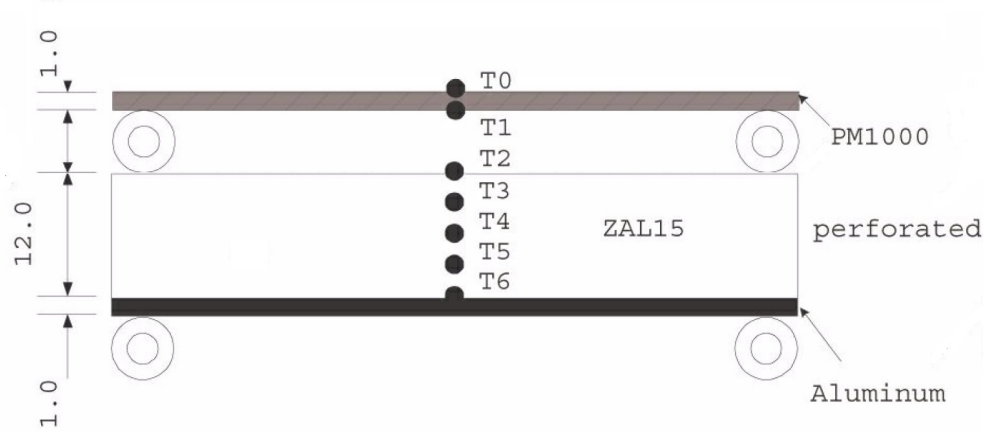

Figure 4-6: Location of thermocouples in the test setup Buursink (2005).

To do so, the heat flux incident on the outer skin must be approximated from the test data, as no measurements of the heat flux are available. Buursink (2005) suggests such an approximation approach to recover the heat flux profile, where the temperature data for an uncooled sample is used and a heat balance is assumed, such that the applied heat load on the skin is a summation of the heat radiated inwards and outwards from it. However, this approach neglects the thermal mass (product of mass and specific heat) of the skin material and the sideways heat transfer to the frame, because of the insufficient measure temperature data.

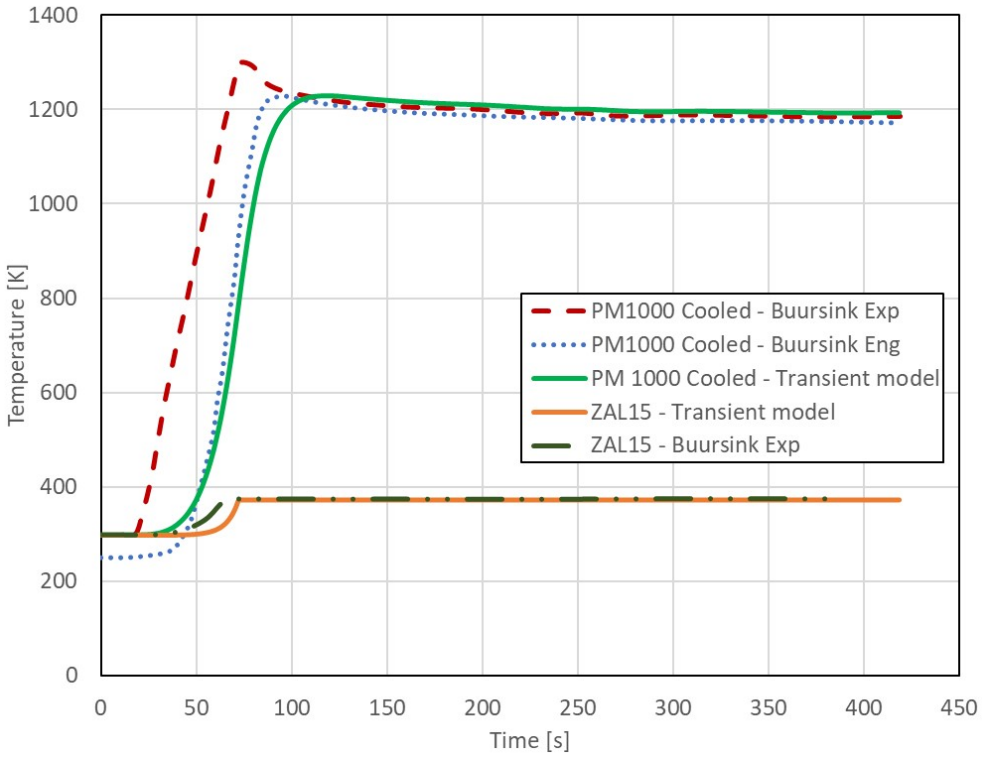

Figure 4-7: Verification of transient model (cooled) using experimental and analytical data given by Buursink (2005).

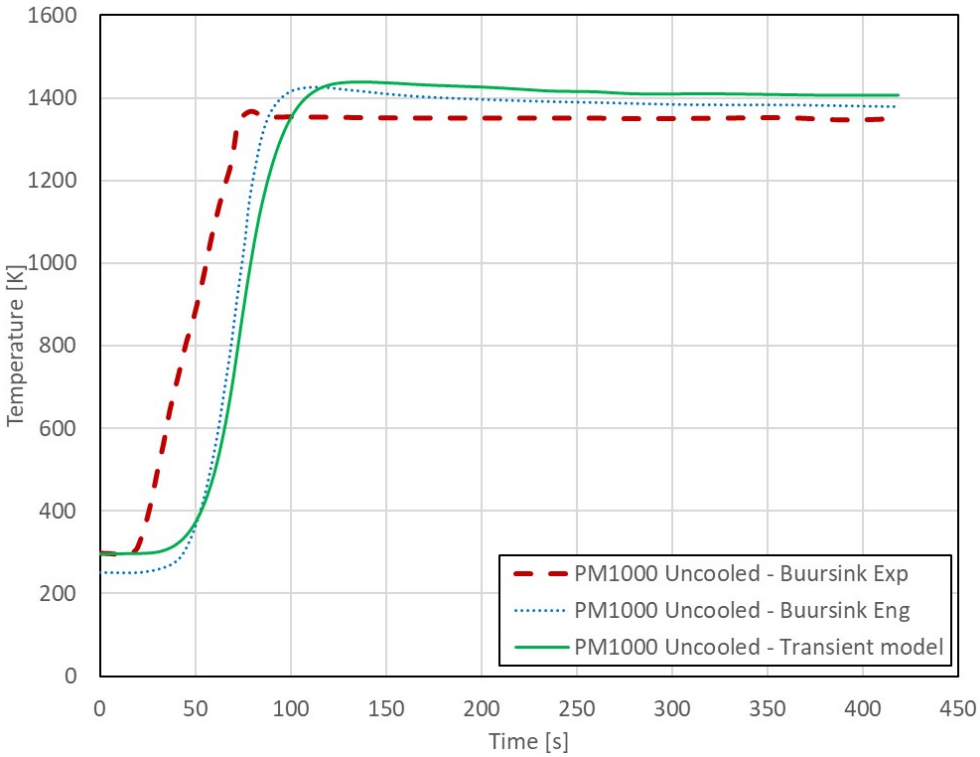

Figure 4-8: Verification of transient model (uncooled) using experimental and analytical data given by Buursink (2005).

Using the above discussed approach, the heat flux profile was recreated and used to simulate the transient model. In Figures 4-7 and 4-8, results for the cooled and uncooled transient model, respectively, are compared with the experimental results provided by Buursink (2005). Additionally, the output is compared to the simple steady state engineering model proposed by Buursink (2005). It is observed that results from both, the transient model and Buursink's (2005) engineering model, are shifted in time. This is because of the approach used to reconstruct the heat flux profile. Otherwise, the difference in temperature for the cooled system, between the measured data and the transient model output, is less than 1%. Also, a larger difference in temperature is seen for the uncooled model because data for the insulation used in the uncooled test setup is not available, therefore, not included. This causes a higher difference between measured and simulated results, of about 5%. There is a slight offset in the heating up phase, between the engineering model and the tool developed in this study, because the engineering model is a first approximation based on steady state analysis, which means the transient effects are neglected. Once the heat flux stabilises, a roughly constant difference is seen between the two models, because the thermal mass of the skin material is neglected in the engineering model. Since Buursink's (2005) engineering model does not provide results for the porous layer, temperature of the upper surface of the porous layer is compared only with results from the experiment. To conclude, the transient model is verified by means of this test case and is found to satisfactorily replicate the heat transfer phenomena, for both cases, cooled and uncooled.

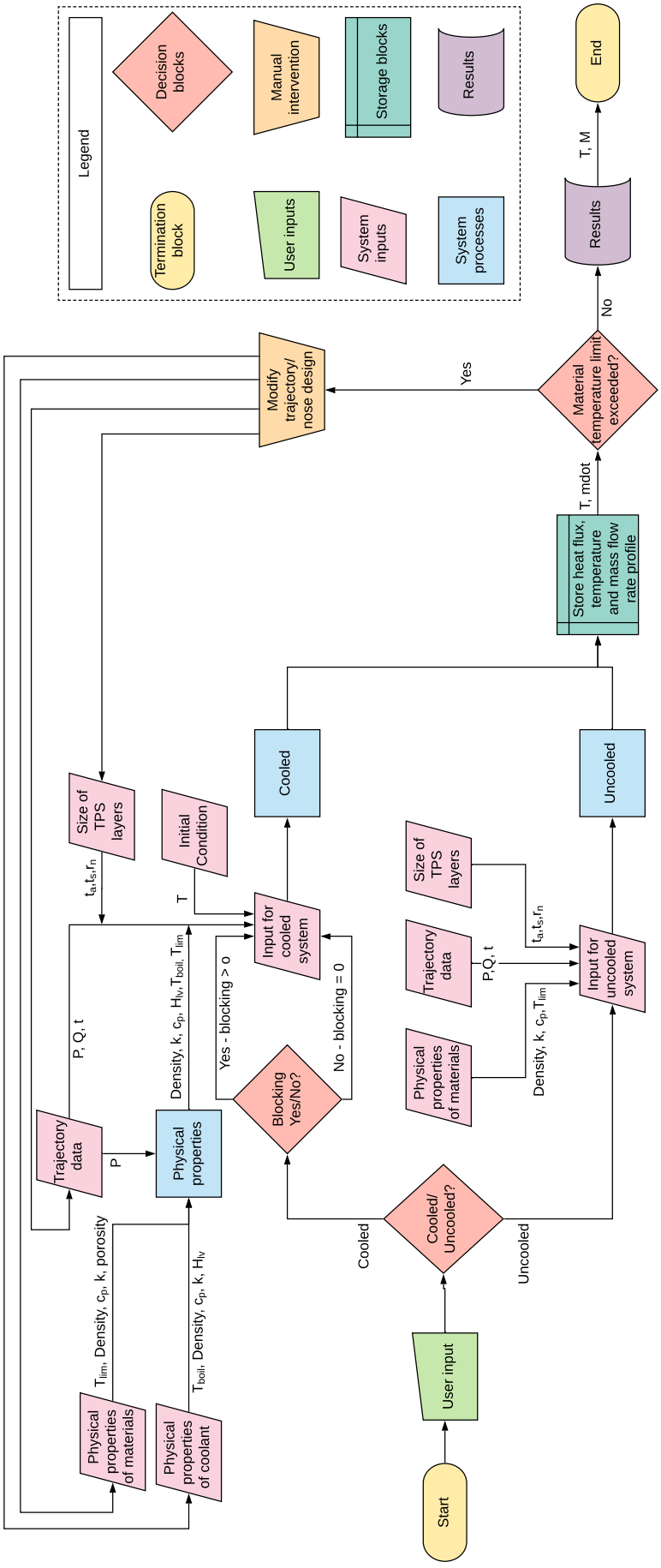

Figure 4-3: Flow chart for transient model.

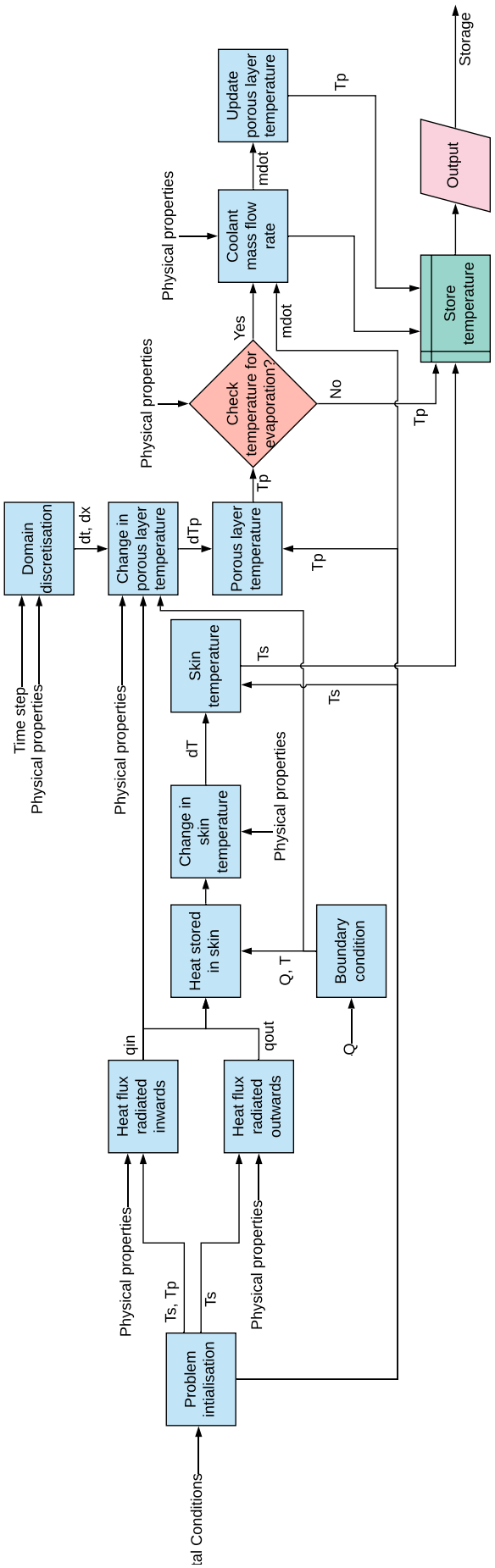

Figure 4-4: Flow chart for cooled model.

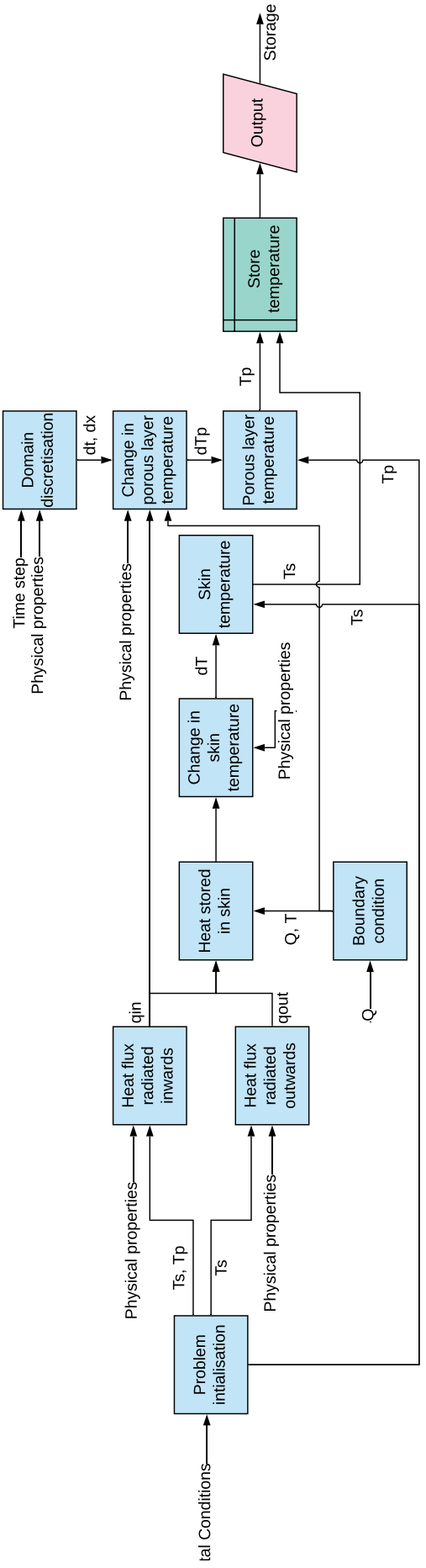

Figure 4-5: Flow chart for uncooled model.

Chapter 5

Proposed Conceptual Design

In this chapter, the results obtained, after simulating the preliminary design, are discussed in Section 5-1. Based on performance of the TPS, certain modifications to the design are proposed and analysed in Section 5-2, including a discussion about the consequences of these modifications. Sizing of the modified design is then discussed in Section 5-3, followed by a proposal of the conceptual design in Section 5-4, including a brief discussion on the proposed cooling system's operation.

5-1 Analysis of preliminary design

Using the software tool developed, as discussed in the previous chapter, the preliminary design of ERC, proposed in Chapter 3, is simulated and results for the same are discussed in this section. It must be noted that data from the nominal trajectory, described in Section 2-6, is used as input for this analysis. Also, material properties are as obtained from the manufacturer's datasheets, in case of outer skin (PM2000) and porous layer (ZAL-15), and from NIST Chemistry WebBook, SRD 69 for properties of water.

The distribution of heat flux, i.e, the variation of stagnation heat flux incident on the skin, heat flux radiated outwards and heat flux radiated inwards, can be seen in Figure 5-1. It is interesting to observe the data in this plot, to see how the heat energy is being distributed. When correlated with coolant mass flow rate variation, seen in Figure 5-4, it is observed that coolant evaporation starts very early on in the re-entry phase. This means that the inwards radiated heat flux seen in Figure 5-1, is nothing but the heat removed from the system by evaporation of water.

The variation in outer skin temperature, as the vehicle re-enters the Earth's atmosphere is seen in Figure 5-2. This variation in temperature is plotted for both, an actively cooled and an uncooled system. The performance improvement from an uncooled or passive system is clearly seen in this plot. Unfortunately, even in case of an actively cooled system, the outer skin temperature, for a maximum heat flux of 1500 kW/m^2, is higher than the maximum operating temperature of PM2000. This means that the system will fail for this trajectory. Alternate solutions must be found or the design must be modified. This is discussed in Section 5-2, along with consequences of the modification.

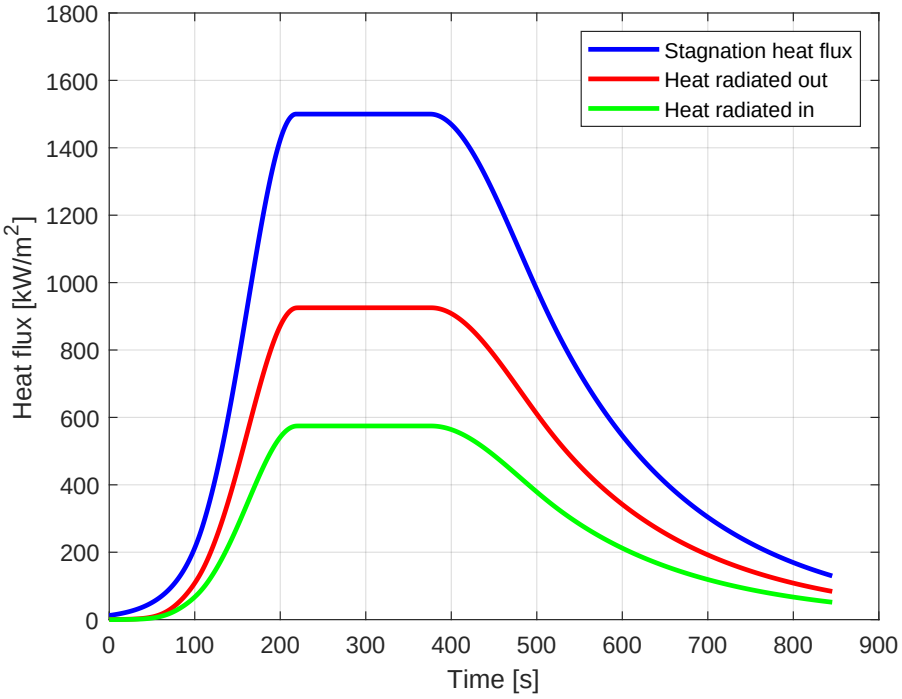

Figure 5-1: Distribution of heat flux (PM2000, cooled).

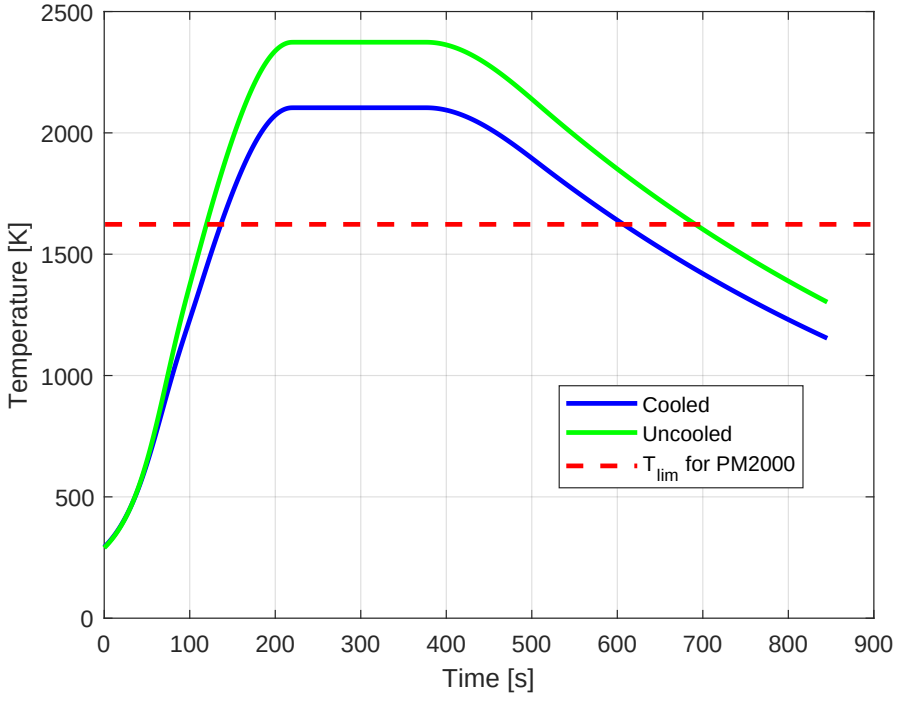

Figure 5-2: Variation of skin temperature as a function of time (PM2000, cooled and uncooled).

The porous layer temperature variation can be seen in Figure 5-3. The plot shows temperature profile for both cases, actively cooled and uncooled system. The temperature of porous layer for an uncooled system, very rapidly attains an equilibrium with the outer

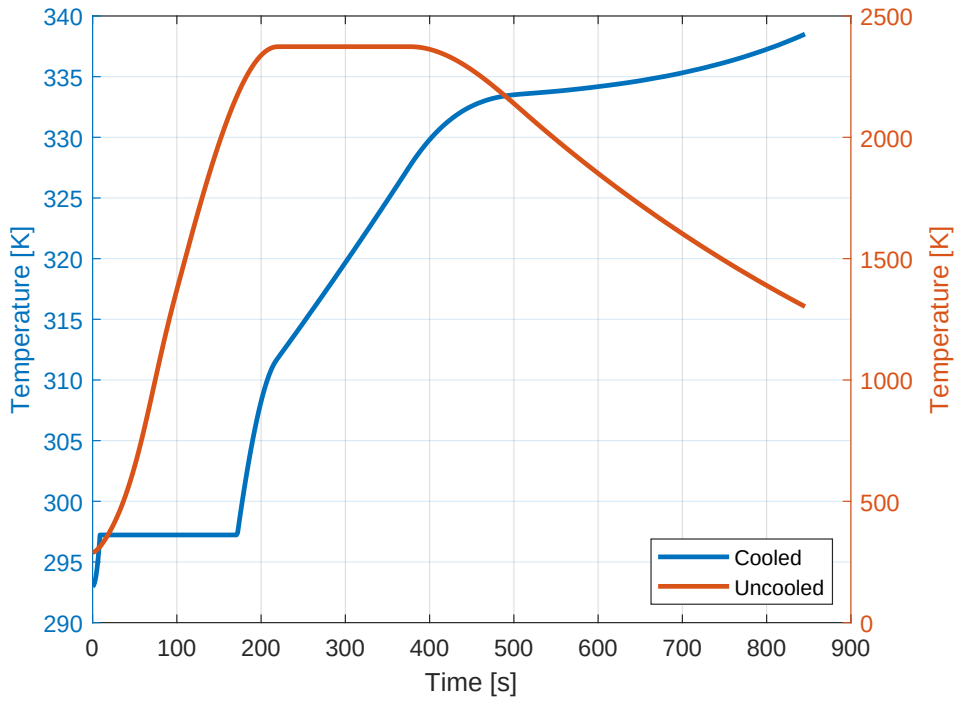

Figure 5-3: Variation of porous layer temperature (outermost surface) as a function of time (PM2000, cooled and uncooled).

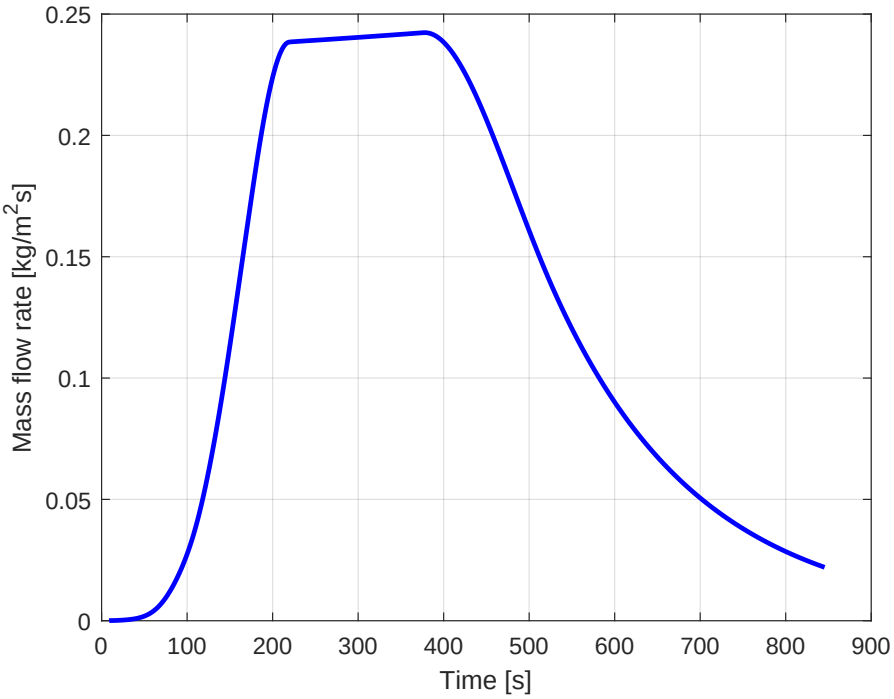

Figure 5-4: Variation of coolant mass flow rate as a function of time (PM2000, cooled).

skin temperature. This means there is negligible or almost no heat flux radiated inwards from the outer skin after a certain point. For the cooled system, as expected, the temperature rises as vehicle re-enters the Earth's atmosphere and the skin temperature rises. The porous

layer temperature is related to the coolant's evaporation temperature, which is dependent on the system pressure. The stagnation pressure increases as the vehicle enters the Earth's atmosphere, correspondingly, the system pressure must be increased, to limit the stress on the outer skin. With this increase in system pressure, the physical properties of the coolant such as the evaporation temperature increases. Therefore, a gradual rise in the porous layer temperature is seen.

5-2 Concept modification

As seen in Section 5-1, PM2000 cannot sustain a maximum heat flux of 1500 kW/m^2. The expected material temperature, for the given heat load constraint, exceeds its maximum operating temperature. Therefore, alternate solutions must be found. A few changes to the enhanced radiation cooling concept are proposed in this section, and the revised concept will be referred to as modified enhanced radiation cooling (or Modified ERC). These changes are implemented in the design, and analysed to study performance of the system. Results for the same are discussed in this section. Each of the design changes proposed has an adverse consequence, which requires attention. This too shall be briefly discussed in this section.

5-2-1 Blocking effect

To increase performance of the ERC concept, it is proposed to introduce small holes in the outer skin of the TPS layer, specifically in the stagnation region. Evaporated coolant will be vented out, from the gap to the surrounding, through these holes. The gaseous coolant will flow out into the boundary layer and provide a thermal blocking effect. This is caused mainly due to the following two reasons.

1. The coolant vapour seeping out undergoes chemical dissociation, which is an endothermic process. This reaction reduces the incident heat flux on the skin surface.

2. The coolant vapour forms a thin layer along the skin surface, which pushes the hot gas layer away from the skin and it is no longer in direct contact with the skin. Some portion of the enthalpy is lost across this additional layer, leading to a reduced heat flux incident on the skin surface.

Blocking effect has been studied earlier, though not for this concept, and is discussed in Section 5-2-1. Followed by a discussion on the consequences of making this change in the concept, in Section 5-2-1. Lastly, in Section 5-2-1, the implementation of blocking effect in the thermal model is discussed, along with performance of the design after introducing this change.

Literature

Blocking effect has been studied by researchers in the past, though not for this concept. It has mainly been studied for transpiration cooling systems. This system consists of only a coolant filled porous layer. The aerodynamic heat flux is directly incident on the porous layer. Coolant evaporates and gaseous coolant seeps into the boundary layer.

Foreest et al. (2009) carried out experiments in an arc jet wind tunnel on three different sized cone shaped nose samples, made up of a porous material known as Procelit 170 (P170) and water as coolant. A simple analysis for investigating the blocking effect in the system

was conducted. Using an analytical model, the expected evaporation rate was estimated and then compared with the flow rate in the experiment. This was done for all three noses and it was seen that in each sample the actual coolant mass flow was less than expected. Blocking effect was speculated as the cause for this difference. The estimated blocking effect lies in the range of 22% to 31%, increasing as the nose radius increases. However, these estimates were limited to the experimental set-up and the wind tunnel conditions.

Glass (2008) conducted a numerical analyses for a convection/ transpiration cooling system, to be used for combustion engines. The viscous flow in the boundary layer was studied, by means of a software developed using implicit finite difference method, which proved that the transpired hydrogen coolant does provide a blocking effect to the system. In this case, blocking effect was attributed to the fact that the coolant forms a layer along the surface, removing the freestream oxygen and facilitates reduction of heat due to oxidation. Also, the work stated that a minimum injection rate is required to ensure significant blocking. Using a finite difference method for thermal analysis of the porous media, it was observed that the evaporation rate was much higher than the minimum injection rate required. No attempt was made to quantify the blocking effect or to give any general relations to make a simple estimate.

Grinberg et al. (1968) developed a complete analytical model for a transpiration cooled nose tip, that consisted of various sub-routines to estimate trajectory paramters, shape optimisation, flow and temperature analysis. Using this model, the blocking effect was shown for a sample case. Blocking effect was said to be 20% in case of turbulent flow and 60% in case of a laminar flow. The model was a first estimate and used simplifying assumptions to analyse the flow field. Experimental validation of the analytical model was not conducted.

Savin (1968) investigates blocking for a different concept. In this work, an ablative system, for a long-range ballistic missile, is numerically analysed and correlated with experiments performed in the Ames entry simulator. The blocking effect obtained due to the vapour formed during ablation is shown, for different thermoplastic materials, under different flow conditions i.e., laminar flow, turbulent subsonic flow and turbulent supersonic flow. The values for blocking are seen to vary, depending on the material and the flow conditions. It is highest for the laminar flow and least for the supersonic turbulent supersonic flow. The values lie in the range of 15% to 50%.

Based on all the past work, it can be concluded that blocking effect will be obtained if the coolant vapour is allowed to seep out into the boundary layer. Although, this cannot be easily estimated and its value varies depending on the flow conditions, the material and size of the nose.

Consequences

There are various consequences of allowing the coolant to seep out into the boundary layer at the stagnation region. Blocking effect is a positive consequence. However, there are other possible negative consequences that must be considered. There is always a risk of contaminating the boundary layer, leading to unexpected or unwanted chemical reactions. Also, depending on the rate at which the coolant vapours seeps out, the boundary layer flow can be disrupted, leading to an unwanted flow disruption.

The number of holes and their location on the nose surface could have an influence on the blocking, which must be studied. Also, when these holes are made in the outer skin, the cooling system is no longer a closed system. This means that the pressure in the gap is directly dependent on the stagnation pressure. And performance of the nitrogen system,

proposed for the closed enhanced radiation cooling system, becomes a critical aspect to the cooling system. If for some reason the pressure in the gap drops below the stagnation pressure, there is a possibility of inflow of hot gas, which can be catastrophic and should be avoided at all costs. More about this has been discussed in Section 5-4-3, along with a possible solution and operating sequence for maintaining the gap pressure.

It must be noted that the above discussed consequences have not been analysed, as that is not possible without detailed numerical simulation of the boundary layer flow, combined with plasma wind tunnel experiments. This means that, although blocking effect is proposed as a solution, it must be thoroughly tested in plasma wind tunnels and numerically analysed, before implementing it for flight experiments.

Implementation and results

Based on literature discussed in Section 5-2-1, an approximate value for blocking effect has been assumed, i.e., 30%. This is a conservative value and lies in the range of values suggested in literature, for different materials, flow conditions and nose radius sizes. In practice, it can be higher or lower, however, a first estimate is needed to obtain some values. In the future, these values can be verified against plasma wind tunnel tests.

According to Foreest et al. (2009), the blocking effect reduces the evaporated coolant mass flow by a certain percentage. Using Equation (4-8), assuming heat of evaporation of water does not change, the result can be extended to say that the incoming heat flux is reduced by the same percentage. Now, for lesser heat flux to be radiated inwards, all other material properties remaining constant, the temperature of the skin is lower, which means that lesser aerodynamic heat flux is incident on the outer skin. This is in line with the expected effect of blocking. Although, it must be noted that this is a very crude approximation.

Equation (4-3) is modified to include the blocking effect, q_{blck}, the heat flux blocked by the coolant vapour layer. The revised equation for estimating skin temperature is as seen in Equations (5-1) and (5-2).

$$\rho_s c_{p,s} x_s \frac{dT_s}{dt} = q_{stag} - q_{in} - q_{out} - q_{blck} \tag{5-1}$$

$$T_{s,new} = T_{s,old} + \frac{dt * (q_{stag} - q_{in} - q_{out} - q_{blck})}{\rho_s c_{p,s} x_s} \tag{5-2}$$

Using the revised formulation and thermal analysis tool, the TPS design proposed in Chapter 3 is analysed for the nominal trajectory. Results obtained for performance of the design, compared with the results without blocking, are seen in Figures 5-5 and 5-6. As expected, performance of the system improves. Maximum temperature of the skin is relatively lesser for the case with blocking, same as the coolant mass flow required. However, the maximum operating temperature of the outer skin material is still reached, meaning the design needs to be further modified.

5-2-2 Skin material

As is seen in the previous section, even after taking the blocking effect into account, PM2000 cannot handle the maximum heat load constraint for the nominal trajectory defined in this study. At this point, there are two possible solutions, to improve performance of the design. First option is, to increase the nose radius, such that the stagnation heat flux reduces

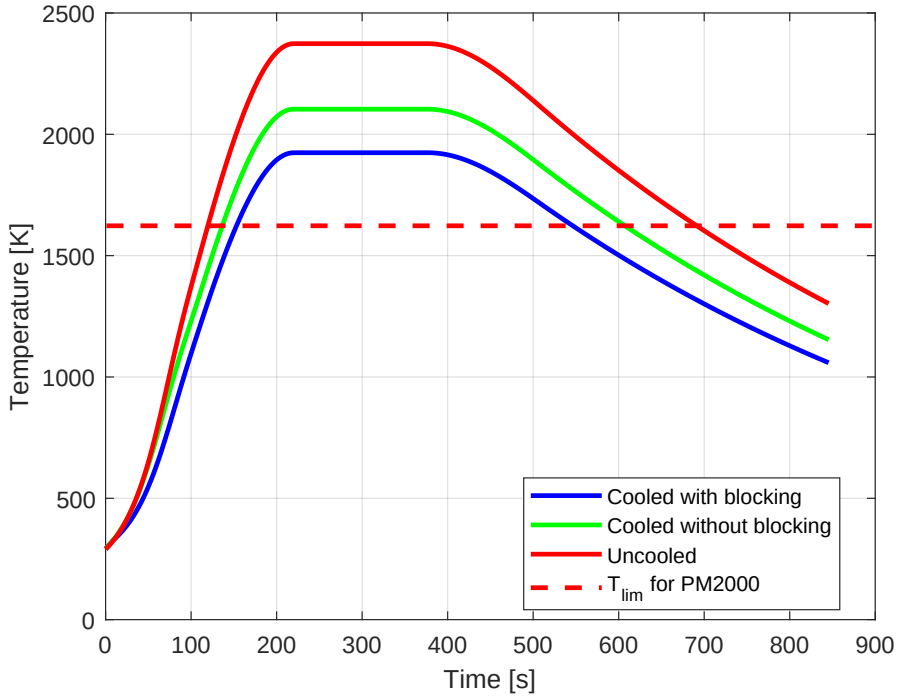

Figure 5-5: Variation of skin temperature as a function of time (PM2000, cooled, with and without blocking).

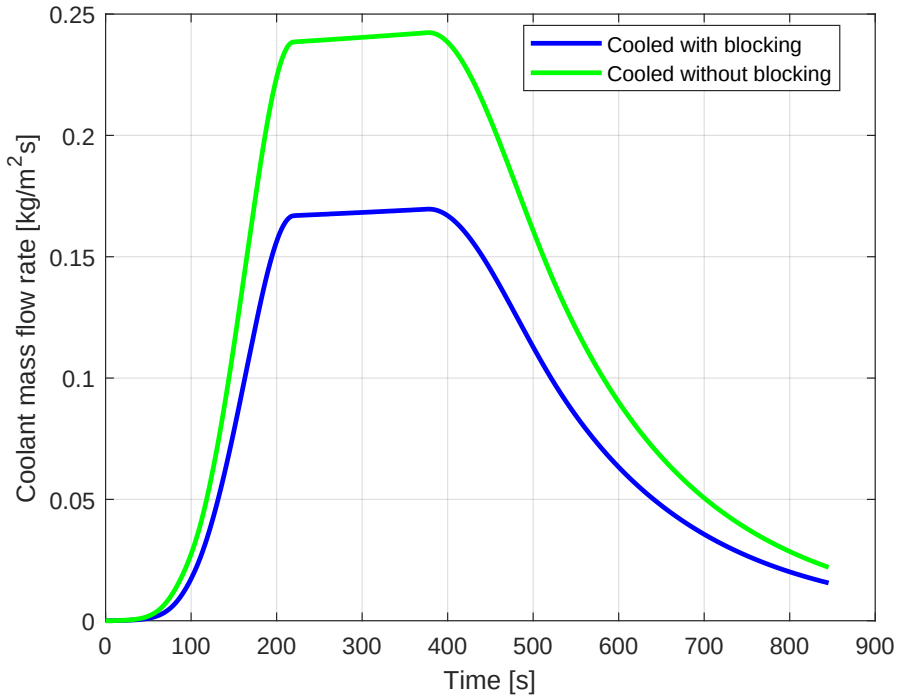

Figure 5-6: Variation of coolant mass flow rate as a function of time (PM2000, cooled, with and without blocking).

(Chapman's equation, stagnation heat flux is inversely proportional to the nose radius). Second option is, to change the material selected for the outer skin from metallic (PM2000)

to ceramic matrix composites (for example C/C-SiC), which have higher maximum operating temperatures (as discussed in Section 3-3-2 and seen in Figure 3-3), and therefore, have the ability to sustain a comparatively higher heat flux.

Consequences

Before comparing the two options and making a choice, it is important to understand the consequences of implementing them. In case of the first option, i.e., increasing the nose radius (changing the vehicle design), has a negative impact on the aerodynamic performance of the vehicle. This is because, the pressure or form drag increases with increase in frontal area of the vehicle. This can also be seen from the drag equation (given in Equation (5-3)), where the drag force (D) increases with velocity (V) and reference area (S_{ref}) of the vehicle. Also, it depends on the drag coefficient (C_D), which is a dimensionless coefficient, and its value depends on the vehicle's geometry. For example, in case of simple shaped objects, such as a sphere, the reference area is the cross sectional area of the sphere, which means a larger sphere will experience a stronger drag force. Similarly, in this case, increasing the nose radius will increase the drag experienced by the vehicle. This is the main drawback. On the other hand, increasing the nose radius is beneficial in terms of the thermal loads experienced by the vehicle. To explain this, the (cold wall) Chapman model for approximating the heat flux can be seen (given in Equation (5-4)), where the heat flux (q) is inversely proportional to the square root of the nose radius (R_N). This means, a vehicle with a larger nose radius will experience relatively lower stagnation heat flux during flight, given everything else remains the same. Therefore, a compromise is required between the aerodynamic performance and thermal loads experienced by the vehicle.

$$D = \frac{1}{2}\rho V^2 S_{ref} C_D \tag{5-3}$$

$$q = \frac{c_1}{\sqrt{R_N}}\sqrt{\frac{\rho}{\rho_0}}\left(\frac{V}{V_c}\right)^{c_2} \tag{5-4}$$

In case of the second option, i.e., changing the material of the outer skin from metallic to ceramic matrix composite (CMC), again there are several positive ad negative consequences. This is discussed further ahead, however, before doing so it is important to discuss more about CMCs and its application in space systems. Ceramic matrix composites consist of a combination of different fibres and matrix materials such as carbon (C), silicon carbide (SiC), alumina (Al_2O_3) and mullite (Al_2O_3-SiO_2). CMCs were developed to overcome the drawbacks of conventional ceramics, such as silicon carbide, carbon, silicon nitride, alumina, etc., including the poor mechanical and thermal load baring ability and poor crack resistance. There are various CMCs available in the market currently, and are differentiated based on the type of fibre and type of matrix material used, as well as based on the manufacturing process. In general, CMCs are light weight, have high thermal shock resistance and high operating temperatures. Compared to oxide based CMCs, non-oxide CMCs, such as carbon fibre reinforced carbon (C/C) and silicon carbide fibres, are found to have relatively better performance, in terms of creep resistance and tensile strength, even at high operating temperatures (up to 2000°C). However, C/C has poor oxidation resistance at temperatures above 450°C, which is a major drawback of this material. Therefore, C/C cannot be used in oxidising atmospheres, unless extra measures are implemented to improve its oxidation resistance. One way is to combine it with a SiC matrix, which is oxidation resistant up to 1000°C, however this is still not sufficient for certain space applications such

as TPS, where temperatures up to 2000°C can be expected. Therefore, additional oxidation resistant coatings are necessary to improve the life and performance of these materials.

There are various techniques that are used to manufacture C/C-SiC, namely chemical vapour infiltration, polymer infiltration and pyrolysis and melt infiltration (liquid solid infiltration). These processes are not discussed in detail here. However, the three general steps involve,

1. Manufacturing of a C fibre preform or a CFRP preform.

2. Build-up of a weak fibre/matrix interphase.

3. Build-up of a SiC matrix.

The quality of C/C-SiC material depends on the manufacturing process as well as the type of C fibre used, these include high tenacity fibres (usually used in liquid solid infiltration), intermediate and high modulus fibres (usually used with polymer infiltration and pyrolysis, chemical vapour deposition) and ultra high modulus fibres. Again, these fibre types are not discussed in detail here. The only important thing to note is that these fibres have an impact on the properties of the final material. As for this application the best manufacturing technique, i.e., polymer infiltration and pyrolysis, which is also the most complex and costly method, must be used to produce the material.

Now, the oxidation resistant coating must satisfy certain requirements for it to be used for this application, described in Bansal and Lamon (2014). The first and most obvious requirement is that it should inhibit the ability of oxygen diffusion. Next, it should have a good match with the C/C-SiC material in the aspect of thermal expansion to avoid development of cracks. Also, the coatings should have low volatility during service process. It should have compatible stability and good interfacial bonding with the main material. An additional requirement, specific to application on the proposed TPS is a self healing property, that can make the use of C/C-SiC comparable to metallic in terms of oxidation resistance. There is a lot of on-going research in the field of self healing coatings, such as the work carried out by Fan et al. (2019) and Chang et al. (2017). Although these studies are very promising, till date a self healing coating has not been successfully developed and demonstrated. In the absence of this property, the coating will degrade over time and there is a possibility of small cracks and holes, which are not easy to inspect. Therefore, the inspection and maintenance cost and time required is higher, as the coating needs to be refurbished after every 4 to 5 flights depending on the rate of degradation.

There are various ways of preparing the coatings, including pack cementation, chemaical vapour deposition, plasma spraying, slurry method, etc. (Bansal and Lamon, 2014). Also, there are different types of coatings, namely glass coatings, metal coatings, ceramic coatings, composite coatings, etc. In earlier times, research was focused on glass coatings, however over time the field of research has expanded to metal and ceramic coatings. Metal coatings such as Hafnium and Chromium are widely used, because of their high melting point and low oxygen permeability (Bansal and Lamon, 2014). Alternately, ceramic coatings have an outstanding performance because of the self healing properties of SiO2 (Bansal and Lamon, 2014). Also, for better matching of the thermal expansion coefficient between the substrate and coating, a gradient coating is applied, such that the different layers of the coating have a gradually varying thermal expansion coefficient. Similarly, composite coatings have been developed that combine ceramic and metal coatings to obtain improved properties (Bansal and Lamon, 2014). It must be noted that the thickness of the coatings are generally a few

microns and this would have an impact on the emissivity of the substrate, however this has been neglected in this study.

Implementation and results

The advantages and disadvantages of increasing the nose radius and of changing the outer skin material are identified and listed in Table 5-3 (can be found on the last page of the chapter). It must be noted that this list is not exhaustive. There could be more advantages and disadvantages for each case, however, the most significant ones have been listed down. From Table 5-3, it is clear that both options have significant drawbacks, and neither can be considered better. The designer has to decide which criteria are given more weight, that will help decide the most suitable design. For example, in most cases, cost is the deciding factor, because of which most designers would chose to compromise on aerodynamic performance of the vehicle and increase the nose radius. Alternately, if in future, a better material than PM2000 is found, with a higher operating temperature limit and without the drawbacks of ceramics, then the second option would be selected. There is plenty of research on-going on oxidation coatings, as discussed above, so if any of these studies are successfully verified and validated, by means of ground (plasma wind tunnel) and flight tests, then ceramics would be an excellent and more preferred choice.

For the purpose of this study, it would be interesting to see how the system would perform under such high heat loads, for example, the amount of coolant required. Therefore, the vehicle design and mission profile is given higher weightage, and it is proposed to change the material to C/C-SiC. It must be noted, in practice this might not be recommended, because of the higher costs. Choosing a C/C-SiC nose means that extra coatings are required and these coatings are not fully oxidation resistant. Therefore, after a few flights they must be reapplied. A possible solution to do this without affecting the flight turn around time is, to have a relatively simple nose assembly and have a spare nose, such that it can be replaced whenever required. As for the increased inspection requirements, the spare nose solution can be implemented to save time between flights. Alternately, a automated inspection technique can be applied, where by the use of AI, the nose can be scanned for damages. However, both these solutions will add to the cost. It must be noted that the effect of changing nose radius will also be studied, but under Section 6-2.

Results for a C/C-SiC nose, including blocking effects, are seen in Figures 5-7 and 5-8. The system performs as expected, the maximum operating temperature of the material is not violated. The total coolant mass required, for the nominal trajectory, is 402 g.

5-3 Design sizing

In Chapter 4, size of the TPS layers is arbitrarily selected, based on literature. Now, before proposing the conceptual design, it is important to understand the influence of sizing on performance of the system. Therefore, the thickness of the outer skin and the air gap is varied, correspondingly thickness of the porous layer varies, such that the nose radius remains the same. As seen in Table 5-1, three skin thickness values, 0.5 mm, 1 mm and 1.5 mm, are considered. 1 mm is the initial value proposed, since the concept is based on a thin skin, a large variation is not considered. Increasing the skin thickness by a large amount, would increase the mass of the TPS layer, also the temperature gradient across a thick layer is larger, leading to higher thermal stresses, which should be avoided. Decreasing

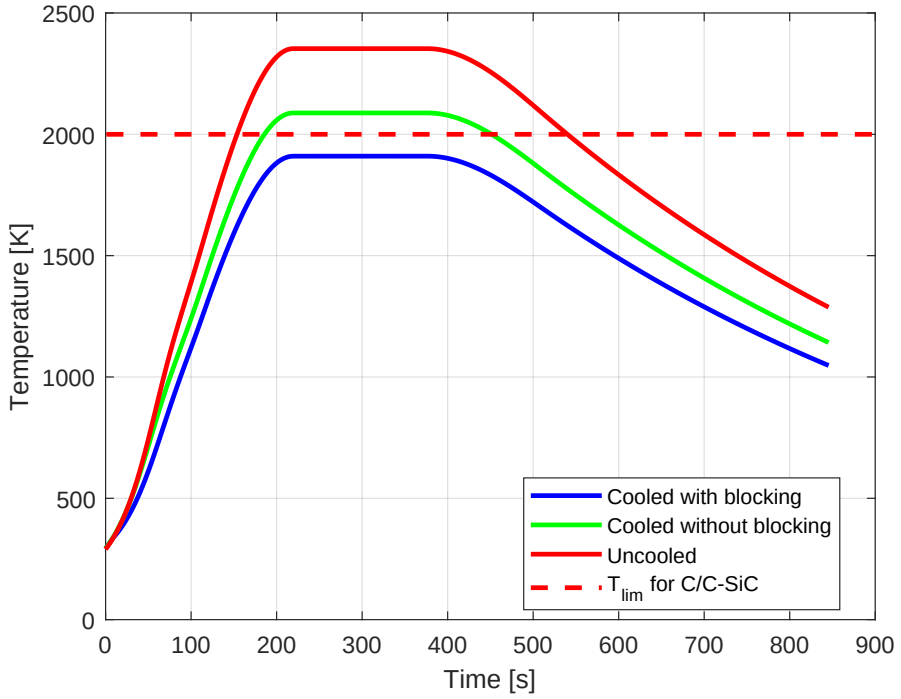

Figure 5-7: Variation of skin temperature as a function of time (C/C-SiC, cooled with blocking, 5mm gap).

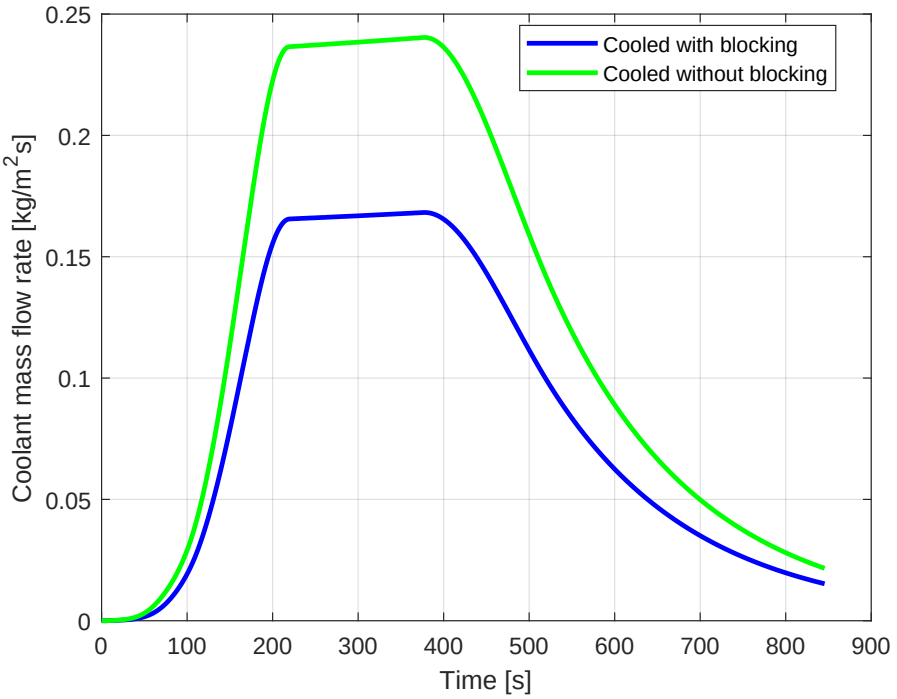

Figure 5-8: Variation of coolant mass flow rate as a function of time (C/C-SiC, cooled with blocking, 5mm gap).

the skin thickness too much can have an impact on the structural integrity. Therefore, the skin thickness is increased and decreased by 0.5 mm, with respect to the initial thickness.

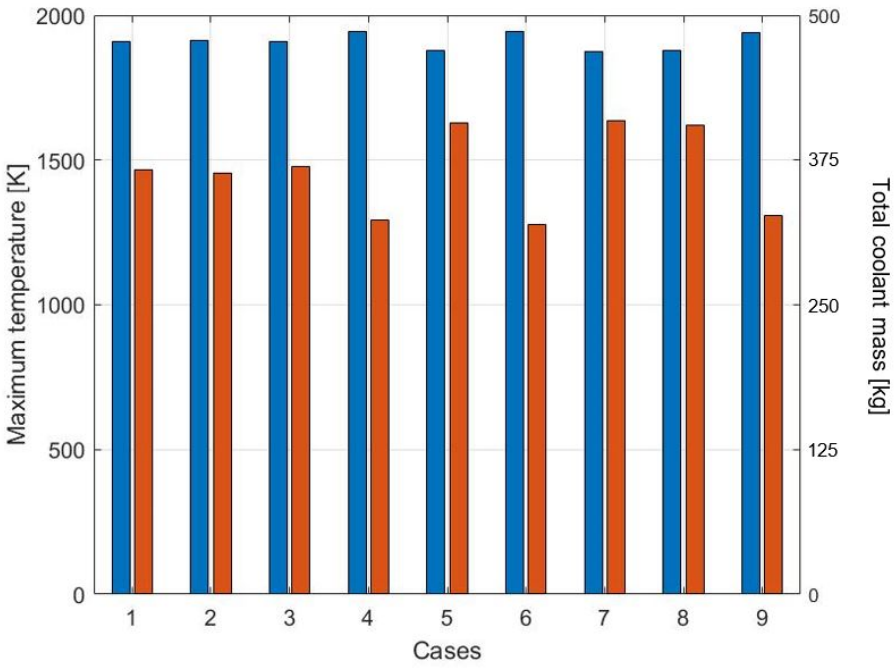

Figure 5-9: Effect of change in skin and gap thickness on the system performance.

Similarly, for the gap thickness, 3 mm, 5 mm and 7 mm, is considered. The flow in the gap is expected to be laminar, however increasing or decreasing the gap by a large value could have an impact on the flow. All possible combinations of skin and gap thickness are explored. The results are seen in Figure 5-9 and in Table 5-1.

Case 1 is the initial design, referenced as nominal design only for this section. Case 5 is found to have the best performance out of all the cases. The maximum operating temperature is reduced by 33 K, with negligible increase in the total coolant mass. Also, it is observed that varying the skin thickness has a negligible impact on the performance. However, varying gap thickness shows a considerable impact, especially on the maximum temperature. This is because, the heat radiated inwards depends on the ratio of inner and outer radius as seen in Equation (4-2), which means it indirectly depends on the gap thickness.

Table 5-1: Comparison of system performance based on different skin and gap thickness.

Case	**Skin thickness [mm]**	**Air gap [mm]**	**Max. skin temperature [K]**	**Coolant mass [g]**
1	1	5	1910	367
2	1.5	5	1912	364
3	0.5	5	1908	369
4	1	7	1944	323
5	1	3	1877	384
6	1.5	7	1946	319
7	0.5	3	1876	409
8	1.5	3	1878	405
9	0.5	7	1941	327

5-4 Proposed conceptual design

In Section 5-4-1, the conceptual design of the active cooling TPS is proposed, followed by the results with respect to its performance, in Section 5-4-2. It should be noted that the conceptual design proposed in this section is based on relatively simplified thermal analysis. This is just the first step towards developing the system, using a simple engineering approach. More detailed thermo-structural analysis and numerical simulations are required, including optimisation, before a complete design can be proposed. The operation sequence of the cooling system is discussed in Section 5-4-3, along with a schematic diagram of the system for better understanding. Additionally, many experiments are required before all teething problems of the system and design can be solved, these are also briefly addressed. Lastly, in Section 5-4-4, drawings for the proposed conceptual TPS design for a nose is given.

5-4-1 Concept description

Modified enhanced radiation cooling, an active cooling thermal protection system, is proposed for cooling the nose of the Hyperion II test vehicle. It consists of a coolant filled porous layer, covered by a thin outer skin, with a gap in between the two layers. In this case, water is selected as a coolant, along with a 22 mm thick ZAL-15 porous layer and a 1 mm thick C/C-SiC outer skin, with a 3 mm gap. Five small holes in the skin, of 1 mm radius each, are proposed, to be located in the stagnation region. It must be noted that the number and size of holes is a first assumption and should be analysed in detail, in the future. When heated, the outer skin radiates heat in both directions, inwards to the underlying porous layer and outwards back to the environment. Heat radiated inwards, heats up the porous layer and the coolant. Once evaporation temperature of the coolant is reached, the incoming heat energy is absorbed by the coolant during phase change, from liquid to vapour. In the stagnation region, small holes are drilled in the nose cap, so as to allow the evaporated coolant to be vented out from the gap.

Sufficient coolant for the complete re-entry flight has to be carried, for which a coolant tank is required. Control valves can be used to start, stop or vary the supply of coolant to the porous layer, along with a processor and sensors (details are discussed in Section 5-4-3). Some part of the coolant supply line is pierced into the porous layer, so that the portion of porous layer closest to the stagnation region is rapidly filled with coolant, as heat flux in this area is the highest. To maintain the gap pressure, above the triple point pressure of coolant; and if needed, to push coolant into the porous layer, a nitrogen gas system is proposed. Once again, depending on the amount of nitrogen required during flight, a nitrogen tank is necessary. Based on some simple calculations, it can be stated that the nitrogen tank will be smaller in size, as compared to the coolant tank. Similar to the coolant tank, control valves are required in the nitrogen supply lines to start, stop or vary the flow. This cooling system has been schematically represented in Figure 5-10. This diagram is useful to understand the sequence of operation of the cooling system, explained in Section 5-4-3.

The steps described below, discuss an analytical approach for roughly estimating the mass flow rate and amount of Nitrogen gas required. This approach is useful in making a first estimate of the size of the nitrogen tank.

1. *Calculate velocity or mass flow rate of nitrogen lost through the small holes*
   To do this, the assumptions of a restrictor plate/ orifice plate are used. By assuming steady-state, incompressible (constant fluid density), inviscid, laminar flow (no change

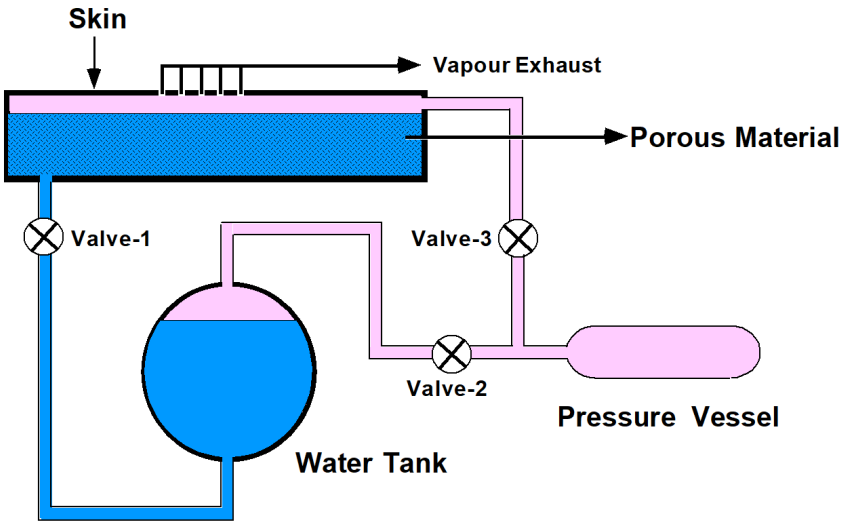

Figure 5-10: Schematic representation of the proposed cooling system.

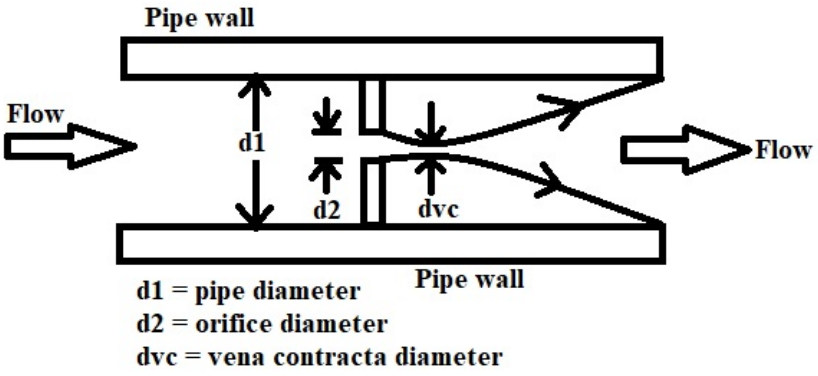

Figure 5-11: Schematic representation of vena contracta.

in elevation) with negligible frictional losses, Bernoulli's equation reduces to an equation relating the conservation of energy between two points on the same streamline:

$$P_1 + \frac{1}{2}\rho V_1^2 = P_2 + \frac{1}{2}\rho V_2^2 \tag{5-5}$$

As per the continuity equation,

$$Q = A_1 V_1 = A_2 V_2 \tag{5-6}$$

Using Equation (5-6) in Equation (5-5) and after re-arranging the terms we get,

$$P_1 - P_2 = \frac{1}{2}\rho \left(\frac{Q}{A_2}\right)^2 - \frac{1}{2}\rho \left(\frac{Q}{A_1}\right)^2 \tag{5-7}$$

Further, solving for Q we get,

$$Q = A_2 \sqrt{\frac{2\left(P_1 - P_2\right)/\rho}{1 - \left(A_2/A_1\right)^2}} \tag{5-8}$$

$$Q = A_2 \sqrt{\frac{1}{1 - (d_2/d_1)^4}} \sqrt{2\left(P_1 - P_2\right)/\rho} \tag{5-9}$$

The above expression for Q gives the theoretical volume flow rate. Introducing the beta factor $\beta = d_2/d_1$ as well as the coefficient of discharge C_d:

$$Q = C_d A_2 \sqrt{\frac{1}{1 - \beta^4}} \sqrt{2\left(P_1 - P_2\right)/\rho} \tag{5-10}$$

Multiplying by density of the fluid to obtain an equation for the mass flow rate,

$$\dot{M}_{loss} = C_d A_2 \sqrt{\frac{1}{1 - \beta^4}} \sqrt{2\rho\left(P_1 - P_2\right)} \tag{5-11}$$

Deriving the above equations used the cross-section of the orifice opening and is not as realistic as using the minimum cross-section at the vena contracta. In addition, frictional losses may not be negligible, plus viscosity and turbulence effects may be present. For that reason, the coefficient of discharge C_d is introduced. For rough approximations, the coefficient of discharge may be assumed to be between 0.60 and 0.75. For a first approximation, a value of 0.62 can be used as this approximates to a fully developed flow. In general, Equation (5-11) is applicable only for incompressible flows. It can be modified by introducing an expansion factor Y to account for the compressibility of gases. Y is 1 in case of incompressible flows.

$$\dot{M}_{loss} = Y C_d A_2 \sqrt{\frac{1}{1 - \beta^4}} \sqrt{2\rho_1\left(P_1 - P_2\right)} \tag{5-12}$$

The expansion factor Y, which allows for the change in the density of an ideal gas as it expands isentropically, is given by:

$$Y = \sqrt{r_p^{2/k} \left(\frac{k}{k-1}\right) \left(\frac{1 - r_p^{(k-1)/k}}{1 - r_p}\right)} \tag{5-13}$$

where, $r_p = P_2/P_1$ and k is the specific heat ratio (c_p/c_v). Equation (5-13) gives the mass flow rate of the nitrogen gas lost through a small hole in the stagnation region of the nose.

2. *Calculate volume of air gap.*
The volume of the air gap can be obtained from the volume formula of a half hemisphere. In this case, the air gap is formed between two concentric hemispheres, namely the skin and the porous layer. Therefore, the volume of the air gap is given as,

$$v_{gap} = \frac{2}{3}\pi r_{skin}^3 - \frac{2}{3}\pi r_{porous}^3 \tag{5-14}$$

3. *Calculate mass of the gas required to fill the gap and to maintain a required pressure.*
The equation of state, as seen in Equation (11), is used for calculating the mass of nitrogen required to fill the gap.

$$m_{gap} = \frac{P_1 v_{gap}}{RT} \tag{5-15}$$

where, m is the mass of nitrogen gas required to maintain a pressure P_1 at temperature T. Here, R is the specific gas constant i.e., universal gas constant divided by the molar mass of the gas.

4. *Calculate the mass flow rate required to fill the gap and to maintain a desired pressure.* The mass flow rate required for filling the gap and maintaining the desired pressure can be estimated by calculating the mass of nitrogen lost over the time period t and the mass required to fill the gap at the desired pressure. This gives the total mass of nitrogen required, which when divided by the time period, gives the mass flow rate with which the air gap shall be filled.

$$m_{total} = \dot{M}_{loss} t + m_{gap} \tag{5-16}$$

$$\dot{M}_{required} = \frac{m_{total}}{t} \tag{5-17}$$

Thus, in this manner the total mass of nitrogen and its mass flow rate can be estimated. In addition to this mass, extra nitrogen should be carried as buffer. It can be used for pushing the coolant into the porous layer and also be required in case gap pressure drops because of some reason.

5-4-2 Results

Performance of the design for the proposed cooling system, for nose radius of 26 mm, expected to fly along the nominal trajectory, is measured by means of the temperature profile and coolant mass requirements. From Figure 5-12, it can be seen that for a maximum heat load constraint of 1500 kW/m^2, operating temperature of the skin material is less than the maximum operating temperature. Also, from Figure 5-13, the coolant mass flow rate variation with respect to the time of flight can be seen. The total coolant mass required is 384 g. However, the actual requirement is expected to be lesser, because this estimation assumes that the heat flux over the entire nose is the same as that for stagnation point, which will not be the case. The heat flux in the region surrounding the stagnation point can be approximated as $q = q_{stag} cos^{1.5}\theta$ (Simeonides, 1995) when $\theta \leq 70°$, where θ is the surface inclination with respect to the tangent at the stagnation point. So for a hemispherical nose, assuming $\theta = 70°$, the heat flux $q = 0.2 q_{stag}$, which correspondingly reduces the coolant mass evaporated. Nonetheless, the coolant mass estimated here is a conservative value and is a good first estimate for the design's performance.

It must be noted that the results produced here are a first estimate based on a simplified thermal analysis, and are considered sufficient to prove that the concept has potential. However, more detailed analysis, using numerical solutions is recommended, other than experiments in plasma wind tunnel, before going for flight testing. The performance of this concept is limited by the maximum operating temperature of the outer skin material. For this study, a carbon matrix ceramic is chosen over a metallic material, to meet the set requirements. However, doing so has many consequences as discussed in Section 5-2. A metallic material would be preferred if the nose radius of the vehicle was larger, in which case, a compromise is made on the aerodynamic performance of the vehicle. This means that in the future, the design has to be optimised such that satisfactory aerodynamic performance of the vehicle and thermal performance of the TPS is obtained. It is very much possible that a metallic skin is preferred for design in the future, simply because it is less costly.

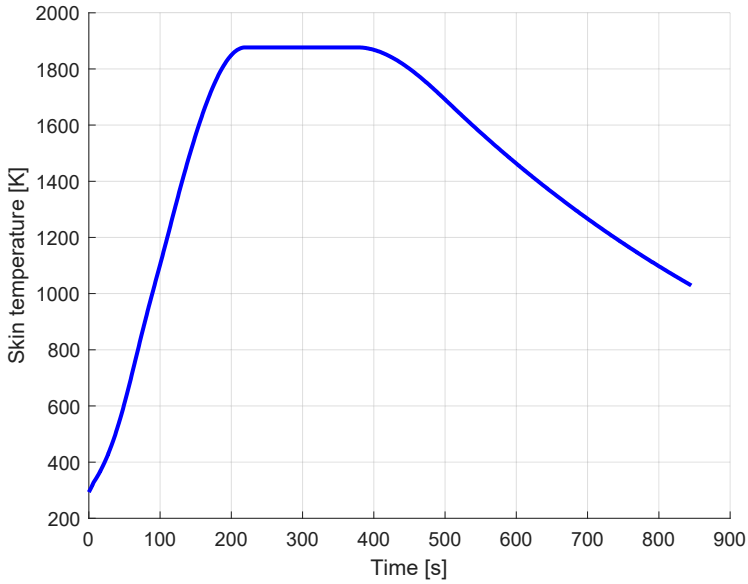

Figure 5-12: Variation of skin temperature as a function of time (C/C-SiC, cooled with blocking).

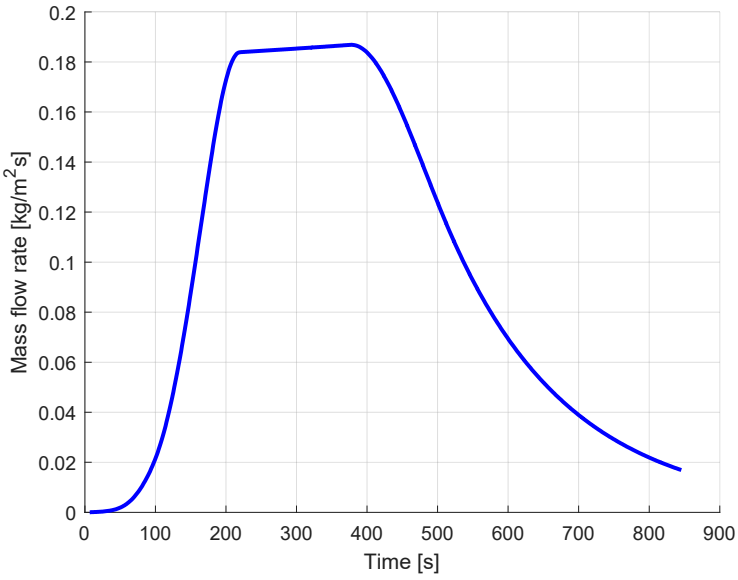

Figure 5-13: Variation of coolant mass flow rate as a function of time (C/C-SiC, cooled with blocking).

However, there is plenty of research on-going in the field of ceramics and oxidation resistant coatings, which if successful, could be a major breakthrough for the space industry.

5-4-3 Cooling system operation sequence

Operation sequence of the cooling system is explained using the case analysed in this study. Therefore, the data provided is specific to that design and trajectory. The entry and end conditions for the vehicle's re-entry phase are given in Table 5-2.

Table 5-2: Entry and final conditions of the vehicle's re-entry phase as per nominal trajectory.

Parameter	Value
Entry altitude (H_E)	120 km
Entry velocity (V_E)	3300 m/s
Final altitude (H_F)	20 km
Final velocity (V_F)	907 m/s

As the vehicle begins to enter the Earth's atmosphere, the stagnation pressure as well as the stagnation point heat flux start increasing. During the ascent phase and time in space, the active cooling system is dormant, this means the porous layer is dry and coolant supply valve is kept shut. Now, as the vehicle begins its descent phase, the stagnation heat flux starts increasing. Pressure in the gap is approximately equal to the pressure in the stagnation region. If the coolant is supplied to the porous layer from the start, the low pressures will cause the coolant in the porous layer to freeze. Now, the problem is not the frozen coolant, it will still absorb heat causing sublimation. However, the capillary transport of coolant through the porous layer is not possible in the absence of a liquid phase, which leads to the sublimation plane to descend into the porous layer. This causes a rise in temperature for the porous layer, correspondingly a rise in the skin temperature.

As the altitude decreases, the stagnation heat flux increases rapidly. If active cooling is not initiated till pressure in the stagnation region is higher than triple point pressure, the stagnation heat flux can be as high as 400 kW/m^2 and correspondingly, temperature of the porous layer and skin can reach values as high as 1600-1800 K, depending on the design. Now at this point, after the materials have heated up, if the active cooling is initiated, the temperature of the porous layer is expected to drop to the coolant's evaporation temperature, which for water at low pressures is very low. This is not recommended, as it could add additional thermal stress to the layer. Also, it might lead to a lag in cooling. More water will be required, for reducing temperature of the porous layer. Plus, there is a chance that in some cases the maximum operating temperature of the porous layer is achieved, during the uncooled phase. Therefore, active cooling must be initiated earlier, to enable this, nitrogen gas is used to increase the pressure in the gap as compared to the pressure in the stagnation region. Nitrogen gas is proposed because, it has a very low freezing point.

For the first 120-130 seconds of the flight, when pressure in the stagnation region is lower than triple point pressure of the coolant, supply of nitrogen gas is required to maintain the pressure in the gap above the triple point pressure and to prevent the coolant from freezing. The nitrogen gas supply valve is opened, when the temperature in the skin/ porous layer reaches 273 K. To do so, a system of pressure and temperature transducers are proposed, which are attached to the skin and porous layer and communicate with a processor that controls the coolant and nitrogen supply valves. This processor is placed very close to the nose, to minimise wiring, and preferably it is programmed to operate with no or minimum intervention from the on-board computer, to enable quick system response. Alternately, these sensors can be avoided and the on-board computer can be used to control the valves based on estimates of the vehicle's altitude and velocity. However, this is not a preferred option, as the cooling system should be capable of functioning independent of the on-board computer. The pressure in the gap between the porous layer and skin is maintained at a pressure of 3000 Pa (which must be higher than the triple point of water, i.e., 612 Pa) . This pressure value has been arbitrarily selected and a different choice can be made, however

it is important to keep in mind the stress produced on the skin, due to the difference in pressure between the gap and the stagnation region. Nitrogen will expand as it is released from its compressed state and momentarily cause the temperature to drop in the system.

As the descent continues, the stagnation pressure and the stagnation point heat flux increase. Correspondingly, the temperature of the skin and porous layer will continue to rise. Once the temperature reaches 275 K (this is arbitrarily selected, it can be set at any value between 273.16 K and 280.12 K, which is the triple point temperature and the evaporation temperature of coolant at the gap pressure, respectively) and gap pressure is 3000 Pa, the coolant supply valve is opened, and the porous layer is filled with coolant.

The nitrogen supply is continued till the stagnation pressure increases above 3000 Pa. After which, the nitrogen gas supply is not required because the continuous evaporation of the coolant from the edge of the porous layer, will ensure a slightly higher pressure in the gap as compared to the pressure in the stagnation region. This difference in pressure should always be present to prevent inflow of hot air from the stagnation region to the air gap, through the holes in the skin. Therefore, the nitrogen gas carried should always be more than that required for the first phase of the flight, such that if for any reason the pressure in the gap is lower than the pressure in the stagnation region, nitrogen is supplied to increase the gap pressure. Also, if needed, nitrogen gas can be used to pump the coolant into the porous layer.

It must be noted that at least one temperature sensor is recommended to be installed in the porous layer and on the inner surface of the skin. Also, at least one pressure sensor is recommended to be installed on the inner surface of the skin. More sensors are always preferred for the purpose of gathering reliable and quality data. However, installing sensors in this system and finding the right location that is both, convenient for installation and is an ideal spot for data measurement, can be very difficult. Most temperature sensors need to be welded, these welds cannot be relied upon, as they are weak and detached welding is often observed. Alternately, a needle type temperature sensor can be used, in which the tip of the needle has a thermocouple that senses the temperature. Such a sensor can be pierced into the porous layer at a suitable location to obtain the temperature data. However, there is one problem, the material will expand when heated and contract when cooled, making it difficult to ensure contact of the sensor with the material at all times. An additional mechanism, possibly a spring mechanism, must be used to ensure the contact at all times. However, this further complicates the system. As for the pressure sensor, because the gap between the skin and porous layer is only 3 to 5 mm, once again installation is tricky. Similar to the temperature sensors, suitable locations must be found to install the pressure sensor. Therefore, use of sensors in this system is necessary, but has a lot of limitations and will require a lot of testing, making the system more complex and the development more costly. It is recommended to conduct a detailed study on sensors suitable for this application, along with easier installation techniques and ways to ensure good quality/ reliability of the measured data. Additionally, it is encouraged to find alternate solutions to control the system with minimum intervention from the on-board computer, other than relying on sensors for data. The sequence of events are listed below:

1. The cooling system is dormant for most part of the flight, during ascent and the time in space.

2. The cooling system is initiated by a command from the on-board computer, just prior to beginning the re-entry phase. This command is then passed on to the sensors, to start measurements. This means that the cooling system is dependent on the on-

board computer for initialisation, however once initialized, it is independent of the on-board computer. It is not recommended to rely on the sensors to initialise the cooling system, because any malfunction of the sensors or erroneous measurements due to poor contact, can prematurely initialise the system, leading to a loss in the mass of nitrogen and water, which is not acceptable.

3. Vehicle begins re-entry phase.
4. Pressure in the stagnation region and stagnation point heat flux start increasing.
5. Temperature and pressure sensors continuously send data to the controller.
6. Temperature of the skin/ porous layer rises to 273 K.
7. Controller opens the valve for the nitrogen supply line.
8. Nitrogen gas fills the gap.
9. Temperature of the skin drops, due to introduction of nitrogen and pressure in the gap is increased to 3000 Pa.
10. Temperature of the porous layer increases to 280 K and pressure is maintained at 3000Pa.
11. Once the temperature and pressure requirements are met, the controller sends a command to open the coolant supply line valve. To check this, data from the pressure sensor attached to the inner surface of the skin and temperature sensor in the porous layer can be used.
12. Coolant fills the porous layer.
13. Coolant evaporation from the edge of the porous layer begins, once the evaporation temperature for 3000 Pa i.e., 297 K, is reached.
14. As the vehicle descends, pressure in stagnation region and stagnation heat flux continue to increase.
15. Once pressure in stagnation region reaches 3000 Pa, controller closes the nitrogen supply valve, based on the data relayed by the pressure sensor. It must be noted that to measure the stagnation pressure, using a sensor is problematic, because of the difficulties in attaching a sensor in that region. Also, the location at which the sensor should be attached, to obtain correct data, is difficult to determine. Therefore, alternately, the expected stagnation pressure for a given altitude and velocity, can be obtained from the on-board computer. This data can then be used to check the pressure in the gap, by comparing it to the pressure data obtained from the pressure sensor attached to the skin. Another possible solution is, to use the data from the temperature sensor attached in the porous layer. If an abnormal temperature rise is observed, the nitrogen system should be initiated. Obviously, it is preferred to use data from both, the pressure and temperature sensor, to ensure that the sudden change is not due to a malfunction of the sensor or due to poor contact.
16. A check must always be conducted, to look for any anomalies in the pressure of the system for remainder of the flight.

17. If pressure of the system is less than the expected stagnation pressure, nitrogen supply valve is opened. Valve is closed once pressure stabilises.

18. Stagnation heat flux continues to rise till maximum heat load constraint is met along the trajectory. After which, the stagnation heat flux remains constant at the maximum value. Correspondingly, temperature of the skin rises and reaches a steady state temperature. Coolant evaporation continues.

19. As the coolant evaporates, the capillary action enables the porous layer to be continuously replenished with coolant.

20. The temperature sensor keeps a check on the porous layer temperature, if a rise in temperature is observed, it means that the rate of evaporation is higher than the rate at which coolant is being filled. In this case, nitrogen gas can be used to press the coolant into the porous layer, so as to rapidly fill the porous layer and to prevent it from reaching its critical saturation level.

21. As the vehicle further decelerates, the stagnation heat flux reduces, simultaneously reducing the temperature of the skin.

22. The coolant supply valve is closed once the temperature reaches 400 K.

5-4-4 Concept drawing

A 3D sectional view of the modified enhanced radiation cooled TPS concept discussed above, for a vehicle's nose, is seen in Figure 5-14, for better understanding of the concept. The TPS is mounted on a supporting plate, which has holes for connecting the coolant and nitrogen supply lines. The coolant is proposed to be filled from the centre and the supply pipe is inserted into the porous layer. This way in the stagnation region, where the heat load is higher, the coolant is rapidly supplied, followed by filling of the remaining layer. For the nitrogen supply, one or more supply ports can be used. Additional ports can be included for redundancy. The porous layer fits into a cavity in the supporting plate. As is seen in the figure, the outer skin has five holes in the stagnation region from where the water vapour is vented out. It must be noted that impact of the number and size of these holes on the system performance has not been analysed. Same applies for the coolant and nitrogen supply ports. Additionally, the material used for the supporting structure should be selected such that joining the outer skin and porous layer is possible. Also, the differential expansion between the supporting structure and the TPS layer should be accounted for and necessary seals must be included. In Figure 5-15, a cut section view of the nose with TPS layer is provided.

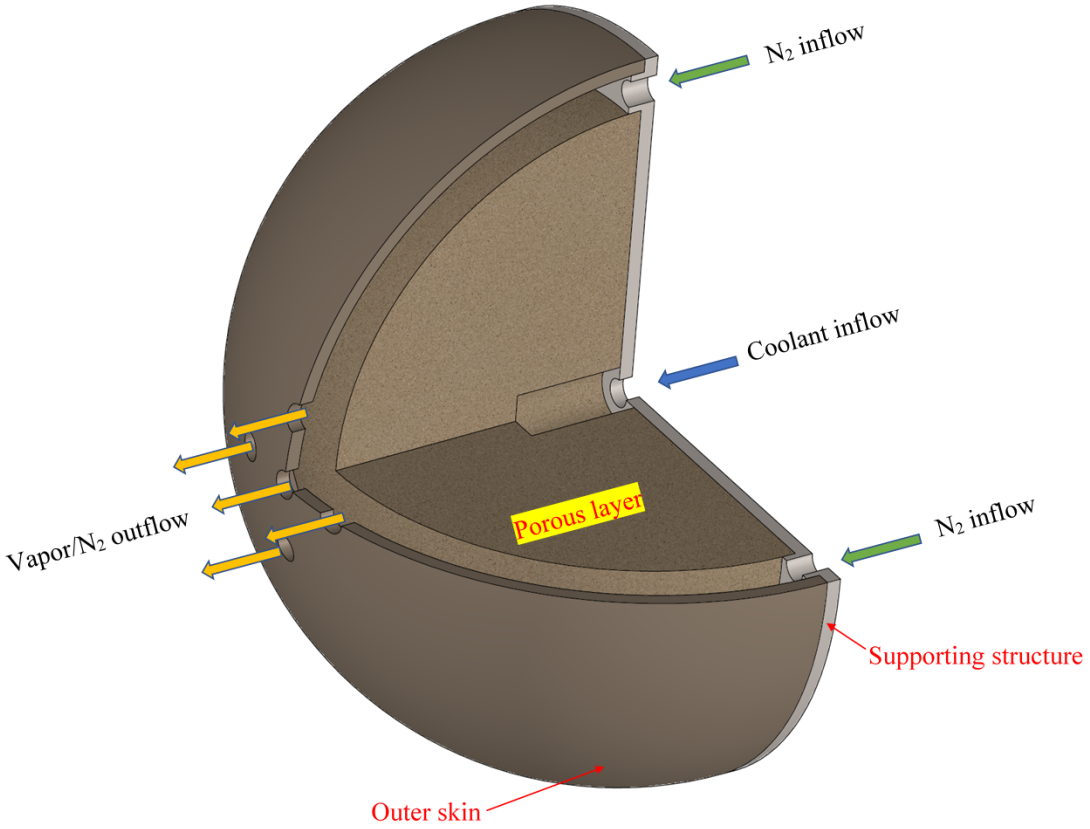

Figure 5-14: 3D view of the nose with a modified enhanced radiation cooled TPS.

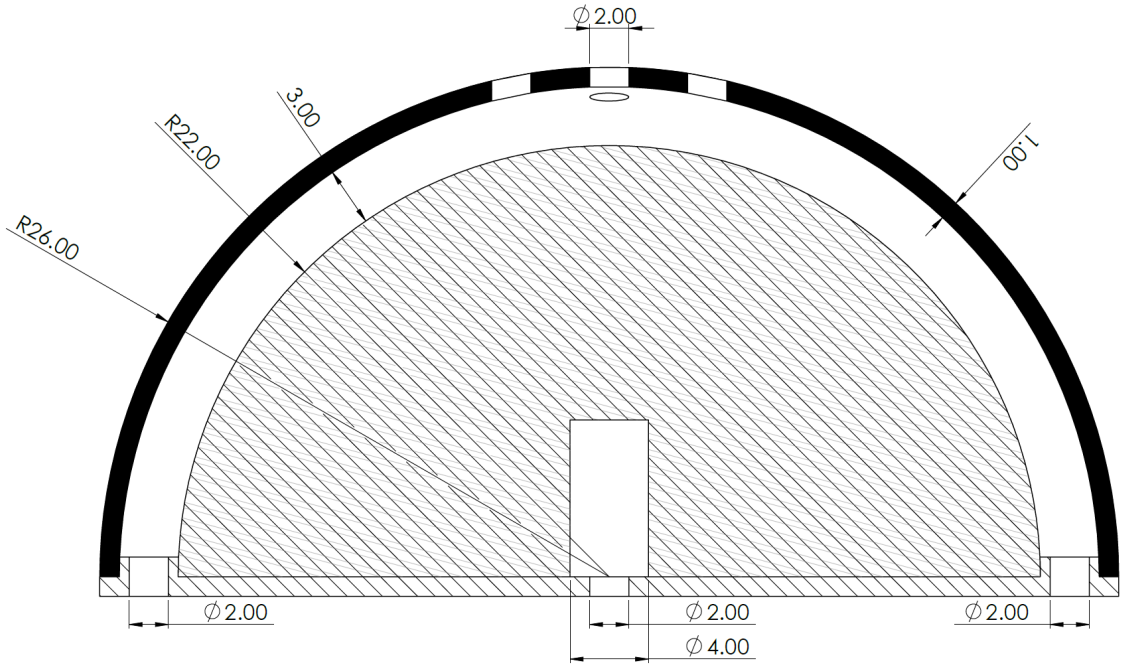

Figure 5-15: 2D view of the nose with a modified enhanced radiation cooled TPS (dimensions in mm).

Table 5-3: Advantages and disadvantages of changing nose radius and skin material.

	Increasing nose radius	**Changing material of outer skin**
Advantages	Maximum stagnation heat flux is reduced.	Maximum heat load constraint set for nominal trajectory can be sustained.
	Metallic skin used, which is relatively more resistant to impact, for example from ice particles. Therefore, inspection is relatively easier and less crucial.	Vehicle design does not have to be changed.
	Metallic skin used, which is relatively more resistant to oxidation.	Aerodynamic performance is not compromised.
	Comparatively less costly in terms of manufacturing and maintaining	Total coolant mass required will increase, but lesser as compared to mass for a bigger nose radius.
		Ceramics are relatively less dense, therefore mass of the layer is reduced.
Disadvantages	Vehicle design needs to be modified.	Ceramics have poor oxidation resistance at higher temperatures, because of which additional coatings are required.
	Aerodynamic performance of the vehicle reduces, as drag increases.	Ceramics are brittle and relatively less resistant to impact, so inspection is crucial.
	Increase in total coolant mass required for the re-entry flight.	Coatings will need to be applied on both surfaces of the ceramic, inner and outer. This will affect the emissivity of the material.
		Self-healing coatings are not yet found. So the coating will have to be refurbished after few flights.
		More costly, because ceramics are expensive to manufacture and maintain. Development cost of coatings is an additional factor.

Chapter 6

Sensitivity and Robustness

A conceptual design of a thermal protection system is proposed in Chapter 5. Now, the next step is to study the performance of this design under various uncertainties. This is interesting because it provides an insight into the behaviour and limitations of the proposed design to different controllable and uncontrollable changes in the system. This study is carried out in two steps. First, the response of the design to unpredictable changes in the system is investigated in Section 6-1. Second, the response of the design to conscious changes in the mission parameters is studied in Section 6-2.

6-1 Sensitivity analysis

Sensitivity of a design is described as the response of a design to an unforeseen change or a perturbation in the vehicle or environment. This includes behaviour of materials under extreme conditions, perturbations in the gravity field, solar radiation pressure, wind and many more. The aim is to understand the sensitivity of the performance to the effect of uncertainties. For this study, unforeseen changes in the design are investigated and this is seen in the physical properties of the materials used, as discussed earlier in Section 4-1-1. Based on the mathematical model, discussed in Section 4-1-2, it is clear that the system under consideration depends on the physical properties of the skin, porous layer and coolant. It must be noted that the uncertainties in estimation of physical properties of the coolant, in this case water, are less than 0.001% (NIST Chemistry WebBook, SRD 69). Therefore, coolant properties have not been taken into consideration for this sensitivity analysis.

Now, most of the material properties of the porous layer are used in combination with the coolant properties, except for emissivity, to obtain the temperature of the coolant/ porous layer. Based on the assumptions used to develop the mathematical model (discussed in Section 4-1-1), it is evident that the influence of these properties, i.e., density, specific heat and conductivity of the porous layer, is negligible, given the material porosity is 91%. Therefore, only uncertainties in emissivity of the porous layer is considered, along with the physical properties of the outer skin, which include density, specific heat and emissivity. Additionally, as discussed in Section 5-2-1, there is a high uncertainity in the value of blocking effect. A lot of experimental data and numerical analysis is required to predict the

blocking effect, even then the accuracy might not be sufficient. Therefore, for this study it is included as a parameter in this sensitivity analysis.

Now, to study the effect of varying the design variables on output of the design, certain performance criteria must be identified. In this case, the steady state temperature or the temperature achieved by the TPS layer when the stagnation heat flux is maximum, along with the total coolant mass required for the re-entry flight, are used as performance criteria.

Once the design variables and performance criteria are defined, the next step is to select a suitable methodology that can be implemented to study effect of the variation. There are many different methods that can be used, the simplest being one-at-a-time variation. Other methods include a Monte Carlo analysis (unstructured approach), full factorial design (structured approach), a fractional factorial design and many more. The choice depends on the expected behaviour of the design variables. If the outcome of varying one design variable affects that of another variable, this means that there is an interaction between the factors. In that case, using the one-at-a-time variation approach is not efficient. Also, interactions can be between more than two factors. Other quadratic or higher order effects can be present, depending on the mathematical model that describes the system and to study these effects, more than a two level variation in factors is necessary. Another important aspect that is considered before selecting a simulation method is the number of simulations required to be performed. For example, a 3-level full factorial design consisting of five factors requires $3^5 = 243$ simulations. This is computationally very expensive and in many cases not feasible.

For this study, as discussed earlier, there are 5 factors that are identified critical to the performance of the design. Based on the mathematical formulation of the physical problem, in Chapter 4, some interactions are expected between these variables, especially between the physical properties. Therefore, one-at-a-time variation is not recommended. The influence of these interactions cannot be quantified without simulation, so the method selected for analysis must consider interaction effects. Also, higher order effects are ruled out, however, quadratic effects are included, although not expected, to perform a thorough investigation.

To cover the full range of possible outcomes, a full factorial design is a preferred approach. Plus, to include quadratic effects, at least a 3-level variation in the factors, i.e., minimum, nominal and maximum, is necessary. This means a total of $3^5 = 243$ simulations are required for a full factorial design. This is computationally expensive, therefore, an alternate method is selected, which provides an efficient way of studying the entire solution space using comparatively lesser simulations. Mooij et al. (1999) proposed a method and used it for doing an aerodynamic design of a low-cost re-entry vehicle. A similar approach is also used by Stanley et al. (1994) to conduct a configuration selection and design of a rocket-powered single-stage vehicle. According to this approach, a second order response surface is used to study the design space and a central composite design (CCD) is proposed to find the coefficients of this response surface. To develop the fractional factorial part of the CCD, the Taguchi method (Taguchi, 1988) is implemented. Before proceeding further, CCD and the Taguchi method are briefly explained.

A schematic representation of a 2-factor CCD is seen in Figure 6-1. A CCD includes,

- a full or fractional, Resolution V 2^n factorial design, where the levels are normalised and represented as +1 and -1,
- two axial points on the axis of each design variable, at a distance α from the nominal value (centre point) i.e, $2n$,
- lastly, $n0$ centre points ($n0 \geqslant 1$),

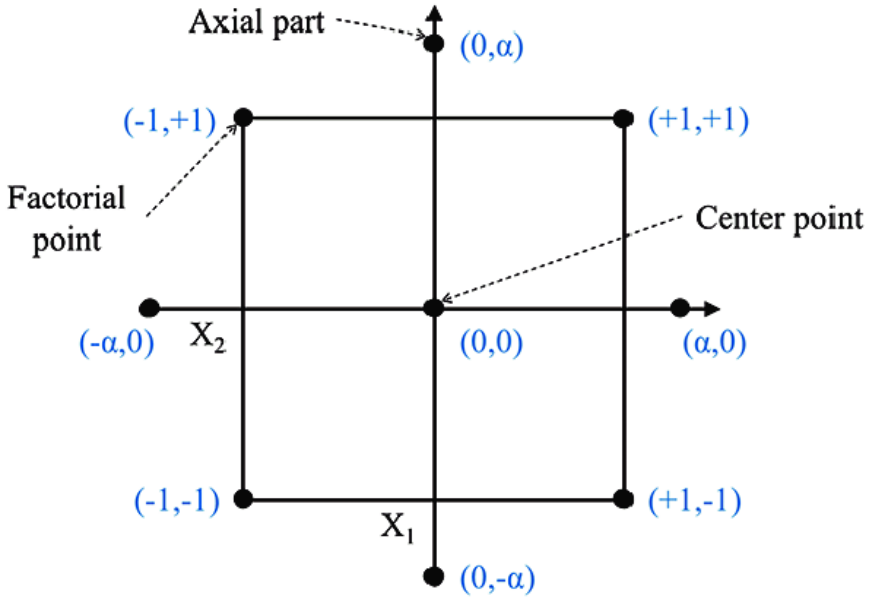

Figure 6-1: Schematic representation of a 2-factor CCD.

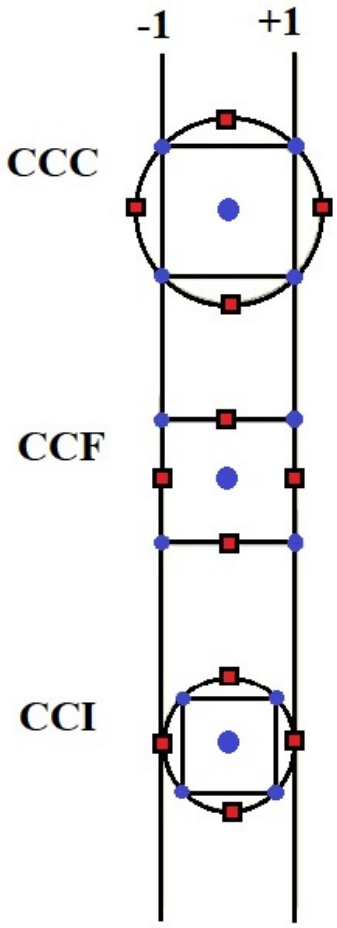

Figure 6-2: Schematic representation of the types of Central Composite Designs.

where, n stands for number of factors. The axial points represent new high and low values for each factor. Based on the value of α, there are three possible varieties of CCD, namely

Circumscribed CCD (CCC), Face Centred CCD (CCF) and Inscribed CCD (CCI). These are schematically represented in Figure 6-2, using which the different types of CCD can be easily understood. CCC is the conventional form of CCD, where the axial points are new extreme values of the factors and are combined with the factorial design, leading to a 5-level variation in each factor. However, if there is a physical limitation on the possible extreme values of the factors, then the CCD is modified to a CCF or CCI. If the factorial part of the CCD is set at a lower values than the maximum possible extreme values a CCI is obtained, consisting of 5-level variation in factors. Alternately, if the extreme values for both the factorial and axial part of the design is set at the maximum possible extreme value, a 3-level variation in each factor is seen and this type of CCD is called a CCF. A CCC covers the largest possible solution space, on the other hand CCI covers the smallest possible solution space, this can also be seen from Figure 6-2. For this study, the value of α is set at 1, as setting new extreme values outside the available bounds for the factors lead to unreal are not feasible values. Therefore, a CCF is implemented for this investigation.

While performing an experiment, the number of centre points in a CCD are generally more than 1. The centre point represents the nominal design, without any variation of parameters. Performing repeated experiments at this point is useful for checking repeatability of the results and to obtain the pure error. Generally, 5 or 6 runs for the centre point design are recommended to be performed randomly in between other runs. However, in this investigation, computer simulations are being performed and the outcome of these simulations does not vary for a fixed set of input variables, as there is no random generator involved. Repeating the same simulation multiple times is not expected to affect the prediction capability of the response surface. Therefore, only one centre point simulation is included in this CCF.

The Taguchi Method is a technique for obtaining a fractional factorial design, found in the field of design and product process optimisation by Taguchi (1988). It uses orthogonal arrays to obtain the parameter setting combinations, using a concept known as 'balancing property', such that in every column pair, all combinations occur equal number of times. Preparing the orthogonal array is a crucial part of the analysis, especially when a 3-level factor variation is used. This is because, interactions can take up to two columns and there is a risk of confounding. For example, for a three factor factorial design, if the first two columns are assigned to the first two factors, the third column records the interaction between the two factors. Now, if the third factor is assigned the third column, the effect of the third factor and the interaction between the first two factors is combined, this is known as confounding. To avoid this, Taguchi (1988) has developed various 2-, 3- and other higher level arrays.

The number of simulations required for this investigation is given as L16 + 2*5 + 1 = 27, where L16 is Taguchi's array, which is a Resolution V fractional factorial design for five factors. From this, the advantage of this method is clearly visible, the number of simulations required to study the complete solution space, is reduced by 216 simulations.

The physical properties and blocking effect, along with the respective variation range, are listed in Table 6-1. This set of parameters is referred to as design variables or factors for this section. The uncertainty in emissivity and density of the outer skin have been obtained from Dittert et al. (2018), and is relatively small. As for the uncertainty in specific heat, a large range is considered because, the specific heat of a C/C-SiC material depends on various aspects, such as the carbon fibres used, the manufacturing method and many more. Plus, the specific heat varies with temperature. After the material is prepared, its specific heat is estimated by means of experiments, but generally these experiments do not cover

Table 6-1: Sensitivity - parameter variation in CCD

Factors	Nominal value	Range (CCD)	Range (axial)
Emissivity of skin ε_s	0.88	± 0.01	± 0.01
Density of skin ρ_s **(kg/m^3)**	1900	± 100	± 100
Specific heat of skin $c_{p,s}$ **(J/kgK)**	1350	± 450	± 450
Emissivity of porous layer ε_p	0.91	± 0.01	± 0.01
Blocking effect (%)	40	± 20	± 20

the complete temperature range, that would be experienced by the material in flight. So, the largest possible range of specific heat seen in Bansal and Lamon (2014) is used for this study, to take into account maximum uncertainty. Similarly, for the blocking effect, a large range of possible values was seen in Section 5-2-1, therefore, the maximum possible range has been considered. It must be noted that the nominal value of blocking effect is taken as 40% for this analysis, unlike that used for the design in the previous chapter. This is done to cover the complete range.

The outcome of this approach was a response surface for each performance criteria. The goodness of fit was ensured for both, and negligible interactions or quadratic effects were observed. The response surface is verified by comparing the predicted results to the actual value obtained, for the same parameter setting, from the simulation. ANOVA (Analyis of Variance) is performed on the fractional factorial part of the CCD, to overcome any confounding and to check, if there are any interactions or quadratic effects that are being missed out. This is done by comparing sum of squares for each factor (S_i) to the total sum of squares (S_T), to give a ratio P_i per factor that determines the factor's importance to the response variation. The results for P_i in percentage for different factors are seen in Table 6-2. The values for the interaction and quadratic terms are not included in this table because, the values negligible and in many cases zero. This confirms that there are no significant interactions or quadratic effects. Additionally, a response gradient is prepared, and the same observation is made from the steepness of the lines. Therefore, it is safe to say that there are no significant interactions or quadratic effects between the selected design variables for the nominal design under study. The actual variation in output parameters for each simulation can be seen in Figure 6-3. A significant variation is seen for both performance parameters, a maximum variation of 300K in temperature and 250 g in coolant mass is observed.

It is important to note that blocking effect is the most significant contributor to the variance as seen in Table 6-2. Due to this, it is difficult to identify the contribution of other variables. Therefore, a second set (Set 2) of sensitivity analysis is conducted, using the same variables minus the blocking effect, and the same approach. The number of simulations required for Set 2 are $2^4 + 2*4 + 1 = 25$, considering a CCD with full factorial design.

The results for response gradient is similar to Set 1 and ANOVA of Set 2 is seen in Table 6-3. Once again, no significant interactions or quadratic effects are observed. The actual variation in output parameters for each simulation can be seen in Figure 6-4, for set 2. The variation observed is comparatively lesser for this set, maximum variation of 12 K and 8 g. It is interesting to note that the first performance criterion, i.e., temperature is more strongly affected by emissivity of the skin, as opposed to the second criterion, i.e., coolant mass, that is affected by emissivity of porous layer. The variation of density and

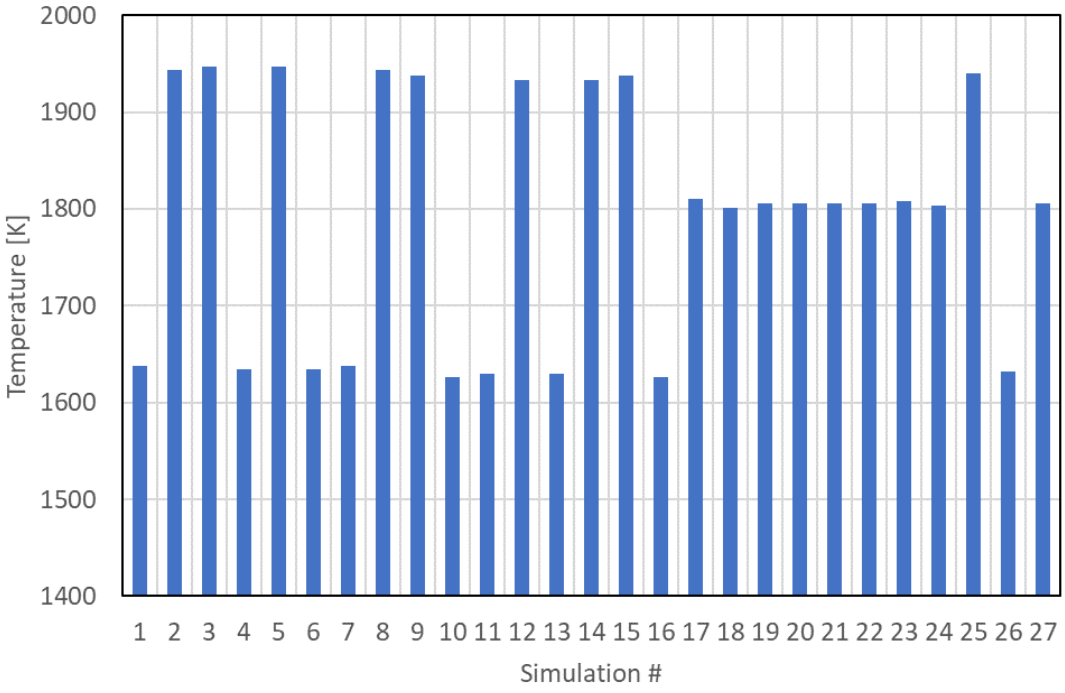

(a)

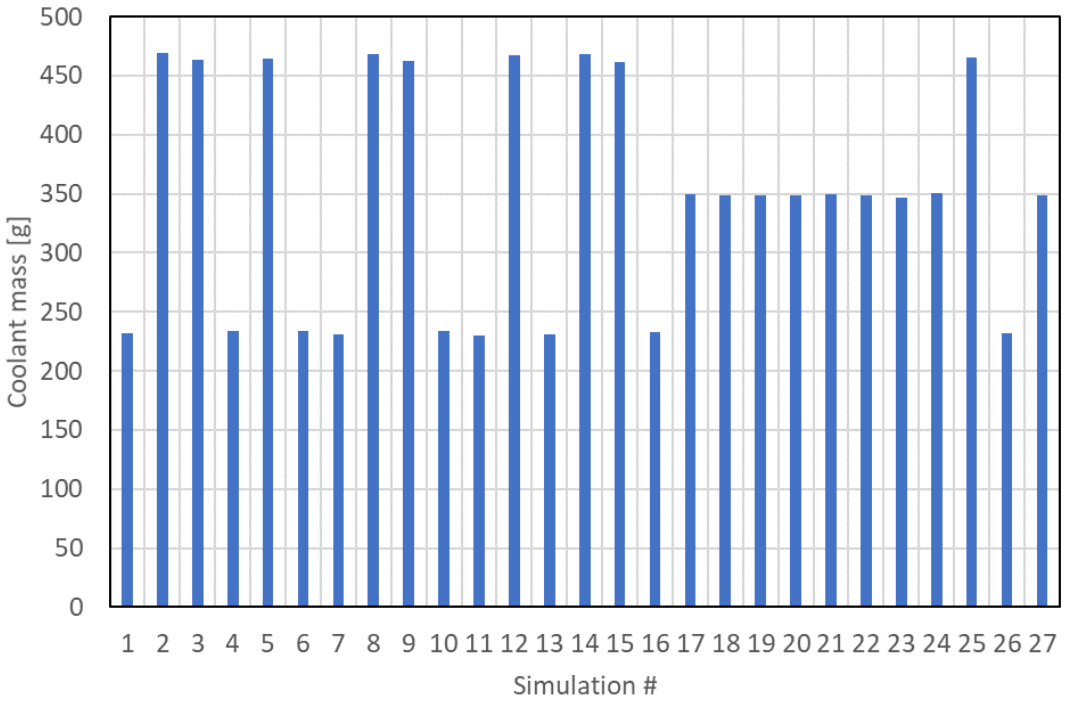

(b)

Figure 6-3: (a) Temperature and (b) Coolant mass variation for different combinations of design variable settings (Set 1).

specific heat of skin is seen to have negligible influence on the temperature of the outer skin, this is because the temperature values are so high and the variation is too small to make a significant impact. Plus, the skin temperature depends on radiative heat transfer, where

Table 6-2: Set 1 - Contribution of each parameter to the variation.

Factors	**Temperature (%)**	**Coolant mass (%)**
$\varepsilon_{\mathbf{s}}$	0.08	0
$\rho_{\mathbf{s}}$	0	0
$\mathbf{c_{p,s}}$	0	0
$\varepsilon_{\mathbf{p}}$	0.01	0.03
Blocking effect	99.90	99.96

Table 6-3: Set 2 - Contribution of each parameter to the variance

Factors	**Temperature (%)**	**Coolant mass (%)**
$\varepsilon_{\mathbf{s}}$	85	8
$\rho_{\mathbf{s}}$	0	0.1
$\mathbf{c_{p,s}}$	0	5.4
$\varepsilon_{\mathbf{p}}$	15	86.4

temperature to the fourth power is the largest contributing factor, compared to that such a small variation in properties does not affect the outcome. As for coolant mass, the effect of density and specific heat is still negligible, but more than that for temperature.

The above analysis provides an understanding of the relative impact of the design variables on the performance criteria. This means that the order of importance/ contribution of design variables to a performance criteria is obtained. So for temperature, the order is blocking effect $\geqslant \varepsilon_s \geqslant \varepsilon_p \geqslant \rho_s, c_{p,s}$. Similarly, for coolant mass, blocking effect $\geqslant \varepsilon_p \geqslant \varepsilon_s \geqslant c_{p,s} \geqslant \rho_s$. To conclude,the design is relatively more sensitive to blocking than the uncertainties in physical properties of the materials. A good thing is that for all uncertainties, no solution set reached a failure point, i.e., for all combinations of design variable setting. Temperature of the skin was less than maximum operating temperature of the skin material. It is important to note that the outcome of this analysis is limited to the nominal mission and design parameters as well as to the assumptions of the mathematical model. For a more complex formulation (having different assumptions) and for a different design (material), the outcome might not be the same. Therefore, it should be analysed before extrapolating the results. Nonetheless, this being a first estimate, it is useful for understanding the system and possible trends.

6-2 Robustness

The effect of a conscious change in one or more design parameters, helps to understand the robustness of a design. It is interesting to see the impact of varying the mission and system parameters, to understand limitations of the proposed design or bounds of the design space. Also, it helps understand possible scalability of this concept. In this study, the mission and system parameters, such as the entry conditions, maximum heat load constraints, mass and nose radius of the vehicle, etc., are obtained from the mission and system requirements.

Now, if for some reason any or all these parameters were changed, the performance of the proposed TPS design would be affected. By means of this robustness analysis, the impact

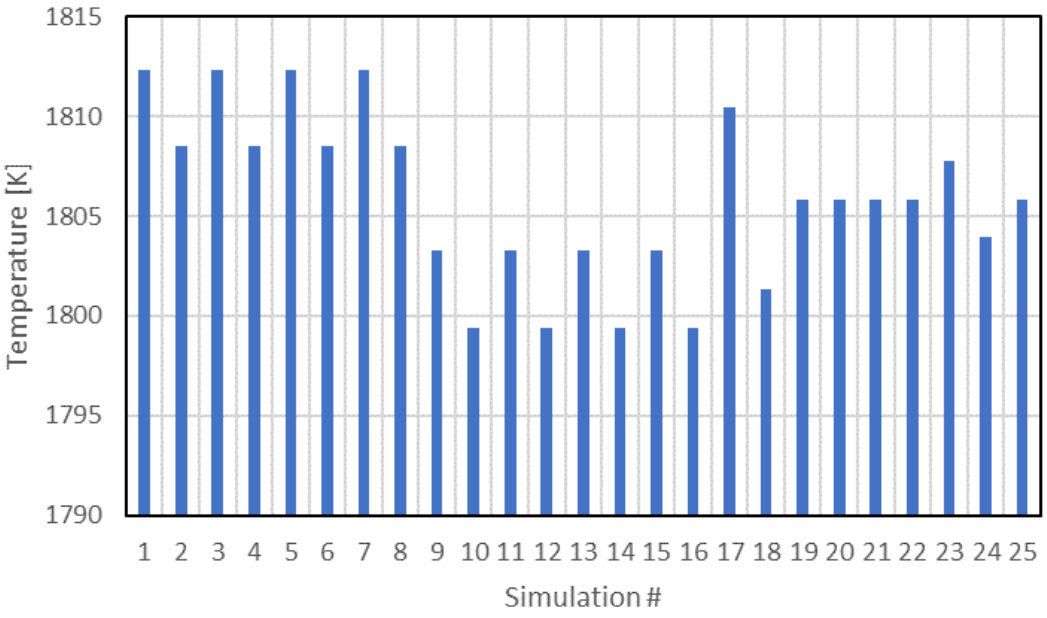

(a)

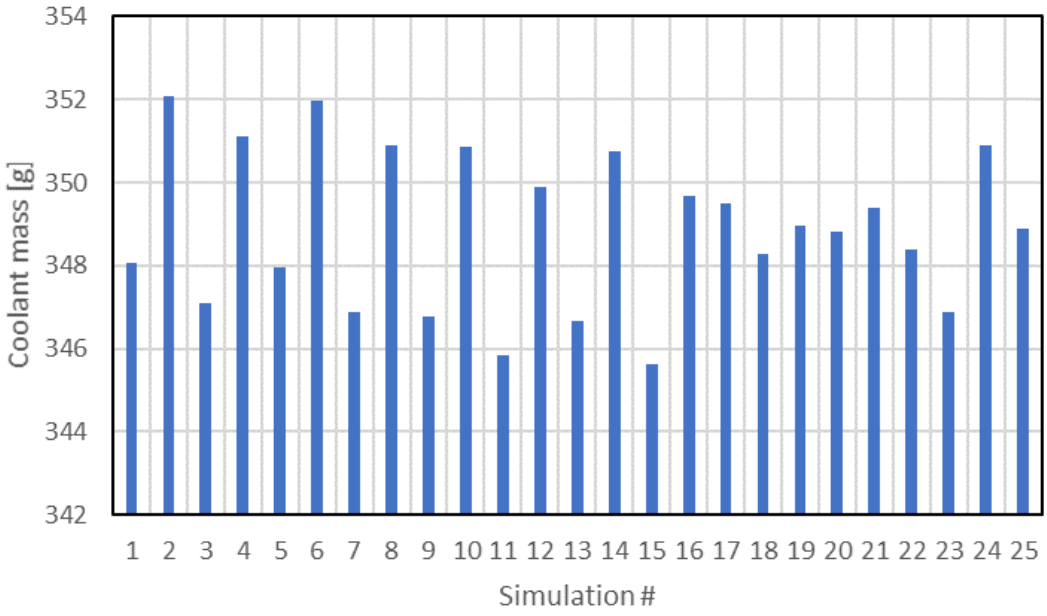

(b)

Figure 6-4: (a) Temperature and (b) Coolant mass variation for different combinations of design variable settings (Set 2).

of varying mission and design parameters, on the performance of the design, is studied. Every parameter affects the outcome, mission parameters have an impact on the trajectory flown, for example increasing the q-load constraint or increasing the entry velocity changes the trajectory to be flown. Similarly, the design parameters, which includes the shape and mass of the vehicle, aerodynamic parameters, lthermal and mechanical load baring ability, etc., influence the vehicle design and the trajectory. With a change in trajectory flown,

Table 6-4: Parameter variation for robustness.

$\mathbf{R_N}$ **(mm)**	13	26	52	–
$\mathbf{V_E}$ **(m/s)**	–	3300	6450	–
$\mathbf{q_{max}}$ **(kW/m^2)**	1000	1500	1900	2000

the integrated heat load (total heat load per unit area, MJ/m^2) experienced by the vehicle varies, because flight time and heat loads are different. Therefore, this has an impact on the performance of the TPS and is interesting investigation.

With the assumptions used to obtain a nominal trajectory (discussed in Section 2-6), there is a limitation on the mission parameters that can be varied. The entry velocity and q-load constraint are the only mission parameters that are varied. If the trajectory is modelled using the conventional method (by propagating the equation of state), a much more detailed robustness analysis, for example impact of varying the entry flight-path angle, angle of attack, etc., is possible and recommended for future. Similarly, for design parameters, only the impact of varying the nose radius is investigated. It would be interesting to study the impact of vehicle mass, aerodynamic parameters such as L/D ratio, mechanical load constraint, controllability of the vehicle, etc., on the performance of the TPS design. However, this is possible only when an integrated design of trajectory, vehicle shape and TPS is conducted. Once again, this is recommended to be done in the future, to better understand and optimise the design.

The nose radius and entry velocity of the vehicle, along with the heat load constraint are varied. This means that both, the trajectory and vehicle shape, are being modified simultaneously. The revised trajectories are obtained in the same way, as the nominal trajectory (described in Section 2-6) and the same assumptions as the nominal trajectory are applicable here, i.e., the vehicle is assumed to have sufficient aerodynamic performance and control, to enable its flight along the trajectory.

For this analysis, other than nominal value of the nose radius, two more values are considered, half the size and double the size with respect to the nominal value. This range is selected to investigate the influence of a smaller nose on the temperature performance parameter. Similarly, the larger nose radius is used to investigate influence on the total coolant mass. As for the velocity, the nominal value was obtained based on the launcher, a lower value is not selected because it is not practical. However, the impact of a higher value is interesting to study, because many launcher's the entry velocity is in the range of 6-7 km/s, also for flights returning from LEO, the range is similar. Next, the maximum heat load constraint is varied between 1 and 2 MW/m^2, as is the range identified in the mission requirements (seen in Section 2-4-1). Other than the maximum, minimum and nominal value, an additional value of 1.9 MW/m^2 is considered, because that is the maximum heat load that can be sustained by the nominal design, so it is included to see the performance of other solutions at the same point. All possible combinations of the three parameters are analysed.

Results of the robustness analysis is seen in Table 6-5, for the first performance criteria, i.e., temperature and in Table 6-6, for the second performance criteria, i.e., total coolant mass. Additionally, total heat load is also taken into consideration here, as with change in trajectory, this parameter will be affected. Results for the same are seen in Table 6-7. In each table, the value of a performance criteria is provided for a specific parameter combination. For example, reading Table 6-6, given a combination of a 13 mm nose radius, entry velocity of 3300 m/s and maximum heat flux of 2000 kW/m^2, the coolant mass required is 108 g.

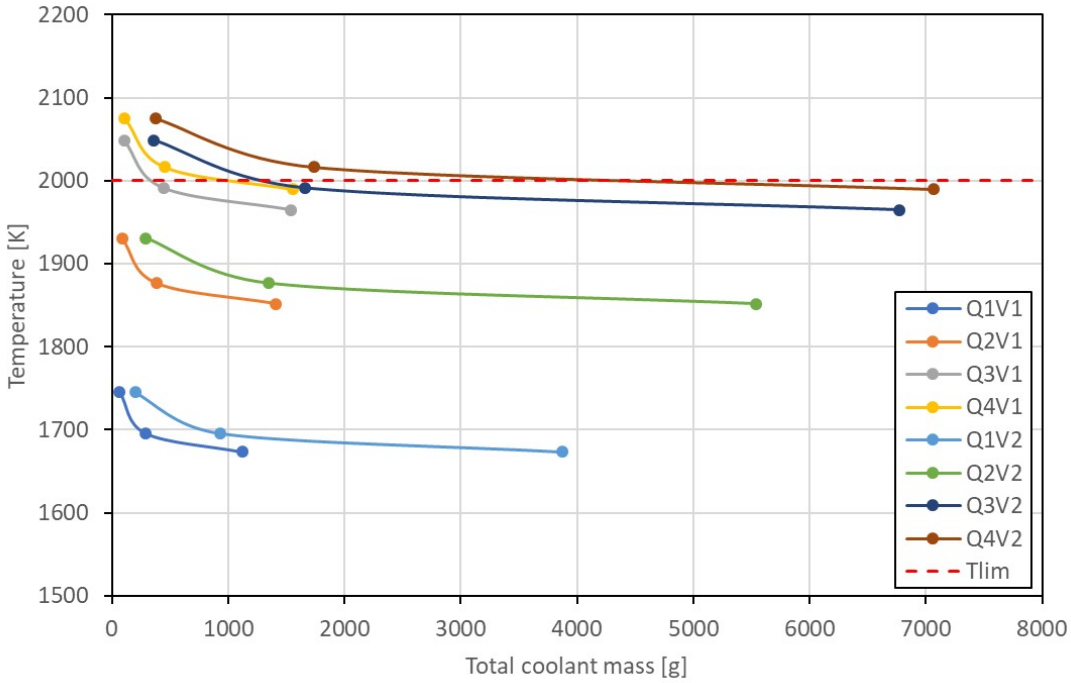

Figure 6-5: Results for TPS design robustness.

Also, the outcomes are colour coded, varying from green for lower values to red for higher values, to visual the trends better. Additionally, the solution space for the design robustness is visualised in Figure 6-5. It shows a plot of the temperature variation against the coolant mass requirement for all input parameter combination sets. The different coloured lines are for different heat flux and entry velocity combination and the three dots seen on each curve represent a different nose radius, going from lower to higher sizes (left to right). A dotted line is shown to indicate the maximum operating temperature of the outer skin material, solutions above this line are not feasible. It is preferred to have a design that lies in the left half of the figure below the dotted line, such that the maximum operating temperature of TPS material is not exceeded and the required coolant mass for the flight is not very large.

Based on this analysis, it is found that for a nose radius of 52 mm, the proposed TPS concept can sustain a maximum stagnation heat flux of 2 MW/m^2 and a total heat load of 3159 MJ/m^2 (V_E = 6450 m/s), for a given vehicle mass (250 kg) and aerodynamic performance (L/D = 2.21). However, the coolant mass required is approximately 4.5 times more than for a lower entry velocity. In reality, the shape of the vehicle (nose radius) has an impact on many other parameters such as, vehicle mass. Therefore, the performance could be worse than predicted here. However, this being a first estimate, a general performance trend and design bounds are obtained. As mentioned earlier, a combined trajectory, vehicle shape and TPS design will give a more accurate and detailed insight. Nonetheless, it is safe to conclude that the proposed concept can sustain higher heat loads as compared to an uncooled metallic system.

Change in entry velocity

From the results, various observations can be made with respect to change in entry velocity as listed below.

1. The outer skin temperature is not affected by a change in the entry conditions, as long

as the maximum heat load constraint is not varied.

2. On the other hand, the coolant mass requirement increases by more than 3 times. This increase in coolant mass for an increase in entry velocity, increases as the nose radius and heat load constraint are increased.

3. Similar trend is observed in case of total heat load per unit area. This is logical, because as the total heat load increases, coolant required also increases.

Change in heat load constraint
From the results, various observations can be made with respect to change in heat load constraint as listed below.

1. As the heat load constraint is increased, a non-linear increase in temperature is observed, for any nose radius or entry velocity. This is as expected.

2. Similarly, for coolant mass, an increase in aerodynamic heat flux, means a higher incoming heat flux and therefore, more coolant is required.

3. In case of total heat load per unit area, the flight time increases and the maximum heat load constraint is increasing, so the trend observed is obvious.

Change in nose radius
From the results, various observations can be made with respect to change in nose radius as listed below.

1. With an increase in nose radius, the temperature for a given heat load constraint reduces. A 13 mm nose radius can sustain a maximum heat load of 1500 kW/m^2, whereas a bigger nose can handle a maximum heat flux of 2000 kW/m^2.

2. As for the coolant mass, observations are as expected, larger nose means a larger surface area, therefore, an increase in coolant mass with increasing nose radius, irrespective of change in entry velocity and heat load constraint. The coolant mass for the nominal heat flux (1500 kW/m^2) and velocity (3300 m/s), reduces by 76% when the nose radius is decreased by 50%, and increases by 267%, when the nose radius is increased by 100%.

3. In case of total heat load per unit area, as the nose radius increases, its value reduces, for a given entry velocity and heat load constraint.

By looking at the data, the earlier assumption made while comparing an increase in nose radius to change in material (Section 5-2-2) that a larger nose radius will lead to a rather large increase in mass, is confirmed. To conclude, this robustness analysis has provided a good first estimate of performance of the TPS design for different trajectories and nose sizes. This information can be used to optimise both the vehicle and trajectory, such that an optimal aerothermodynamic performance of the system is found. The analysis can be extrapolated to obtain a first estimate of the performance of the TPS design for any spaceplane mission.

Table 6-5: Robustness - results for maximum temperature.

Temperature (K)					
$\mathbf{R_N}$ **(mm)**	$\mathbf{V_E}$ **(m/s)**	$\mathbf{q_{max}}$ **(kW/m$_2$)**			
		1000	1500	1900	2000
13	3300	1745	1931	2049	2075
	6450	1745	1931	2049	2075
26	3300	1696	1877	1991	2017
	6450	1696	1877	1991	2017
52	3300	1674	1852	1965	1990
	6450	1674	1852	1965	1990

Table 6-6: Robustness - results for total coolant mass.

Coolant Mass (g)					
$\mathbf{R_N}$ **(mm)**	$\mathbf{V_E}$ **(m/s)**	$\mathbf{q_{max}}$ **(kW/m^2)**			
		1000	1500	1900	2000
13	3300	64	89	105	108
	6450	198	290	360	378
26	3300	289	384	442	453
	6450	930	1348	1664	1741
52	3300	1119	1411	1539	1557
	6450	3873	5543	6774	7069

Table 6-7: Robustness - results for total heat load.

Total heat load (MJ/m^2)					
$\mathbf{R_N}$ **(mm)**	$\mathbf{V_E}$ **(m/s)**	$\mathbf{q_{max}}$ **(kW/m^2)**			
		1000	1500	1900	2000
13	3300	595	811	955	987
	6450	1852	2698	3343	3504
26	3300	553	730	835	856
	6450	1808	2608	3206	3351
52	3300	497	622	676	683
	6450	1751	2490	3030	3159

Chapter 7

Conclusions and Recommendations

As discussed in Chapter 1, the aim of this work is to identify a suitable reusable TPS design for a winged RLV, and to investigate its influence on designing a flight test. A summary of the outcomes obtained from the work carried out during the course of this thesis is discussed in Section 7-1. Based on this, some recommendations for future work, to develop the proposed TPS concept/ design and the software tools required to model it, is discussed in Section 7-2

7-1 Conclusions

The main research question and the corresponding sub-questions for the thesis work is as listed below. In this section, each of these questions has been addressed based on the outcomes obtained from the work.

How does the thermal protection system design influence the mission and system design of an experimental winged RLV?

1. What are the mission and system requirements that must be fulfilled by a TPS for an experimental winged re-entry vehicle?
2. Which TPS design is expected to satisfy the desired mission and system requirements?
3. How can the performance of the TPS design be analysed?
4. Is the TPS design suitable for multiple flights?
5. How do the limitations of the TPS design influence the flight test mission and the vehicle design?

RLV development has evolved over the years and it is found that one of the next steps in development requires improvement of the TPS technology. The TPS needs to be reusable and at the same time have a better thermal performance. Most of the existing RLVs, proposed and developed, are ballistic or low L/D vehicles. For a comfortable manned mission, such as space tourism, a high L/D vehicle is preferred. This is because the lift component

allows it to decelerate at a higher altitude and glide back to Earth, experiencing comparatively lower g-loads during flight and a global cross-range, allowing multiple options for landing sites. One of the major drawbacks of these vehicles is the high heat load experienced by the vehicle, due to longer time period of flight. Also, the stagnation point heat flux is higher because of the smaller nose radius and sharp leading edges, that are a must for a high L/D vehicle. If an air breathing propulsion system is implemented, the ascent phase thermal loads are more demanding than the descent. However, there are various difficulties involved in using such a propulsion system. Therefore, in the next phase of RLV development a rocket powered launch is expected, combined with a gliding entry. This implies that the thermal loads during re-entry are relatively more significant for designing a TPS. The existing TPS designs and materials are not suitable for sustaining such high heat loads over repeated flights. Here, arises the need to develop a TPS design that can address this problem.

The outcome a thorough literature survey lead to the finding of a probable solution, a cooled metallic TPS design, called Enhanced radiation cooling, proposed by Buursink (2005). Using ground-based experiments, Buursink (2005) investigated the performance of the cooling system and gave a proof of concept. Cooled metallic TPS has the ability to sustain almost twice the thermal loads as compared to an uncooled system, for the same temperature. This implies that the TPS, if applied in the nose region of a vehicle, can permit reducing the size of the nose radius, enabling an improvement in the aerodynamic performance of the vehicle. This concept is studied in more detail through the course of this thesis.

Enhanced radiation cooling is a metallic TPS design, cooled by means of a coolant filled porous layer. The aerodynamic heat flux incident on the surface of the vehicle, heats up the outer metallic skin by means of convection. The outer skin looses this heat by means of radiation to the environment and the underlying porous layer. The advantage of filling the porous layer (ZAL-15) is that the coolant (water) takes up a large portion of the incoming heat flux as it heats up and undergoes a phase change. The metallic outer skin is preferably chosen to be a ODS alloy (PM2000). One of the many reasons for this choice is the self healing property in oxidising environments (good oxidation resistance). This property is very beneficial, as it makes inspection and maintenance after a flight easier and less costly. The porous layer material and coolant selected for the design are the same as proposed by Buursink (2005). This is because the desired properties of these materials are excellent and almost no improvement is expected from other materials.

To analyse the performance of the cooling system, a mathematical model is developed that helps in translating the physical phenomenon of cooling to a software tool. A one-dimensional transient thermal analyser is developed, with some simplifying assumptions. The tool is verified using the data obtained from the experiments performed by Buursink (2005) on a similar system. Using the transient thermal analysis tool, the performance of the system is analysed and it is found to sustain a maximum heat flux of 700 kW/m^2. The thermal analysis performed in this thesis gives a first estimate of the cooling system's performance and can be used as a starting point for developing the design. The ERC concept is found to be limited by the maximum operating temperature of the outer skin material. Although, the performance is better than other existing systems, the heat flux requirement identified for this work is higher. Therefore, a few design modifications are proposed and investigated.

Based on the proposed design improvements, including a change in the skin material from metallic to C/C-SiC and venting of evaporated coolant through small holes in the

stagnation region of the skin, a modified enhanced radiation cooling concept is proposed. A transient thermal analysis of this concept shows that it can sustain stagnation heat flux up to 1900 kW/m^2. This is possible because of two main reasons, first, ceramic materials have higher operating temperatures (2000 K) as compared to metallic and second, venting the evaporated coolant in the stagnation region introduces a thermal blocking effect. However, these modifications have their own limitations. Firstly, the poor oxidation resistance of the C/C-SiC material at temperatures above 1200 K, makes it unfit for use unless additional coatings are applied. Existing coating materials and technologies are rapidly developing, however the research in the field self-healing coatings is still on-going. Therefore, if the currently available oxidation resistant coatings are applied, there will be an additional cost of refurbishing the layer after a few flights. Also, inspection is more difficult, time consuming and expensive. Secondly, although the existing literature on blocking effects proves that it has a significant impact as a barrier, quantifying this is not easy. Plus, there is a risk of adverse effects due to contamination of the boundary layer, which to estimate requires intensive numerical simulations and experiments. Nonetheless, the performance improvement of this concept is significant and is recommended for future study.

Both concepts, ERC and modified ERC, are seen to perform better than a passive system. Therefore, for future spaceplane applications, both these systems are suitable solutions. The performance of ERC is limited, however, it is a relatively simpler system and is expected to have lesser inspection and maintenance cost. As for development costs, this is expected to be lesser as compared to modified ERC, which is a relatively complex system. The choice of TPS depends on the constraints and requirements of the desired mission and vehicle, including the costs involved.

For the operation of both concepts, a gap pressurisation system is necessary, in order to maintain a desired system pressure, for this a nitrogen pressure tank system complete with control valves, sensors and a controller is proposed. This mechanism is more crucial for the modified ERC concept because it is an open system, and has a risk of inflow of hot air if the pressurisation is not maintained. A sensitivity analysis of the modified ERC concept showed that the design has negligible sensitivity to the uncertainty in material properties. However, the performance is sensitive to the blocking effect. A considerable variation in the performance is seen for the variation in blocking effect. Therefore, while designing a flight test, it is recommended to take the variation in blocking parameter into account and to incorporate ways for measuring the value. Detailed numerical simulations might provide accurate values, however, flight testing is essential for validation. This analysis is a preliminary step and a much detailed sensitivity is required to gather a complete understanding of the system.

Studying robustness of the design gave interesting insights about the performance trends of the TPS with respect to different mission and system parameters, as discussed earlier. The important take-away from this analysis is that a nose with a smaller radius heats up more and experiences a higher total heat load for the same heat flux constraint, but requires lesser coolant mass for the entire trajectory because of the smaller area. This should be considered while designing and optimising a mission and vehicle. Once again, this analysis is a first step, considering only a few mission and system parameters. A more detailed study, taking into account other critical parameters such as flight-path angle L/D ratio and vehicle mass, is recommended.

To conclude, the thermal protection system influences the mission and system design of an experimental vehicle in many ways. As seen from the design robustness investigation, the different trajectory and vehicle parameters influence the thermal performance of the TPS,

which has an impact on its design. Depending on the vehicle size and mission constraints, either of the two concepts, ERC or the modified version, can be selected (although there are other factors such as cost at play too). Vice versa for a chosen TPS design, a suitable trajectory and vehicle shape can be selected, this would be the case when a flight test is designed specifically for the TPS. In most cases, the cost of flight testing is significant, so it is preferred to test multiple systems at a time. Therefore, it is recommended to conduct a integrated design of the vehicle, trajectory and TPS, to obtain the most optimal flight test mission. Moreover, the flight test should be designed such that the various sub-systems for example, gap pressurising system, can be tested, and data can be obtained for critical parameters such as blocking effect.

Performance of the TPS observed in this study is very promising for future RLV missions. It is reusable and has a positive influence on the aero-thermodynamic performance of a vehicle. Currently, this design is proposed to be implemented only in the critical heating regions such as nose tips and leading edges, because to cool the entire vehicle a large amount of coolant is required, which has a negative impact on the TPS mass and is not necessary. For an existing spaceplane, for example the selected reference mission (FSSC 15-OAE, 500 kW/m^2), the stagnation region heat flux and reusability requirements can be met using a simple ERC design. For missions like DLR's SpaceLiner (2000 MW/m^2) and ISRO's RLV-TD (900 kW/m^2), the modified ERC is a possible TPS solution.

7-2 Recommendations

Based on the work carried out in this thesis, a few recommendations have been made in this section for future work. This has been divided into three parts, depending on the type of work,i.e., software development / numerical modelling, experimental work and research based.

Numerical modelling
A few steps that can be taken from the software modelling aspect have been listed below, in no specific order.

1. In this study, a simple tool for thermal analysis has been developed. This can be further improved by adding a sub-routine for structural analysis.

2. Integrated trajectory-vehicle shape-TPS design and optimisation is one of the very next steps that can be taken to develop this design. From this tool, preliminary information about the heat load bearing capacity of the TPS can be obtained and used to set as a constraint in the trajectory design and vehicle shape. The expected outcome is a mission and vehicle combination having an optimal aerothermodynamic performance.

3. Finite element analysis (FEA) of a two dimensional system is also necessary, to investigate the structural and thermal loads on the TPS.

4. Numerical investigation of flow and convection heat transfer in the gap, is a recommended task for the future, to correctly size the gap. This will help not only to understand the system better, but also, there is a possibility of identifying certain limitations on the gap size.

5. Analysis of the boundary layer is recommended, to study the effect of introducing the coolant vapour in the boundary layer. It is important to investigate how the flow in the boundary layer behaves when this is done and to study the effect on chemistry of the boundary layer.

6. A multidisciplinary optimisation (MDO) of the TPS concept, taking into account parameters such as aerodynamic, trajectory, structural, aerothermal and cost, would facilitate in improving the technology readiness level (TRL) of this system.

Experimental work

Alongside developing software models for designing the TPS concept, a lot of experimental work is also recommended to support this development. All the subsystems must be tested before the concept can be undergo flight testing. Experimentation is vital, not only for understanding the system and testin sub-systems, but also for verification and validation of the software models.

1. Plasma wind tunnel experiments are a must to validate the proposed TPS concept, including the investigation for blocking effect and testing of the proposed nitrogen system for pressurizing the gap. Additionally, the coating and boundary layer flow can also be investigated. These experiments will provide the necessary proof of concept.

2. Vibrational tests are recommended for the proposed ZAL-15, because it was seen during the research for this thesis that such tests have not been performed. If the material cannot sustain these tests, design modifications could be made so as to strengthen the porous layer, a honeycomb structure using metal wire meshes, is a possible solution. However, this too must be tested.

3. Sub-system tests, for example, to test the performance of sensors, the attachment techniques and the reliability of the data under vibration, is recommended.

4. Experiments for testing estimating the capillary transport rate must be done. This can be useful in identifying limitations, if any, of the transport rate on the system.

5. Lastly, flight testing is proposed for future work, as it is very essential to develop the design, before it can be flown in an actual mission. Hypersonic flight data is limited and the wind tunnel tests are not sufficient to fully validate the system. Plus, flow data can be obtained from flight tests, this data to better model the environment that is used to simulate the design.

Research

A few research based studies have been identified, which if carried out could help develop the concept and also address some of its limitations.

1. A detailed material study is recommended. This includes coatings, skin material, porous layer and coolants. This could help improve the performance of the design or it could help resolve its limitations and help making it a less complex system. One of the major drawbacks of the proposed concept is the poor oxidation resistance of the C/C-SiC material. A detailed research into coatings might help find better solutions to the problem. Also, water is proposed as a coolant, and there is little to no room for finding a better coolant. Nonetheless, there are still some drawbacks of using water, because when dissociated it will produce more nascent oxygen. Therefore, a study on

coolants is proposed, so as to weigh out all possible options and do a proper coolant selection. Similarly, research can be conducted for finding optimal materials for the porous layer and skin.

2. Another research project would be to study the different instruments and sensors that can be used in such a TPS system. Additionally, efficient methods of installing these instruments in the system need to studied. Welding is not always the best and most reliable solution. To assess performance of the design in ground or flight testing, instrumentation plays a major role. Therefore, it is important to conduct a detail study for the same.

3. Lastly, if C/C-SiC is used as skin, then inspection costs are expected to be higher. Finding and developing efficient inspection methods is recommended for future work. With growing technology in the field of neural networks and artificial intelligence, there could be ways of automating the inspection process to some extent. Advanced scanners can be developed for checking the vehicle's outer TPS layer, such that even small cracks and dents can be rapidly identified. This could possibly save inspection time and cost.

Bibliography

[1] Anderson Jr, J. D. *Hypersonic and high-temperature gas dynamics*. American Institute of Aeronautics and Astronautics, 2006.

[2] Bansal, N. P. and Lamon, J. *Ceramic matrix composites: materials, modeling and technology*. John Wiley & Sons, 2014.

[3] Böhrk, H. Transpiration-Cooled Hypersonic Flight Experiment: Setup, Flight Measurement, and Reconstruction. *Journal of Spacecraft and Rockets*, 52(3):674–683, 2015.

[4] Buursink, J. *On the development of a cooled metallic thermal protection system for spacecraft*. PhD thesis, TU Delft, Delft University of Technology, 2005.

[5] Chang, Y., Sun, W., Xiong, X., Chen, Z., Wang, Y., Hao, Z., and Xu, Y. A novel design of Al-Cr alloy surface sealing for ablation resistant C/C-ZrC-SiC composite. *Journal of the European Ceramic Society*, 37(2):859–864, 2017.

[6] Curry, D., Rochelle, W., Chao, D., and Ting, P. Space shuttle orbiter nose cap thermal analysis. Proceedings of the *24th Aerospace Sciences Meeting*, p. 388, 1986.

[7] Dijkstra, M. *Trajectory Optimization of Hyperion-II for the Study of Hypersonic Aerothermodynamic Phenomena*. PhD thesis, Master's thesis, Delft University of Technology, 2012.

[8] Dijkstra, M., Mooij, E., and Sudmeijer, K. Trajectory Optimization to Support the Study of Hypersonic Aerothermodynamic Phenomena. Proceedings of the *AIAA Atmospheric Flight Mechanics (AFM) Conference*, p. 4501, 2013.

[9] Dissel, A. F., Kothari, A. P., and Lewis, M. J. Comparison of horizontally and vertically launched airbreathing and rocket vehicles. *Journal of spacecraft and rockets*, 43(1):161–169, 2006.

[10] Dittert, C., Böhrk, H., and Elsässer, H. Design of a transpiration cooled sharp leading edge for SHEFEX III. Proceedings of the *8th European Conference on Aerothermodynamics for Space Vehicles*. European Space Agency, 2015.

[11] Dittert, C., Kütemeyer, M., Kuhn, M., and Wagner, A. Process Optimization of Ceramic Matrix Composites for Ultrasonically Absorptive TPS Material. AIAA 2018-2947. 2018 Joint Thermophysics and Heat Transfer Conference, 2018.

[12] Dujarric, C. Possible future European launchers- A process of convergence. *ESA bulletin*, 97, 1999.

[13] Fan, S., Ma, X., Ji, B., Li, Z., Xie, Z., Deng, J., Zhang, L., and Cheng, L. Oxidation resistance and thermal shock properties of self-healing SiCN/borosilicate glass-B4C-Al2O3 coatings for C/C aircraft brake materials. *Ceramics International*, 45(1):550–557, 2019.

[14] Fischer, W., Gülhan, A., Esser, B., Faerber, J., and Reger, N. Plasma-Windtunnel Tests on a New Metallic TPS Material. volume 521, pp. 199–204, 2003.

[15] Foreest, A. V., Sippel, M., Gülhan, A., Esser, B., C. Ambrosius, B., and Sudmeijer, K. Transpiration cooling using liquid water. *Journal of Thermophysics and Heat Transfer*, 23(4):693–702, 2009.

[16] Glass, D. Ceramic matrix composite (CMC) thermal protection systems (TPS) and hot structures for hypersonic vehicles. Proceedings of the *15th AIAA International Space Planes and Hypersonic Systems and Technologies Conference*, p. 2682, 2008.

[17] Gong, L., Ko, W. L., Quinn, R. D., and Richards, W. L. Comparison of flight-measured and calculated temperatures on the space shuttle orbiter. 1987.

[18] Grinberg, I., Whitacre, G., Lane, W., and Ungar, E. Development of an Analytic Model of the Response of Self-contained, Transpiration-cooled Nose Tips to Reentry Environments. Technical report, Albuquerque, New Mexico, and Livermore, California, 1968. SC-CR-68-3585.

[19] Heppenheimer, T. A. Facing the heat barrier: a history of hypersonics. NASA SP-2007-4232. Government Printing Office, NASA, 2007.

[20] Hollis, B. R., Horvath, T. J., Berry, S. A., Hamilton, H. H., Thompson, R. A., and Alter, S. J. X-33 computational aeroheating predictions and comparisons with experimental data. *Journal of Spacecraft and Rockets*, 38(5):658–669, 2001.

[21] Jenkins, D. R., Landis, T., and Miller, J. American X-Vehicles: An Inventory X-1 to X-50 Centennial of Flight Edition. 2003.

[22] Korabelnikov, A. and Kuranov, A. Thermal protection using endothermic fuel conversion. AIAA 2005-3368. AIAA/CIRA 13th International Space Planes and Hypersonics Systems and Technologies Conference, 2005.

[23] Kors, D. Design considerations for combined air breathing-rocket propulsion systems. AIAA 1990-5216. 2nd International Aerospace Planes Conference, 1990.

[24] Mahulikar, S. P., Khurana, S., Dungarwal, R., Shevakari, S. G., Subramanian, J., and Gujarathi, A. V. Transient aero-thermal mapping of passive Thermal Protection system for nose-cap of Reusable Hypersonic Vehicle. *The Journal of the Astronautical Sciences*, 56(4):593–619, 2008.

[25] Marini, M. Body-Flap Efficiency Prediction of a FESTIP Concept Vehicle. Proceedings of the *Second International Symposium on Atmospheric Reentry Vehicles and Systems, Arcachon, France*, 2001.

[26] McMurry, J. and Fay, R. *McMurry Fay chemistry.* Belmont: Pearson Education International, 2004.

[27] Modlin, J. M. Hypersonic aerospace vehicle leading edge cooling using heat pipe, transpiration and film cooling techniques. Technical report, 1991. AD-A236 406.

[28] Mooij, E., Sudmeijer, K., and Kremer, F. Mission analysis of a low-cost re-entry test vehicle. AIAA 1999-4935. 9th International Space Planes and Hypersonic Systems and Technologies Conference, 1999.

[29] Mooij, E., Sudmeijer, K., and Kremer, F. Aerodynamic design of a low-cost re-entry test vehicle using a Taguchi approach. AIAA 1999-4831. 9th International Space Planes and Hypersonic Systems and Technologies Conference, 1999.

[30] Ratti, F., Gavira, J., Passarelli, G., and Massobrio, F. EXPERT: The ESA experimental re-Entry test-bed: System overview. AIAA 2009-7224. 16th AIAA/DLR/DGLR International Space Planes and Hypersonic Systems and Technologies Conference, 2009.

[31] Reed, R. D. and Lister, D. *Wingless flight: the lifting body story*, chapter 8: Lifting-Body Racehorses. University Press of Kentucky, 2015.

[32] Reimer, T., Stubicar, K., Koppenwallner, G., Müller-Eigner, R., Lein, S., and Steinbeck, A. Overview about the instrumented nose assembly development for the expert capsule. Proceedings of the *16th AIAA/DLR/DGLR International Space Planes and Hypersonic Systems and Technologies Conference*, p. 7233, 2009.

[33] Rotelli, R. X-20 Design and Development. *Annals of the New York Academy of Sciences*, 134(1):80–92, 1965.

[34] Savin, R. C. *Ablative Properties of Thermoplastics Under Conditions Simulating Atmosphere Entry of Ballistic Missiles.* National Aeronautics and Space Administration (NASA), November 1968. Technical memorandum X-397.

[35] Schwanekamp, T. System studies on active thermal protection of a hypersonic suborbital passenger transport vehicle. AIAA 2014-2372. 19th AIAA International Space Planes and Hypersonic Systems and Technologies Conference, 2014.

[36] Schwanekamp, T., Garbers, N., and Sippel, M. Conceptual Design of the SpaceLiner Thermal Protection System. 8th European Symposium on Aerothermodynamics for Space Vehicles, 2015.

[37] Simeonides, G. Simple theoretical and semi-empirical convective heat transfer predictions for generic aerodynamic surfaces. *ESA, Propulsion and Aerothermodynamics Division TR-YPA/1576/GS*, 1995.

[38] Sippel, M. SpaceLiner Technical Progress and Mission Definition. AIAA 2015-3582. 20th AIAA International Space Planes and Hypersonic Systems and Technologies Conference, 2015.

[39] Sippel, M., van Foreest, A., Bauer, C., and Cremaschi, F. System Investigations of the SpaceLiner Concept in FAST20XX. AIAA 2011-2294. 17th AIAA International Space Planes and Hypersonic Systems and Technologies Conference, 2011.

[40] Sivamurugan, T., Anoop, P., and Desikan, S. Aerothermal design, qualification and flight performance. *Current Science (00113891)*, 114(1), 2018.

[41] Stanley, D. O., Engelund, W. C., Lepsch, R. A., McMillin, M., Wurster, K. E., Powell, R. W., Guinta, T., and Unal, R. Rocket-powered single-stage vehicle configuration selection and design. *Journal of spacecraft and rockets*, 31(5):792–798, 1994.

[42] Sudmeijer, K. An Enhanced Radiation Cooling System for re-entry vehicles, principle and mathematical modeling. Unpublished, obtained via personal communication, 2005.

[43] Taguchi, G. System of experimental design; engineering methods to optimize quality and minimize costs. Technical report, 1988. QA279 T3.

[44] Van Baten, T. and Buursink, J. Spaceship with heat-isolating outer skin. *WO 02066326 (A1)*, 2002.

[45] van Foreest, A., Gülhan, A., Esser, B., Sippel, M., Ambrosius, B., and Sudmeijer, K. Transpiration Cooling Using Liquid Water. *39th AIAA Thermophysics Conference*, (AIAA 2007-4034), 2007.

[46] Vollmer, K. Heatloads calculation for Concept No. 15 OAE. (FSS-DASARI-RP-4008A/FSSC-15oae), 1992.

[47] Yamaguchi, M., Inui, H., and Ito, K. High-temperature structural intermetallics. *Acta materialia*, 48(1):307–322, 2000.

[48] *Alumina Type ZAL-15*. Zircar Ceramics, 2019. online at https://www.zircarceramics.com/wp-content/uploads/2017/01/ZAL-15.pdf (accessed March 4, 2020).